

Master Thesis in Reservoir Chemistry

# **Modelling of Low Salinity Surfactant Polymer Coreflood Experiments**

**Sivert Mordal Nerbøvik**



Centre for Integrated Petroleum Research

Department of Chemistry

University of Bergen

November 2018



## Acknowledgement

First and foremost, I would like to thank my supervisor Arne Skauge for his excellent guidance and support throughout the process of writing this thesis.

I would also like to express gratitude to UniResearch CIPR for giving me the opportunity to write my thesis for them, and for providing me with great working conditions.

Thank you to my fellow students Diderik Olav Jarlsby, Vilde Loug Pedersen, and Trude Sætnan Sæther for contributing to a positive and collaborative working environment.

Also thank you to my family for their constant support and encouragement through all my years of studying.

Finally, a special thank you goes to Andrea. Thank you for being who you are, and for supporting me throughout this process. Your positive attitude has lifted my spirits when things have been difficult, and for that I am very grateful.

Sivert Mordal Nerbøvik

Bergen, November 2018

## Abstract

In recent years, there has been a growing interest in the effect of varying brine composition during waterflooding. Several studies on low salinity water injection have been conducted, and the results indicate a potential for increased oil recovery at reduced salinity. Further studies have also shown a significant increase in oil recovery when low salinity injection is combined with surfactant and polymer flooding. This is attributed to the mobilization of oil during low salinity and surfactant floods, and the increased volumetric sweep from polymer injection.

In this thesis, modelling of low salinity surfactant polymer (LSSP) coreflood experiments is investigated. The simulations presented in the study was conducted by using the chemical simulator STARS by CMG (Computer Modelling Group). Sensitivity and verification studies were performed in order to confirm STARS' capabilities of modelling coreflood experiments, and to determine how altering key parameters affected the simulation results. This was followed by a history matching study of a LSSP coreflood experiment conducted by UniResearch CIPR.

For the history matching, salinity dependent oil and water relative permeability was used to model low salinity waterflooding. This was based on an assumption that the injection of low salinity brine induced a wettability alteration in the core. Low salinity surfactant injection was modelled by enabling interpolation based on capillary number. The low salinity polymer solution was modelled as a viscosity effect only, due to interpolation problems when adding a third interpolation routine in the model.

The experimental oil recovery and differential pressure from the experiment was successfully history matched using the described model. The results thus confirmed that STARS is capable of modelling complex coreflooding processes such as LSSP floods. However, since the model was limited to only two interpolation routines, the physical effects of each injection sequence was not accurately represented.

# Nomenclature

## Variables

$A$	Area	[cm <sup>2</sup> ]
$Ad$	Adsorption	[gmol/cm <sup>3</sup> ] [mg/g]
$ca$	Mole fraction of component subject to adsorption	Dimensionless
$D_{ijk}$	Total dispersion component	[cm <sup>2</sup> /min]
$dP$	Differential pressure	[Pa]
$dP/dx$	Pressure drop over distance $x$	[Pa/cm]
$dv/dy$	Shear rate	[1/s]
$E_D$	Microscopic displacement efficiency	Dimensionless
$E_R$	Oil recovery factor	Dimensionless
$E_{vol}$	Volumetric displacement efficiency	Dimensionless
$f_j$	Fractional flow of phase $j$	Dimensionless
$G$	Gibbs Free Energy	[J]
$I_{AH}$	Amott-Harvey index	Dimensionless
$I_w$	Amott-Harvey water index	Dimensionless
$I_o$	Amott-Harvey oil index	Dimensionless
$I_{USBM}$	USBM index	Dimensionless
$h$	Height	[cm]
$J_{ijk}$	Total dispersive flux	[g/min <sup>-1</sup> cm <sup>-2</sup> ]
$K$	Absolute permeability	[mD]
$k_{ej}$	Effective permeability of phase $j$	[mD]
$k_{rj}$	Relative permeability of phase $j$	Dimensionless
$k_{rj}^o$	End-point relative permeability of phase $j$	Dimensionless
$L$	Length	[cm]
$m$	Mass	[g]
$M_{wo}$	Mobility ratio between oil and water	Dimensionless
$M_{wo}^o$	End-point mobility ratio between oil and water	Dimensionless
$N_{vc}$	Capillary number	Dimensionless
$n_{w/o}$	Corey exponent for water/oil	Dimensionless

$P$	Pressure	[Pa]
$PV$	Pore volume	Dimensionless
$q$	Flow rate	[cm <sup>3</sup> /min]
$r$	Radius	[cm]
$S$	Saturation	Dimensionless
$S_w^\circ$	Normalized water saturation	Dimensionless
$S_{or}$	Residual oil saturation	Dimensionless
$S_{oi}$	Initial oil saturation	Dimensionless
$S_{wi}$	Irreducible water saturation/ Initial water saturation	Dimensionless
$t$	Time	[min]
tad1, tad2	Langmuir adsorption isotherm	[gmol/cm <sup>3</sup> ]
tad3	Langmuir adsorption isotherm	Dimensionless
$u$	Darcy velocity	[cm/min]
$V$	Volume	[cm <sup>3</sup> ]
$v$	Interstitial velocity	[cm/min]
WC	Water Cut	Dimensionless
$\nabla k$	Concentration gradient	[g/cm <sup>4</sup> ]
$\Delta$	Difference	Dimensionless
$\theta$	Contact angle	[°]
$\lambda$	Mobility	[mD/cP]
$\lambda^\circ$	End-point mobility	[mD/cP]
$\rho$	Density	[g/cm <sup>3</sup> ]
$\sigma$	Interfacial tension	[mN/cm]
$\tau$	Shear stress	[Pa]
$\mu$	Viscosity	[cP]
$\phi$	Porosity	Dimensionless
$\Pi(h)$	Disjoining pressure	[N/m <sup>2</sup> ]

## Subscripts

<i>abs</i>	Absolute
<i>b</i>	Bulk
<i>c</i>	Capillary
<i>D</i>	Microscopic
<i>eff</i>	Effective
<i>g</i>	Gas
<i>j</i>	Component (phase)
<i>i</i>	Initial
<i>i</i>	Irreducible
<i>o</i>	Oil
<i>p</i>	Pore
<i>r</i>	Relative
<i>r</i>	Residual
<i>R</i>	Recovery
<i>tot</i>	Total
<i>vol</i>	Volumetric
<i>w</i>	Water

## Abbreviations

1D	One-dimensional
2D	Two-dimensional
3D	Three-dimensional
CDC	Capillary desaturation curve
CMC	Critical micelle concentration
CMG	Computer Modelling Group
COBR	Crude oil/brine/rock system
Ca <sup>2+</sup>	Calcium ion
Cl <sup>-</sup>	Chloride ion
CIPR	Centre for Integrated Petroleum Research
EOR	Enhanced Oil Recovery
IFT	Interfacial Tension
IPV	Inaccessible pore volume
HPAM	Hydrolyzed polyacrylamide
LS	Low salinity
LSS	Low salinity surfactant
LSP	Low salinity polymer
LSSP	Low salinity surfactant polymer
MIE	Multicomponent ionic exchange
Mg <sup>2+</sup>	Magnesium ion
Na <sup>+</sup>	Sodium ion
NaCl	Sodium Chloride
NCS	Norwegian Continental Shelf
OOIP	Original oil in place
PAM	Polyacrylamide
ppm	Parts per million
SCAL	Special core analysis
SOB	Surfactant-oil-brine
SSW	Synthetic seawater
STOOIP	Stock tank oil in place
SWCTT	Single-well chemical tracer test

## STARS Keywords

ADMAXT	Maximum adsorption capacity	[gmol/cm <sup>3</sup> ]
ADRT	Residual adsorption level	[gmol/cm <sup>3</sup> ]
ADSCPOMP	Specify component to which the adsorption function will apply	Dimensionless
ADSLANG	Denote composition dependence via Langmuir isotherm coefficients	[gmol/cm <sup>3</sup> ] Dimensionless
AVISC	Liquid viscosities	[cP]
DISPI/J/K_WAT	Effective total dispersion coefficients of component in water phase	[cm <sup>2</sup> /min]
DTMAX	Maximum allowed time-step size	[min]
DTRAPW	Value of water phase interpolation parameter	Dimensionless
IFTTABLE	Interfacial tension input values	[dyne/cm]
INTCOMP	Assign interpolation component	Dimensionless
KRINTRP	Assign interpolation set number	Dimensionless
KRTYPE	Assign rock type number to each grid-block	Dimensionless
LOWER_BOUND	Define lower bound of interpolation parameter	Dimensionless
PORFT	Accessible pore volume	Dimensionless
RPT	Define rock type number for rock-fluid data	Dimensionless
RPT_INTRP	Specify interpolation between two rock types	Dimensionless
TUBE-END	Specify linear flow model of well indices	Dimensionless
SHEARTAB	Specify shear effects on fluid viscosity	Dimensionless
SWT	Water-oil relative permeability table	Dimensionless
UPPER_BOUND	Define upper bound of interpolation parameter	Dimensionless
UPPERB_RPT	Specify which rock type number is used as upper bound for interpolation	Dimensionless
VSMIXCOMP	Specify component to which viscosity mixing is assigned	Dimensionless
VSMIXENDP	Specify minimum and maximum mole fractions of component subject to mixing	Dimensionless
VSMIXFUNC	Define mixing rule function	Dimensionless

# Contents

<b>Acknowledgement .....</b>	<b>i</b>
<b>Abstract .....</b>	<b>ii</b>
<b>Nomenclature.....</b>	<b>iii</b>
Variables.....	iii
Subscripts .....	v
Abbreviations .....	vi
<b>STARS Keywords.....</b>	<b>vii</b>
<b>Contents.....</b>	<b>viii</b>
<b>List of Figures .....</b>	<b>xi</b>
<b>List of Tables.....</b>	<b>xiv</b>
<b>1 Introduction.....</b>	<b>1</b>
<b>2 Theory .....</b>	<b>2</b>
2.1 Petrophysical properties .....	2
2.1.1 Porosity.....	2
2.1.2 Absolute permeability .....	2
2.1.3 Effective and relative permeability.....	3
2.1.4 Saturation.....	4
2.1.5 Residual oil saturation .....	4
2.2 Fluid properties.....	6
2.2.1 Viscosity.....	6
2.2.2 Mobility .....	6
2.2.3 Mobility ratio.....	6
2.2.5 Miscibility .....	8
2.2.6 Interfacial tension .....	8
2.2.6 Capillary pressure.....	9
2.2.7 Drainage and imbibition .....	10
2.2.8 Capillary number and capillary desaturation curves (CDC).....	11
2.2.9 Wettability .....	12
2.2.10 Effect of wettability on waterflooding and Sor .....	14
2.2.11 Effect of wettability on relative permeability.....	16
2.2.12 Wettability alteration .....	17

<b>3</b>	<b>Enhanced Oil Recovery .....</b>	<b>18</b>
3.1	Low salinity waterflooding.....	19
3.1.1	Laboratory studies .....	19
3.1.2	Field studies.....	21
3.1.3	Low salinity mechanisms .....	22
3.1.4	Modelling of low salinity waterflooding.....	26
3.2	Surfactant flooding .....	27
3.2.1	Surfactants .....	27
3.2.2	Phase behavior.....	29
3.2.3	Surfactant retention .....	31
3.2.4	Laboratory studies on low salinity surfactant (LSS) injection .....	31
3.2.5	Modeling of low salinity surfactant (LSS) injection .....	32
3.3	Polymer flooding.....	33
3.3.1	Polymers.....	33
3.3.2	Viscosity of polymer solutions .....	34
3.3.3	Polymer retention and inaccessible pore volume (IPV) .....	36
3.3.4	Laboratory studies on low salinity polymer (LSP) injection.....	36
3.3.5	Modeling of low salinity polymer (LSP) flooding .....	37
<b>4</b>	<b>CMG STARS – Reservoir Simulator .....</b>	<b>38</b>
4.1	Relative permeability interpolation .....	39
4.2	Dispersion.....	40
4.3	Adsorption.....	41
4.4	Multiple interpolation.....	42
4.4.1	Multiple interpolation scheme – core R14 .....	43
<b>5</b>	<b>Previous Studies at UniResearch CIPR .....</b>	<b>45</b>
5.1	Simulation study of core R3 and R4 by Drønen.....	45
5.2	Simulation study of core R10 by Jarlsby.....	51
<b>6</b>	<b>Sensitivity and Verification Studies .....</b>	<b>54</b>
6.1	Corey relative permeability parameters.....	54
6.1.1	Sensitivity - varying <i>no</i> .....	55
6.1.2	Sensitivity - varying <i>nw</i> .....	57
6.1.3	Sensitivity - varying <i>krw(Sor)</i> .....	60
6.1.4	Sensitivity - varying <i>Sor</i> .....	63
6.2	Dispersion.....	67

6.2.1	Numerical dispersion.....	67
6.2.2	Physical dispersion .....	71
6.2.3	Dispersion over distance.....	72
6.2.4	Effect of dispersion on relative permeability .....	73
6.3	Surfactant and polymer viscosity .....	74
6.4	Interfacial tension and capillary number .....	76
6.5	Surfactant and polymer adsorption.....	79
<b>7</b>	<b>History Matching of Core R14.....</b>	<b>81</b>
7.1	R14 – synthetic seawater (SSW) flooding.....	84
7.1.1	Wettability evaluation .....	84
7.1.2	History matching .....	87
7.2	R14 – Low salinity water (LS) flooding.....	90
7.2.1	History matching .....	90
7.3	R14 - Low salinity surfactant (LSS) flooding .....	94
7.4	R14 – low salinity polymer (LSP) flooding .....	95
7.5	R14 – combined low salinity surfactant polymer (LSSP) flooding.....	96
7.5.1	Sensitivity of LSSP matching parameters .....	96
7.5.2	History matching .....	105
<b>8</b>	<b>Summary and Conclusions.....</b>	<b>111</b>
<b>9</b>	<b>Further Work .....</b>	<b>112</b>
<b>10</b>	<b>References .....</b>	<b>113</b>
<b>A</b>	<b>Appendix.....</b>	<b>120</b>
A.1	Experimental data.....	120
A.3	STARS input file – History Matching of R14.....	122
A.3	STARS input file – Sensitivity Study of Corey Parameters.....	137

## List of Figures

Figure 2 1: Illustration of Darcy’s law. ....	3
Figure 2 2: Illustration of the pore doublet model [3].....	5
Figure 2 3: Illustration of the snap-off model [3].....	5
Figure 2 4: Effect of end-point mobility ratio on displacement efficiency [3]. ....	7
Figure 2 5: Illustration of molecular attraction in miscible and immiscible fluids. ....	8
Figure 2 6: Motion of molecules within the immiscible phases oil and water [4]. ....	9
Figure 2 7: Relative permeability curves for drainage and imbibition in water wet system [3] .....	10
Figure 2 8: Example of a typical capillary desaturation curve (CDC) [3]. ....	11
Figure 2 9: Measuring of the wetting angle in oil-water system [11]. ....	13
Figure 2 10: Illustration of waterflooding in a water-wet (a) and oil-wet (b) system. ....	14
Figure 2 11: Oil recovery at different wettability conditions [12]. ....	15
Figure 2 12: Oil/water relative permeability for both oil wet and water wet systems [13].....	16
Figure 3 1: Illustration of oil-wettability mechanisms [36].....	25
Figure 3 2: Illustration of a surfactant molecule. ....	27
Figure 3 3: Classification of surfactant molecules [2] .....	28
Figure 3 4: Illustration of the critical micelle concentration (CMC) [3].....	28
Figure 3 5: Illustration of surfactant – oil – brine (SOB) phase behavior systems [2]. ....	29
Figure 3 6: Relationship between interfacial tension and salinity [3]. ....	30
Figure 3 7: Structure and composition of Xanthan, PAM and HPAM [48].....	33
Figure 3 8: The Carreau model for viscosity behavior of polymer solutions [3]. ....	34
Figure 3 9: Effect of increasing salinity concentration on HPAM molecules [48]. ....	35
Figure 4 1: Overview of data files in STARS simulation [55]. ....	38
Figure 4 2: Normalized mole fractions of components in block 50,1,1.....	42
Figure 4 3: Interpolation setup used in history matching of core R14. ....	43
Figure 5 1: Summary of coreflooding sequences of core R3 and R4 [57]. ....	46
Figure 5 2: Oil recovery and water cut during LSSP flooding of core R3 [57]. ....	47
Figure 5 3: Oil recovery and water cut during LSSP flooding of core R4 [57]. ....	47
Figure 5 4: Interpolation setup in Drønen’s modelling of flooding sequences in R3 and R4..	48
Figure 5 5: History match of oil production and differential pressure for core R3.....	49
Figure 5 6: History match of oil production and differential pressure for core R4.....	50
Figure 5 7: Summary of coreflooding sequences in core R10 [58]. ....	51
Figure 5 8: Interpolation setup in Jarlsby’s modelling of core R10 [58]. ....	52
Figure 5 9: History match of oil production and differential pressure for core R10 [58]. ....	52
Figure 6 1: Base case relative permeability curves.....	55
Figure 6 2: Relative permeability curves for varying $n_o$ . ....	55
Figure 6 3: Cumulative oil production for varying $n_o$ . ....	56
Figure 6 4: Differential pressure for varying $n_o$ . ....	56
Figure 6 5: Relative permeability curves for varying $n_w$ . ....	57
Figure 6 6: Cumulative oil production at varying $n_w$ . ....	58
Figure 6 7: Cumulative oil production at varying $n_w$ , with altered x-axis and y-axis. ....	58
Figure 6 8: Differential pressure for varying $n_w$ . ....	59
Figure 6 9: Differential pressure at varying $n_w$ , with altered x-axis. ....	59
Figure 6 10: Relative permeability curves for varying $krw(Sor)$ . ....	60
Figure 6 11: Cumulative oil production at varying $krwSor$ . ....	61

Figure 6 12: Cumulative oil production at varying $krw(Sor)$ , with altered x-axis and y-axis.	61
Figure 6 13: Differential pressure at varying $krw(Sor)$ .	62
Figure 6 14: Relative permeability curves at varying $Sor$ .	63
Figure 6 15: Cumulative oil production at varying $Sor$ .	64
Figure 6 16: Differential pressure at varying $Sor$ .	64
Figure 6 17: Differential pressure at varying $Sor$ , with altered x-axis and y-axis.	65
Figure 6 18: Numerical dispersion of salt concentration in the producer for different amount of grid-blocks.	68
Figure 6 19: Numerical dispersion of salt concentration in the producer for different amount of grid-blocks, with altered x-axis.	68
Figure 6 20: Numerical dispersion of salt concentration for different sized time-steps. 100 grid blocks is used.	69
Figure 6 21: Numerical dispersion of salt concentration for different sized time-steps, with altered x-axis. 100 grid blocks is used.	70
Figure 6 22: Physical dispersion for different dispersion coefficients. 100 grid-blocks and DTMAX 1 is used.	71
Figure 6 23: Physical dispersion at increasing distance from the injector. A model of 100 grid blocks and DTMAX 1 is used, with dispersion set to $0.005 \text{ cm}^2/\text{min}$ .	72
Figure 6 24: Water relative permeability for different dispersion coefficients, with altered x-axis and y-axis.	73
Figure 6 25: Water viscosity as a function of water mole fraction of surfactant (Block 50,1,1)	75
Figure 6 26: Simulated interpolation between interfacial tension entries compared to the expected linear interpolation from the STARS manual.	77
Figure 6 27: Comparison of simulated and calculated capillary numbers.	78
Figure 6 28: Comparison of simulated and calculated adsorption	79
Figure 6 29: Reversible and irreversible adsorption of surfactant	80
Figure 7 1: Coreflooding sequences performed on core R14.	82
Figure 7 2: Experimental oil recovery and water cut for core R14. Plot is taken from laboratory data sheet.	83
Figure 7 3: Experimental differential pressure for core 14. Plot is taken from laboratory data sheet.	83
Figure 7 4: Simulated relative permeability curves for different wettability conditions, with altered x-axis.	85
Figure 7 5: Simulated oil recovery for different wettability conditions.	86
Figure 7 6: Simulated differential pressure for different wettability conditions.	86
Figure 7 7: Relative permeability curves yielding the best match for SSW flooding.	88
Figure 7 8: History match of oil recovery for the SSW flood.	89
Figure 7 9: History match of differential pressure for the SSW flood.	89
Figure 7 10: Relative permeability curves yielding the best match for the LS flood.	91
Figure 7 11: History Match of oil recovery for the SSW and LS floods.	92
Figure 7 12: History match of differential pressure for the SSW and LS floods.	92
Figure 7 13: IFFTABLE defining the interfacial tension in the model.	94
Figure 7 14: shear rate table defining the polymer viscosity at different Darcy velocities.	95
Figure 7 15: Extended LS relative permeability curves (instantaneous vs continuous)	97
Figure 7 16: Differential pressure match for the different extended LS relative permeability curves (instantaneous vs continuous)	97
Figure 7 17: Extended LS relative permeability curves for different $krw(Sor)$ values.	98
Figure 7 18: Differential pressure match for different $krw(Sor)$ values	98

Figure 7 19: Oil recovery for varying $n_o$ .....	99
Figure 7 20: Differential pressure for varying $n_o$ .....	99
Figure 7 21: Differential pressure for varying polymer viscosity .....	100
Figure 7 22: Oil recovery for varying polymer viscosity .....	100
Figure 7 23: Differential pressure for varying surfactant viscosity.....	101
Figure 7 24: Oil recovery for different surfactant viscosity .....	101
Figure 7 25: Differential pressure for varying $S_{or}$ .....	102
Figure 7 26: Oil recovery for varying $S_{or}$ .....	102
Figure 7 27: Differential pressure for varying inaccessible pore volume .....	103
Figure 7 28: Oil recovery for varying inaccessible pore volume .....	103
Figure 7 29: Differential pressure for varying surfactant and polymer dispersion .....	104
Figure 7 30: Differential pressure for varying surfactant and polymer dispersion .....	104
Figure 7 31: Relative permeability curves used in the history matching of LSSP flooding..	106
Figure 7 32: Best match of oil recovery for all flooding sequences.....	107
Figure 7 33: Best match of differential pressure for all flooding sequences.....	107
Figure 7 34: Comparison of water phase viscosity and differential pressure (block 50,1,1).	108
Figure 7 35: Mole fractions of surfactant and polymer in block 50,1,1 .....	109
Figure 7 36: Relative permeability curves from block 2,1,1 of the LSSP best match simulation .....	110
Figure 7 37: Relative permeability curves from block 2,1,1 of the LSSP best match simulation, with logarithmic scale on the y-axis.....	110

## List of Tables

Table 2 1: Wettability classes for an oil-water system [4].	13
Table 2 2: Craig’s rules of thumb for determining wettability [14].	17
Table 6 1: Corey parameters used in calculation of base case relative permeability.	54
Table 6 2: Observations from sensitivity study of Corey parameters.	66
Table 6 3: Input values used in simulation of surfactant injection.	74
Table 6 4: Interfacial Tension values used in the verification study.	76
Table 7 1: Properties of core R14.	81
Table 7 2: Chemical composition of the synthetic seawater used in coreflooding experiments.	84
Table 7 3: Corey parameters for intermediate wet, more water wet and more oil wet cases.	85
Table 7 4: Experimental permeability values.	87
Table 7 5: Experimental, initial guess and best match values for SSW flooding.	88
Table 7 6: Experimental, initial guess and best match values for LS flooding.	91
Table 7 7: Simulated properties of “Recolas 18”.	94
Table 7 8: Simulated properties of HPAM3230S.	95
Table 7 9: Corey relative permeability values used in history matching of LSSP floods.	105
Table 7 10: Values of parameters related to the surfactant and polymer floods.	106
Table A 1: Petrophysical data of core R14.	120
Table A 2: Experimental properties of injected fluids.	120
Table A 3: Experimental properties of injection sequences.	121

# 1 Introduction

According to the Norwegian Petroleum Directorate, the oil recovery factor on the Norwegian continental shelf (NCS) averages at 47%, while the global figures are slightly below 40% [1]. This means that more than half of the oil discovered, both on the NCS and globally, are not recovered. With a growing demand of energy, and oil reserves on decline, the importance of improving the oil recovery factor is increasing.

Oil recovery can be categorized into three phases; primary, secondary and tertiary recovery. Primary recovery is the recovery of oil by use of the natural energy residing in the reservoir, also referred to as pressure depletion. Secondary recovery is the injection of water or gas to act as pressure support and to displace oil towards producers. Tertiary recovery is the implementation of so-called Enhanced Oil Recovery (EOR) methods, which is oil recovery by injection of chemicals, such as surfactants and polymers [3]. Studies suggest that in order to increase the oil recovery factor in the future, further development and utilization of EOR methods is necessary.

Historically, waterflooding have only been used as pressure support and to displace oil towards producers [3]. However, in recent years, several studies have investigated the effect of varying the composition of the injected brine. The results have indicated a potential for increased oil recovery for low salinity waterflooding. Furthermore, investigations on the effect of combining low salinity injection with surfactant and polymer flooding have been conducted. These studies show promising results, with significant increases in oil recovery being observed.

UniResearch CIPR have performed several coreflood experiments investigating the effect of combining low salinity injection with surfactant and polymer flooding. In this thesis, the low salinity surfactant polymer (LSSP) coreflooding of core R14 is analyzed. The thesis is a simulation study, in which the simulator STARS by CMG (Computer Modelling Group) has been utilized. The initial sections of the thesis includes basic theory related to reservoir properties, enhanced oil recovery, and coreflood simulation. This is followed by a presentation of sensitivity and verification studies related to modelling of EOR processes. Finally, a history matching study of the mentioned experiment is presented. The purpose of the thesis is to analyze the effect of low salinity surfactant polymer (LSSP) flooding, and evaluate the simulators' capabilities of modelling such corefloods.

## 2 Theory

In this section, fundamental reservoir properties and concepts related to coreflooding experiments are introduced. Knowledge of this theory is necessary in order to understand the work presented in this thesis.

### 2.1 Petrophysical properties

#### 2.1.1 Porosity

The porosity of a rock determines the rock's ability to store hydrocarbons, and is therefore of great importance when it comes to reservoir engineering. The total porosity is defined as the ratio of total void volume to the bulk volume of the rock [4].

$$\phi_{tot} = \frac{V_p}{V_b} \quad (2.1)$$

Where  $\phi_{tot}$  is the total porosity,  $V_p$  is the total void volume and  $V_b$  is the bulk volume.

In coreflooding experiments, the porosity of the core sample is estimated through single phase flow measurements. This only accounts for the pore space that is interconnected, and where fluids are allowed to flow. This is the effective porosity, which is given by:

$$\phi_{eff} = \frac{V_{p,eff}}{V_b} \quad (2.2)$$

#### 2.1.2 Absolute permeability

Absolute permeability is a measure of a rock's capability of transmitting fluids through its network of interconnected pores [4]. It can be estimated performing single phase flow measurements on a core sample, and applying the measured data to Darcy's law:

$$q = -\frac{KA}{\mu} \frac{dP}{dx} \quad (2.3)$$

Where  $q$  is the volumetric flow rate,  $K$  is absolute permeability,  $A$  is cross-sectional area,  $\mu$  is fluid viscosity and  $dp/dx$  is the pressure loss across the core.

Darcy's law is an empirical law which requires certain basic conditions to be satisfied. The core sample has to be 100% saturated with a single, incompressible fluid, and the flow has to be horizontal, stationary and laminar. In addition, there must be no chemical reaction between the fluid and the rock [4]. Figure 2.3 illustrates the different parameters in Darcy's law for a coreflooding process.

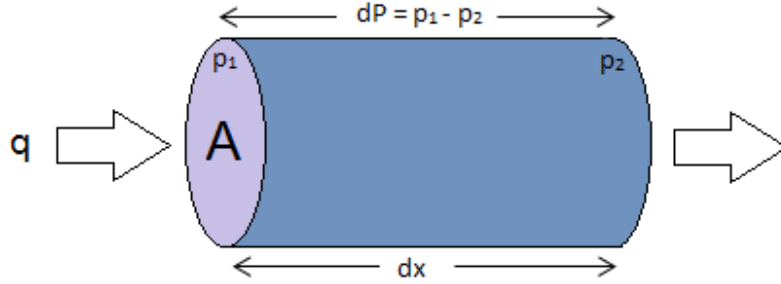


Figure 2 1: Illustration of Darcy's law.

From equation 2.3 it can be found that the unit for permeability is  $m^2$ . In the coreflooding data provided for the simulations in this thesis, permeability is given in the alternative unit Darcy (D). The conversion from  $m^2$  to Darcy is given as:  $1D = 10^{-12} m^2$ .

### 2.1.3 Effective and relative permeability

When there are multiple fluids in a system, the permeability to each fluid is called the effective permeability. Effective permeabilities strongly depend on the fluids' relative saturation, as the presence of one fluid will hinder the flow of the other. To calculate effective permeability, Darcy's law must take into account each separate phase:

$$q_j = -\frac{k_{ej}A}{\mu_j} \frac{dP_j}{dx} \quad (2.4)$$

Where  $j$  denotes the fluid phase and  $k_{ej}$  is the effective permeability of phase  $j$ .

The ratio between the effective permeability and the absolute permeability is called the relative permeability. It is a function of fluid saturation, rock properties and wettability, and is given by [4]:

$$k_{rj} = \frac{k_{ej}}{K} \quad (2.5)$$

Where  $k_{rj}$  is the relative permeability of phase  $j$ .

Modelling of relative permeability curves is a key aspect in history matching of experimental corefloods. In the simulations presented in this thesis, modelling of relative permeability was based on Corey-type functions. These involve calculating the relative permeability as a function of normalized water saturation [5]:

$$k_{rw} = k_{rw}^{\circ} (S_w^*)^{n_w} \quad (2.6)$$

$$k_{ro} = k_{ro}^{\circ} (1 - S_w^*)^{n_o} \quad (2.7)$$

$$S_w^* = \frac{S_w - S_{wi}}{1 - S_{wi} - S_{or}} \quad (2.8)$$

Where  $k_{rw}^{\circ}$  and  $k_{ro}^{\circ}$  are end-point relative permeability for water and oil and  $S_w^*$  is the normalized water saturation.

#### 2.1.4 Saturation

Several fluids can be present at the same time in a porous medium. These fluids are typically water, oil and gas. The pore occupancy for such a system can be described by:

$$V_p = V_o + V_g + V_w \quad (2.9)$$

Where  $V_p$  is the pore volume,  $V_o$  is the oil volume,  $V_g$  is the gas volume and  $V_w$  is the water volume.

In most cases, it is preferred to describe pore occupancy in terms of saturations rather than volumes. The saturation of a fluid is defined as the fraction of pore volume occupied by that fluid [4]:

$$S_j = \frac{V_j}{V_p} \quad j = 1, \dots, n \quad (2.10)$$

Where  $S_j$  is the saturation fluid  $j$ ,  $V_j$  is the fluids volume, and  $V_p$  is the pore volume.

#### 2.1.5 Residual oil saturation

When producing oil from a reservoir, some of the oil will remain in the pore space as residual oil. The fraction of total pore volume containing residual oil is defined as the residual oil saturation ( $S_{or}$ ) [4]. There are multiple models describing the phenomenon of residual oil trapping, with the pore doublet model and the snap-off model being the most acknowledged.

### 2.1.5.1 The pore doublet model

The pore doublet model describes the trapping of residual oil due to local heterogeneities in the system. When a pore channel splits into two, the wetting phase will intrude the narrower channel more rapidly due to larger capillary forces. This results in the non-wetting phase being trapped in the larger channel, as illustrated in figure 2.2.

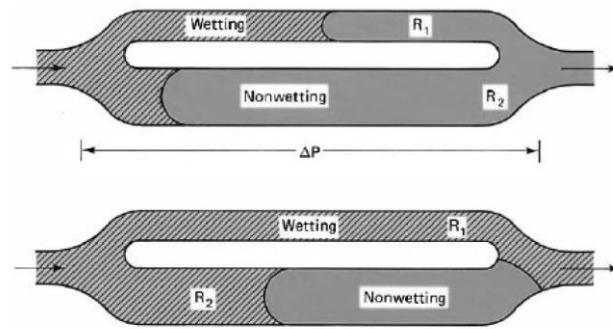


Figure 2 2: Illustration of the pore doublet model [3]

### 2.1.5.2 Snap-off model

The snap-off model illustrates the trapping of residual oil due to surface tension between oil and water. In a water-wet system, the oil will flow in the center of pores, with a thin water film separating it from the pore walls. As water displaces the oil, increasing water saturation causes thickening of water films and thinning of oil films in narrow pore throats. Eventually, the oil will snap-off, causing residual oil globules to be trapped in the center of large pores. An illustration of the snap-off model is seen in figure 2.3.

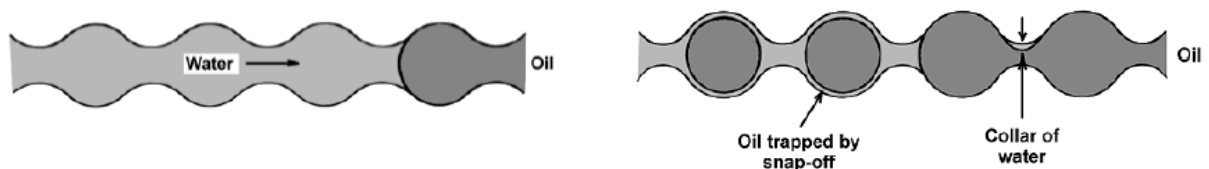


Figure 2 3: Illustration of the snap-off model [3]

## 2.2 Fluid properties

### 2.2.1 Viscosity

Viscosity is a measure of a fluids internal resistance to flow [4], and is defined by:

$$\mu = \frac{\tau}{dv/dy} \quad (2.11)$$

Where  $\mu$  is the viscosity,  $\tau$  is the shear stress and  $dv/dy$  is the shear rate.

Fluids may be classified as Newtonian or non-Newtonian depending on their viscosity behavior. Newtonian fluids have a linear relationship between shear rate and shear stress, meaning that their viscosity is independent of shear rate (e.g water). Non-newtonian fluids have a shear-dependent viscosity (e.g polymer solutions) [3].

In the simulations performed in this thesis, the shear rate interval during polymer flooding is assumed to be constant, and the polymer viscosity is therefore treated as independent of shear rate. This is described in more detail in section 7.4.

### 2.2.2 Mobility

The mobility of a fluid is a measure of how easily a fluid flows through a porous medium at a given saturation [4]. It is defined as the ratio between the fluids effective permeability and viscosity:

$$\lambda_j = \frac{k_{ej}}{\mu_j} = \frac{k_{rj}}{\mu_j} K \quad (2.12)$$

Where  $\lambda_j$  is the mobility fluid  $j$ ,  $k_{ej}$  is its effective permeability and  $\mu_j$  is its viscosity.

### 2.2.3 Mobility ratio

The mobility ratio is the ratio between the mobility of the displacing fluid to the mobility of the displaced fluid [6]. In a scenario where water displaces oil, the mobility ratio is defined as:

$$M_{wo} = \frac{\lambda_{w,or}}{\lambda_{o,iw}} = \frac{k_{rw}}{k_{ro}} \frac{\mu_o}{\mu_w} \quad (2.13)$$

For evaluation of waterflood stability, the end-point mobility ratio is used:

$$M_{wo}^{\circ} = \frac{k_{rw}^{\circ}}{k_{ro}^{\circ}} \frac{\mu_o}{\mu_w} \tag{2.14}$$

Where  $M_{wo}^{\circ}$  is the end-point mobility ratio.

End-point mobility ratio is an important parameter when evaluating waterflooding performance as it has a significant impact on the displacement efficiency ( $E_D$ ). This is illustrated in figure 2.7.

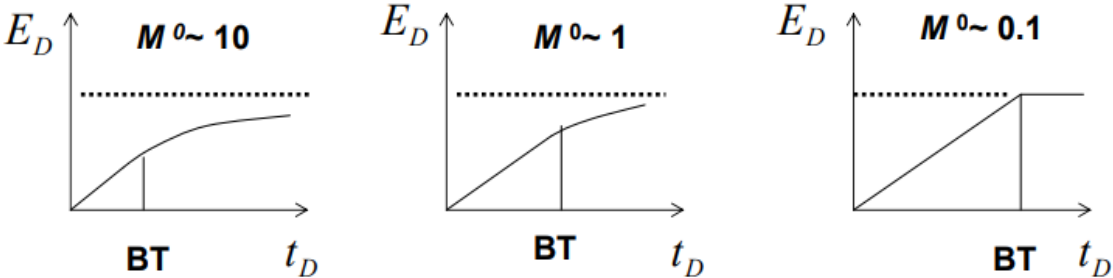


Figure 2 4: Effect of end-point mobility ratio on displacement efficiency [3].

For mobility ratios above 1 ( $M^{\circ} > 1$ ), the viscosity of the injected water is lower than that of the oil. This is considered unfavorable, as the injected water will have a higher mobility and travel faster towards the production well compared to the oil. This results in an unstable displacement front, which yields early water breakthrough and long tail production.

For mobility ratios below 1 ( $M^{\circ} < 1$ ), the viscosity of the injected water is higher than that of the oil. This causes a piston-like displacement, resulting in later water breakthrough and short tail production, which is favorable [3].

## 2.2.5 Miscibility

In reservoirs with more than one fluid, there are electrostatic forces acting both within (intramolecular forces) and between (intermolecular forces) the present fluids. When the intramolecular forces are greater than the intermolecular, the fluids are *immiscible*. This is generally the case with water, oil and gas. In cases where the intermolecular forces are greater than the intramolecular, the fluids tend to mix. These are called *miscible* fluids. A typical example is the mixing of alcohol with water [7]. Figure 2.5 illustrates the molecular attraction in miscible and immiscible fluids.

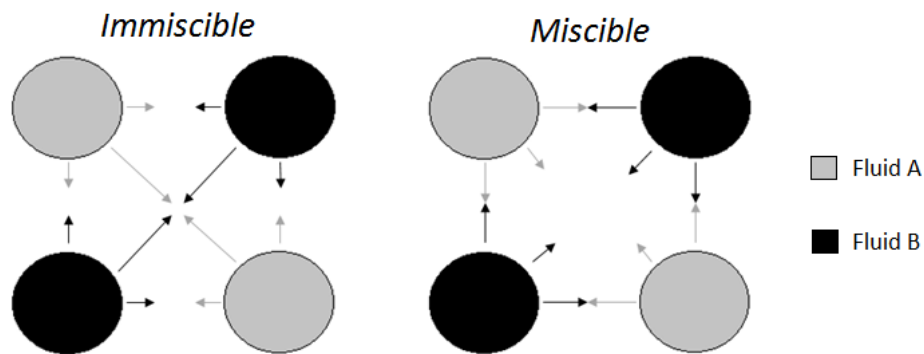


Figure 2.5: Illustration of molecular attraction in miscible and immiscible fluids.

## 2.2.6 Interfacial tension

Interfacial tension (IFT) is the tangential force at the interface between two immiscible fluids representing the work required to keep the fluids from mixing [4]. It is defined by:

$$\sigma = \left( \frac{\partial G}{\partial A} \right)_{T,P,m_{1,2}} \quad (2.15)$$

Where  $\sigma$  is the interfacial tension,  $G$  is Gibbs free energy,  $A$  is the interface area,  $T$  is temperature,  $P$  is pressure and  $m$  is mass.

A positive interfacial tension ( $\sigma > 0$ ) indicates that the fluids are immiscible and their contact surface is minimized. When the interfacial tension is negative ( $\sigma < 0$ ), the fluids are miscible and dissolution will occur. At neutral IFT ( $\sigma \approx 0$ ), slow diffusion will lead to complete mixing, and the fluids are “truly” miscible [4].

Natural reservoir fluids are usually immiscible, although miscibility may occur under certain conditions [4]. Figure 2.6 illustrates the interfacial tension between the immiscible fluids water and oil. It shows how the motion of molecules at the interface is much more limited than in the bulk of the two fluids.

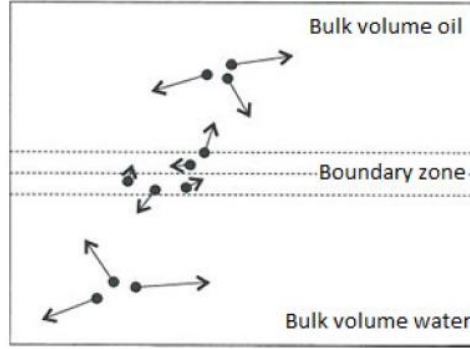


Figure 2 6: Motion of molecules within the immiscible phases oil and water [4].

In the coreflood experiment analyzed in this thesis, the interfacial tension between oil and water was reduced by injecting surfactants. Further description of surfactant flooding is presented in section 3.2.

### 2.2.6 Capillary pressure

Capillary pressure ( $P_c$ ) is defined as the molecular pressure difference across the interface between two immiscible fluids [4]. It is a result of both the internal and external electrostatic forces acting upon the fluids. The capillary pressure is defined by the Laplace equation, which for a water wet system is given as:

$$P_c = P_{non-wetting} - P_{wetting} = P_o - P_w \quad (2.16)$$

For fluid flow in porous mediums, pore channels are treated as capillary tubes. The capillary pressure for flow in tubes is defined by the Young-Laplace equation:

$$P_c = \frac{2\sigma_{ow}\cos\theta}{r} \quad (2.17)$$

Where  $\sigma_{ow}$  is the interfacial tension between oil and water,  $\theta$  is the wetting angle and  $r$  is the pore channel radius.

As can be seen from the parameters in equation 2.17, the capillary pressure is a function of the wettability of the system, pore size distribution, and the interfacial tension between the present fluids [4]. It also depends on saturation history due to the effects of hysteresis [8].

### 2.2.7 Drainage and imbibition

Drainage is the flow process in which the non-wetting fluid displaces the wetting fluid, causing a decrease in the wetting phase saturation. Imbibition is the opposite process, where the wetting fluid displaces the non-wetting fluid, increasing the wetting phase saturation [4]. Figure 2.7 shows typical relative permeability curves for drainage and imbibition in a water wet system.

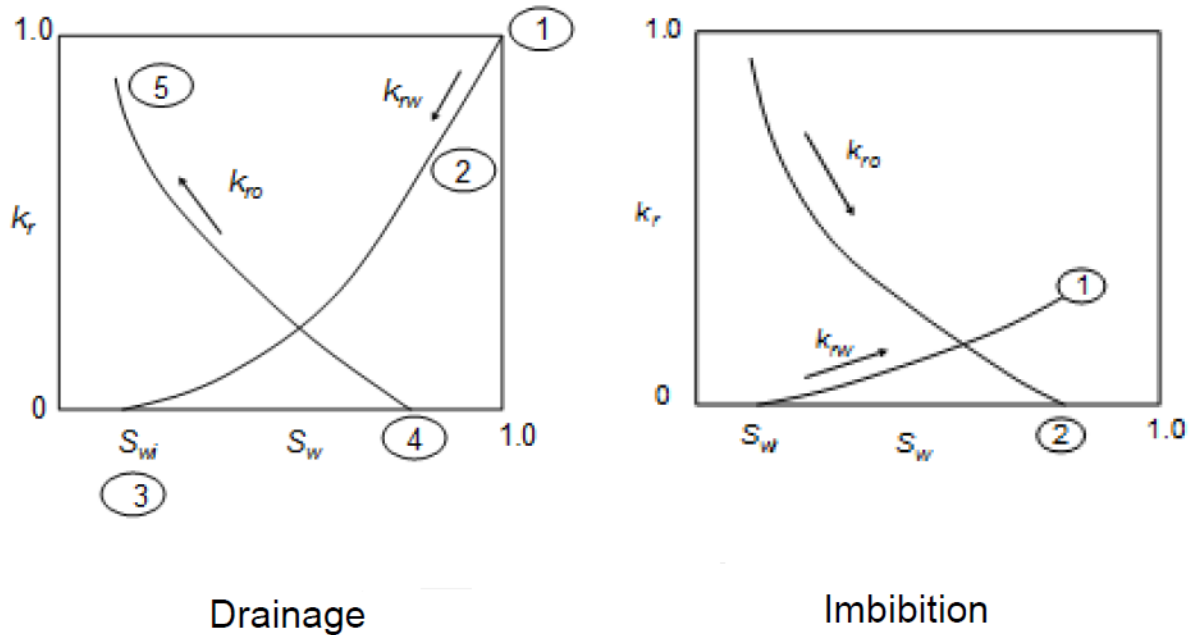


Figure 2.7: Relative permeability curves for drainage and imbibition in water wet system [3]

The pore filling sequence during drainage and imbibition processes are directly related to the capillary pressure. As can be seen from equation 2.17, the largest capillary pressure is found in the pores with the smallest radius. When water is injected into a water wet reservoir, the smaller pores with higher capillary pressure will be filled first due to the “water-loving” nature of the rock. As the pressure in the water phase is increased, pores of increasing radii will be filled. When water is injected into an oil-wet reservoir, the larger pores with lower capillary pressure will be filled first. This is due to the rock being “oil-loving”, meaning that the water phase have to overcome a threshold pressure in order to displace the oil from the pore space. By increasing the water phase pressure, pores of decreasing radii will be filled [4].

## 2.2.8 Capillary number and capillary desaturation curves (CDC)

The capillary number is as a dimensionless number expressing the ratio between the viscous and the capillary forces in a waterflooding process [3] . By applying Darcy's law, the capillary number is given by:

$$N_{vc} = \frac{u_w \cdot \mu_w}{\sigma_{ow}} \quad (2.18)$$

Where  $u_w$  is the Darcy velocity of the injected water,  $\mu_w$  is the water viscosity and  $\sigma_{ow}$  is the interfacial tension between oil and water.

Experimental studies have shown that there is a relationship between the capillary number and the residual oil saturation [2, 4, 9, 10]. This relationship is illustrated a capillary desaturation curve (CSD):

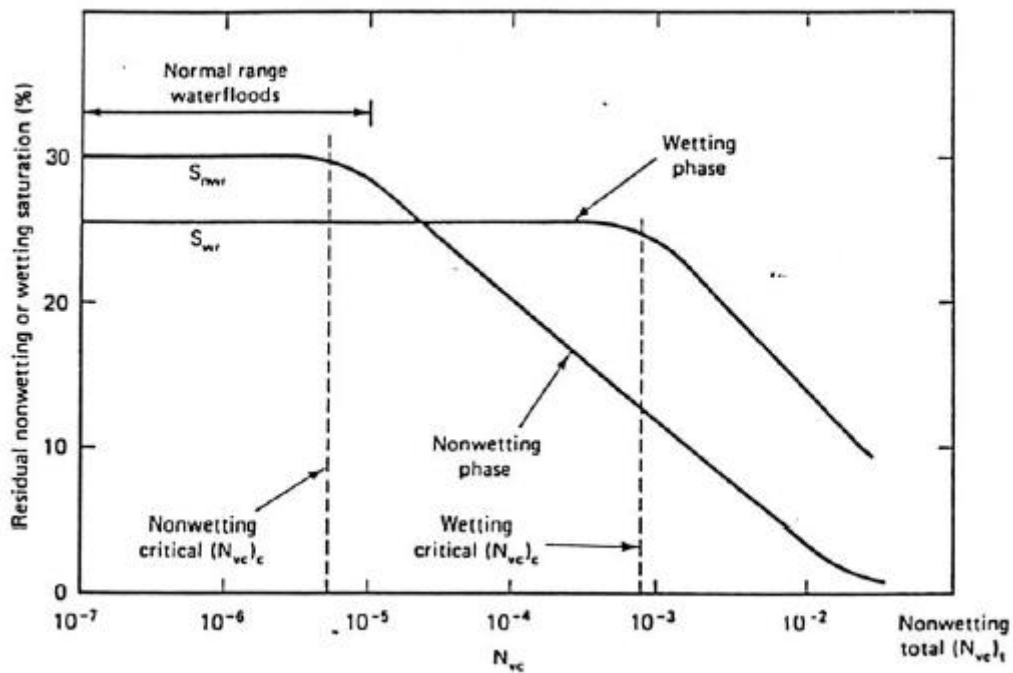


Figure 2 8: Example of a typical capillary desaturation curve (CDC) [3].

At low capillary numbers, the residual oil saturation remains constant for both the non-wetting and the wetting phase. When  $N_{vc}$  is increased to a critical value, the residual oil saturations will begin to decrease. As can be seen from the figure above, the wetting phase has a higher critical capillary number than the non-wetting phase.

In order to reduce the residual oil saturation after waterflooding, a high capillary number is required. As can be seen from equation 2.18, the capillary number can be increased by either increasing the velocity of the injected water, increasing the water viscosity, or reducing the interfacial tension between oil and water.

In practice, increasing the velocity of the injected water is not an option due to pressure limitations. The water viscosity could be increased by adding polymers to the water, however this would result in injectivity issues. Therefore, the most viable option for lowering  $S_{orw}$  is to reduce the interfacial tension between oil and water. This can be done by adding surfactants to the injection water [3].

In the coreflooding experiment simulated in this thesis, a slug of low salinity surfactant solution was injected to mobilize residual oil. In the modelling of this process, interpolation between high salinity and low salinity surfactant curves were based on the logarithm of the capillary number. Evaluation of the capillary number was therefore important in order to obtain a best match.

### 2.2.9 Wettability

The wettability of a rock is defined as the tendency of one fluid to spread on the rock surface when another immiscible fluid is present [4]. Experimental studies have shown that wettability conditions play a significant role in oil displacement [3].

There are several methods of estimating rock wettability. One examples is to measure the contact angle between the liquid-liquid or liquid-gas interface and the solid surface. This is called the wetting angle, which is defined by the Young-Dupré equation [4]:

$$\cos \theta = \frac{\sigma_{os} - \sigma_{ws}}{\sigma_{ow}} \quad (2.19)$$

Where  $\theta$  is the wetting angle and  $\sigma$  is the interfacial tension between the phases.

Figure 2.9 illustrates the measuring of wetting angles in an oil-water systems. In table 2.1, different wettability classes and their corresponding wetting angles are listed.

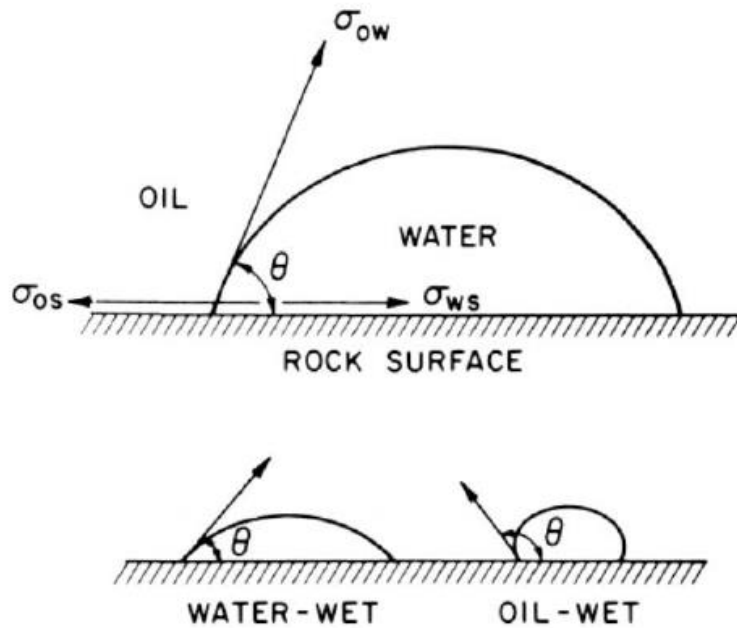


Figure 2 9: Measuring of the wetting angle in oil-water system [11].

Table 2 1: Wettability classes for an oil-water system [4].

Wetting angle (°)	Wettability preference
0 – 30	Strongly water-wet
30 – 90	Weakly water-wet
90	Neutral wettability
90 – 150	Weakly oil-wet
150 – 180	Strongly oil-wet

Skauge and Ottesen [63] presented a comprehensive study on the wettability of multiple North Sea cores, in which most reservoirs were found to have wettability within the intermediate region. In the history matching study presented in this thesis, an evaluation of the wettability of the studied core sample is presented. In the evaluation, the term intermediate wet is used to describe a wettability close to neutral wettability.

### 2.2.10 Effect of wettability on waterflooding and Sor

The wettability of a porous medium will strongly affect its waterflooding behaviour. This is due to wettability being a major factor in controlling the location, flow and distribution of fluids in the medium [12]. Figure 2.10 illustrates a waterflooding process in a water wet and an oil wet system.

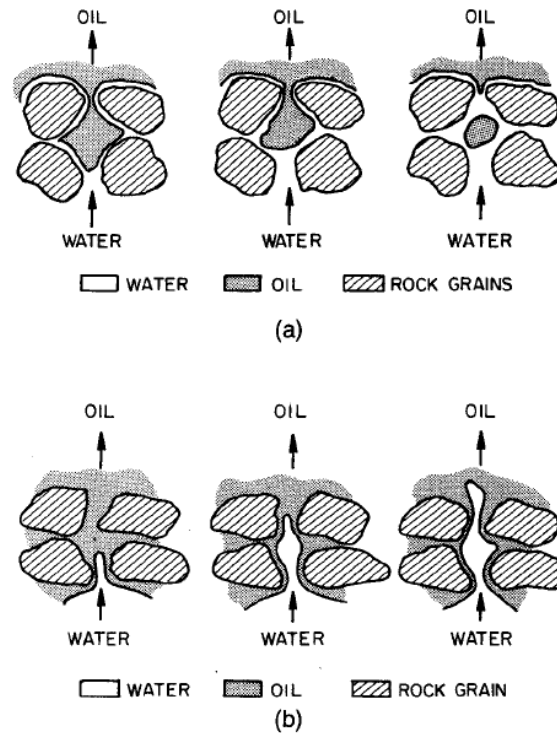


Figure 2 10: Illustration of waterflooding in a water-wet (a) and oil-wet (b) system.

In a water wet system, water will occupy the smaller pores and form thin films across the rock surface in the larger pores. When waterflooding, the injected water will enter the smallest pores first and push the oil into the larger pores where it is easily displaced. The water will move as a fairly uniform front, with only oil moving ahead of the front. When the water front has passed, almost all of the oil left in the pore space will remain as residual oil saturation. [12].

In an oil-wet system, the location of fluids is reversed from that in the water wet case. The injected water will enter the larger pores first and form continuous channels or fingers, displacing oil from the centre of the pores. As water injection continues, the water will enter smaller and smaller pores and form additional water channels. This will be accompanied by a gradual increase in the water oil ratio of the produced fluids. When water is no longer able to invade smaller pores, oil production falls to a very low level [12].

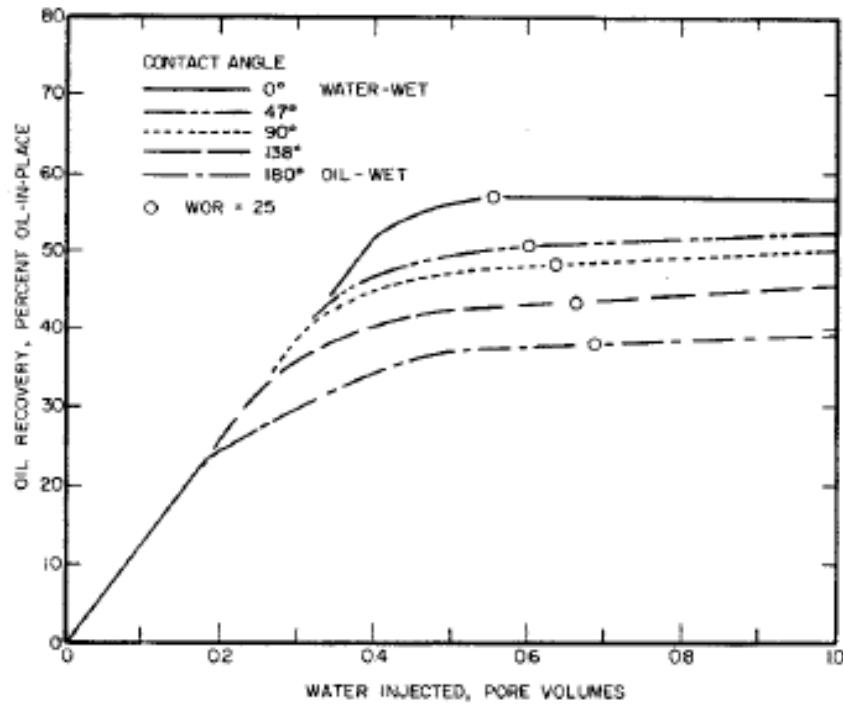


Figure 2.11: Oil recovery at different wettability conditions [12].

Figure 2.11 shows oil recovery curves for different wettability conditions ranging from completely water wet to completely oil wet. When transition from a strongly water wet system to a strongly oil wet system, earlier water breakthrough and longer tail production is observed. Waterflooding in strongly-water wet systems is highly efficient, as most of the oil is produced before breakthrough, and tail production is minimal. Waterflooding in strongly oil-wet systems are less efficient, due to the formation of water channels resulting in early water breakthrough and long tail production. For oil-wet systems, most of the oil is recovered after breakthrough [12].

Oil recovery in water-wet systems are essentially independent of the amount of water injected, due to most of the oil being produced before breakthrough. In oil wet systems however, where most of the production occurs after breakthrough, the recovery depends on the volume of water injected. As a result, more injected water is required to produce a given amount of oil in an oil-wet system compared to in a water-wet system.

### 2.2.11 Effect of wettability on relative permeability

As mentioned in section 2.1.3, relative permeability is a function of the saturations of the fluids present in the porous medium. The wettability of the medium is a major factor in controlling the location, flow and distribution of these fluids [12]. Therefore, wettability has a significant impact on the relative permeability of the medium.

In general, at any given saturation, the relative permeability of a fluid is higher when it is the non-wetting fluid. This is due to the location and distribution of the fluids in the pore space. The wetting fluids tends to travel through smaller, less permeable pores, while the non-wetting fluids flows easily through the centre of larger pores. In addition to this, snap-off at low non-wetting saturations causes trapping of non-wetting phase in the centre of larger pores. This hinders the flow of the wetting phase and reduces its relative permeability [13].

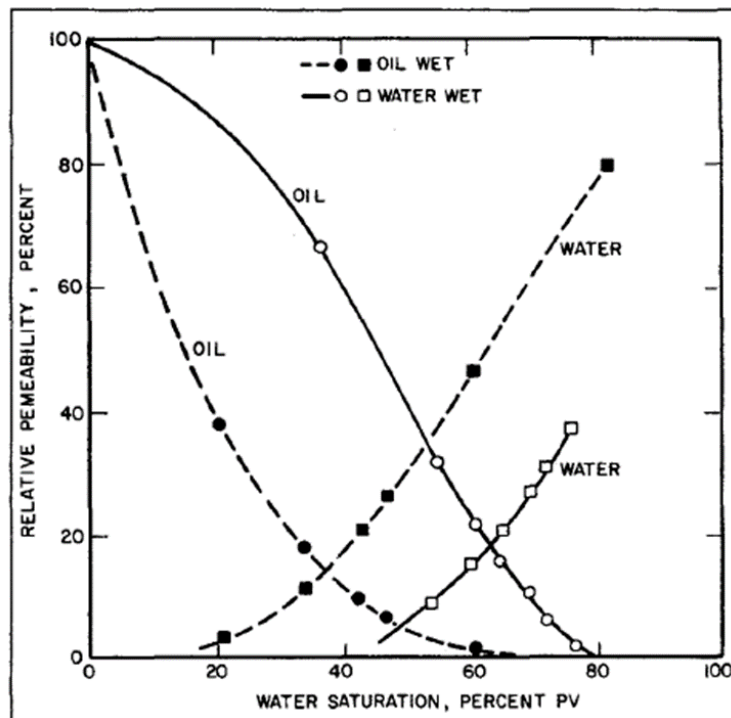


Figure 2.12: Oil/water relative permeability for both oil wet and water wet systems [13].

Figure 2.12 illustrates how relative permeability is affected by wettability conditions. For example, the relative permeability of water is lower in the water wet case than in the oil wet case. This is mainly due to residual oil blocking the flow of water in the centre of larger pores in water wet systems. Likewise, the relative permeability of oil is reduced in the oil-wet case compared to the water-wet case due to trapping of residual water [13].

According to Craig [14], the wettability conditions of a reservoir can be predicted from its relative permeability curves. This is done by looking at end-point relative permeabilities, residual saturations, and the crossover point between the relative permeability curves (Craig point). The following rules of thumb were suggested by Craig:

*Table 2 2: Craig’s rules of thumb for determining wettability [14].*

	<i>Water-wet</i>	<i>Oil-wet</i>
<i>Initial water saturation</i>	<i>Usually greater than 20 to 25% PV</i>	<i>Generally less than 15% PV</i>
<i>Saturation at which oil and water relative permeabilities are equal</i>	<i>Greater than 50% water saturation</i>	<i>Frequently less than 10%</i>
<i>Relative permeability to water at the maximum water saturation</i>	<i>Generally less than 30%</i>	<i>Greater than 50% and approaching 100%</i>

For the history matching presented in section 7, it was desirable to evaluate the wettability of the core at various stages. As the laboratory data from the experiment did not include any measurements directly related to wettability, the wetting conditions were predicted from relative permeability curves using Craig’s rules of thumb.

### 2.2.12 Wettability alteration

The wettability of a reservoir depends on the rock’s mineral composition, in addition to the composition of the reservoir fluids [4]. All reservoirs are thought to be strongly water wet initially, but as oil migrates into the pore space, wettability alteration may occur as a result of crude oil/brine/rock interactions (COBR). Buckley et al [15] presented four main categories of COBR interactions altering wettability. These include:

- Polar interactions due to absence of a water film between the oil and the solid
- Surface precipitation, which depends on the crude oil’s ability to act as a solvent for its asphaltenes.
- Acid/base interactions that control the surface charge at the interface between oil/water and solid/water.
- Ion binding or other specific interactions between higher valency ions and charged sites at the rock surface

### 3 Enhanced Oil Recovery

Due to the world's growing need for energy, the oil demand is higher than ever before. With oil reserves on decline, production optimization becomes increasingly important.

Oil recovery is usually separated into three phases; primary, secondary and tertiary recovery. Primary recovery is the recovery of oil by use of the natural energy in the reservoir, often referred to as pressure depletion. Secondary recovery is the injection of water or gas to act as pressure support and to displace oil towards the producer. Tertiary recovery is the implementation of Enhanced Oil Recovery (EOR) methods [3].

Enhanced Oil Recovery is by Lake [2] defined as “oil recovery by the injection of materials not normally present in the reservoir”. Such methods may be used when the recovery from secondary recovery is no longer sufficient. Examples of EOR methods include polymer flooding, surfactant flooding, and thermal methods [3].

The oil recovery factor is defined by:

$$E_R = E_D \cdot E_{vol} = \frac{\text{Volume oil displaced}}{\text{Volume oil contacted}} \cdot \frac{\text{Volume oil contacted}}{\text{Volume oil in place}} \quad (3.1)$$

Where  $E_R$  is the oil recovery factor,  $E_D$  is the microscopic displacement efficiency, and  $E_{vol}$  is the volumetric sweep efficiency.

The purpose of EOR is to increase the microscopic and volumetric displacement efficiencies to achieve a higher recovery factor [3].

The microscopic displacement efficiency can be increased by adding surfactants to the injection water. Surfactants mobilizes capillary trapped oil by reducing the interfacial tension between oil and water. As a result, a larger fraction of the oil contacted can be recovered.

The volumetric displacement efficiency can be increased by adding polymer to the injection water. The polymer increases the viscosity of the injected solution, allowing for a more favourable mobility ratio and better sweep efficiency during displacement. This results in more oil being contacted.

### 3.1 Low salinity waterflooding

Water injection has been used for decades to give pressure support to reservoirs and to displace oil towards producers. The potential benefits from waterflooding was first recognized in the 1880's, and field applications were initiated in the 1930's. Today, waterflooding is the most commonly used fluid injection process in the world [16].

The source of injection water has usually been chosen based on availability [3]. For offshore reservoirs, the obvious choice has been to inject seawater. For years, little consideration was made of the composition of the injected brine.

In recent years, there has been an increasing interest in the effects of low salinity waterflooding. Several studies indicate that the oil recovery is increased when the salinity of the injected brine is reduced. The underlying recovery mechanisms are not completely understood, but multiple theories have been suggested. In the following sections, laboratory and field studies on low salinity waterflooding will be presented.

#### 3.1.1 Laboratory studies

In a study from 1967, Bernard [17] investigated the effect of floodwater salinity on oil recovery from cores containing clays. The results showed that for salinities between 1-15 wt% NaCl, both oil recovery and differential pressure remained almost unaffected. For salinities below 1 wt% however, increased oil recovery was observed, accompanied by a pressure drop across the core. This tendency was observed in both secondary and tertiary mode.

Jadhunandan and Morrow [18] presented a study on the effect of wettability on waterflood recovery in Berea sandstone cores. A wide range of wetting conditions were generated and evaluated. An increase in oil recovery was observed when transitioning from strongly water wet conditions to close-to-neutral wettability. The highest recoveries were found at weakly water wet conditions. The parameters affecting the wettability were crude oil, brine composition, irreducible water saturation, and aging temperature.

Yildiz and Morrow [19] studied the effect of brine composition on recovery of Moutray crude oil. Two brines of different salt content were used in the experiments. The results showed that brine 2 yielded higher oil recoveries than brine 1. It was also observed that brine 2 had slower imbibition rates, indicating less water-wet conditions. This confirms the findings in

Jadhunandan and Morrow [18], which claimed that weakly water wet conditions are favourable for oil recovery.

Yildiz and Morrow [20] also presented a study on the effect of salinity on recovery of Prudhoe Bay crude oil. The brine compositions and core types were the same as in the previous study [19], however the results were the opposite. Brine 1 yielded 16% higher oil recovery than brine 2, and brine 1 was found to have less water-wet conditions. The conclusion was that the effect of salinity on oil recovery is highly dependent on the specific crude oil.

Tang and Morrow [21] studied the effect of brine composition on recovery by waterflooding and spontaneous imbibition. Three different crude oils were used, and brine salinity was varied by changing the salt concentration by factors of 0.01, 0.1 and 2. The results showed that oil recovery increased with decreasing salinity. In this case however, the higher oil recovery was found for more water-wet conditions. This is contradictory to what was found by Jadhunandan and Morrow [18] and Yildiz and Morrow [19] [20].

Tang and Morrow [22] also presented a study where they investigated the influence of salinity and fines migration on COBR interactions and oil recovery. To determine if fine particles affected the sensitivity of oil recovery to salinity, tests were done on Berea cores after fines had been stabilized by firing at 800 °C. The recovery from these cores were found to be independent of salinity. When comparing to results from unfired cores, it was concluded that fines migration play an important role in salinity sensitivity. Furthermore, the oil recovery from the three different sandstone types were compared. The sandstones with the lower clay content (Bentheim and Clashach) showed less increase in oil recovery for decreasing salinity compared to the clay-rich Berea sandstone. The authors also discovered the importance of an initial water saturation for salinity to affect oil recovery. In addition, the need for crude oil was confirmed, as the recovery of refined oil proved to be independent of salinity.

Sharma and Filico [23] performed centrifuge experiments to study the effect of brine salinity and crude-oil properties on oil recovery. In this study, oil recovery was increased significantly for lower connate brine salinities, while the salinity of the displacing brine did not have much impact. The salinity of the connate brine was proposed to be the primary factor controlling the oil recovery. This was attributed to a change in wettability from water wet towards more mixed wet conditions.

Zhang and Morrow [24] studied oil recovery with change in brine composition for both secondary and tertiary mode. Berea sandstones of varying permeability were used, along with

three different crude oils, two reservoir brines, and brine dilutions representing low salinity brines. By waterflooding the cores at different initial water saturations, oil recovery was found to increase with increasing  $S_{wi}$ . Also, for cases in which low salinity flooding increased production, the response was usually observed in both secondary and tertiary mode. The authors concluded that rock properties was the most significant factor behind the improved oil recovery from low salinity injection.

Shiran and Skauge [25] studied the effect of low salinity injection by performing waterflooding experiments on Berea and Bentheimer cores with different wettability conditions. The results showed no increase in oil production in water wet Bentheimer cores, and only limited increase in recovery for neutral-wet Berea and slightly oil-wet Bentheimer cores. In addition to this, no fines production, pH increase or pressure decrease was observed. This is contradictory to what was expected based on previous studies.

### 3.1.2 Field studies

Webb et al [26] performed a log-inject-log field test to study the effect of low salinity waterflooding within the near well region of a reservoir. The specific well used for testing was carefully selected to ensure the best possible conditions for controlling saturation changes in the near well area. Three different brine salinities were used; high, intermediate and low salinity. The results were in line with previous laboratory studies, showing a 25-50% reduction in residual oil saturation for low salinity waterflooding.

Skrettingland et al [27] presented a study on the potential of low salinity injection for increased oil recovery at the Snorre field. Coreflooding experiments were conducted, along with a single-well chemical tracer-test (SWCTT). The result showed little to no incremental recovery, indicating low potential for low salinity flooding. The conclusion was that the wettability conditions at Snorre already was close to optimal for seawater injection, and that the benefits from low salinity injection would be minimal.

Lager et al [28] reported of a successful injection of low salinity brine into an Alaskan reservoir. The observed effect was a significant drop in the water-oil ratio, accompanied by a doubling of the oil production rate within 12 months. The water chemistry of the produced brine followed a similar trend to that reported in previous studies.

Vledder et al [29] investigated the effectiveness of secondary low salinity flooding in the Omar field in Syria. Low salinity water from the Euphrates River was injected into the reservoir for a

period of almost 10 years. This resulted in a change in wettability from oil-wet to water-wet, and an incremental oil recovery of 10-15% of STOOIP.

Seecombe et al [30] performed a field test to evaluate the efficiency of low salinity waterflooding at inter-well distances. The test was implemented in the Endicott Field in Alaska, and involved an injector and a producer 1040 feet apart. After three months of low salinity injection, the water cut dropped from 95% to 92%. At the same time, breakthrough of low salinity water occurred. After injecting 1.3 PV, an incremental oil recovery of 10% was recorded for the area swept. This confirmed that low salinity waterflooding is applicable at inter-well distances.

### 3.1.3 Low salinity mechanisms

As mentioned in the previous sections, several mechanisms behind the effects of low salinity injection have been suggested. In this section, the most widely accepted mechanisms are presented.

#### 3.1.3.1 Wettability alteration

Wettability has a large effect on the waterflooding performance in a reservoir. Several studies report that the increased recovery from low salinity injection is accompanied by an alteration in wettability [12, 19, 21, 22, 26, 29]. The change in wettability is thought to be one of the main mechanisms behind the incremental production, with a shift towards both more water wet and more oil wet conditions reported to yield increased recovery.

The extent of wettability alteration depends on the stability of the water film between the oil phase and the rock surface. The stability of this film is determined by the disjoining pressure  $\Pi(h)$ . Skauge et al [31] defined the disjoining pressure as “the force acting between two interfaces separated by a thin film of thickness  $h$ ”. The three main factors affecting the disjoining pressure are electrostatic interactions, Van der Waal interactions, and hydration forces. A positive disjoining pressure will cause the interfaces to repel each other, making the water film more stable. A negative disjoining pressure causes the interfaces to attract each other and the film to become unstable. In terms of oil recovery, a destabilization of the water film will promote a wettability alteration towards more oil-wet conditions [8] [31].

In a study from 1998, Sharma and Filico [32] found that higher salinities caused water films to become more unstable, resulting in alteration towards more oil-wet conditions. However, two years later, Sharma and Filico [23] performed a similar study and experienced the opposite effect. This time, higher salinities resulted in more stable water films, promoting more water-wet conditions. This was attributed to changes in hydration forces, which became more repulsive at increasing salinity.

The studies of Sharma and Filico [23, 32] are examples of contrasting results when it comes wettability alteration during low salinity waterflooding. It shows the complexity of wettability and COBR interactions, and the mechanisms behind the increased recovery from low salinity injection.

### 3.1.3.2 Fines Migration

Tang and Morrow [22] studied the impact of clay content on salinity sensitivity during oil recovery. They discovered that the cores with the higher clay content had more incremental production. In addition, production of fine particles in the effluent was observed after low salinity waterflooding. The conclusion was that injection of low salinity water had caused stripping of mixed-wet fines from the rock surface, resulting in increased oil recovery and more water-wet conditions.

The forces determining the stripping of mixed-wet fines from the rock surface depend on a balance of mechanical and colloidal forces. Mechanical forces include capillary forces, resulting from adhesion of crude oil to the fines, and viscous forces, which tend to promote stripping. Colloidal forces is described by the DLVO theory, and depends on the balance between attractive Van der Waal forces and electrostatic repulsion due to overlap of electrical double layers [7, 22].

The electrical double layer is a structure of ions in a solvent that forms in the presence of a charged solid [7]. The thickness of the double layer decreases with ion valence and ion concentration. A decrease in the salinity of the injected brine would result in an expansion of the double layer, which promotes stripping of fine particles from the pore walls [22].

Tang and Morrow [22] proposed that the increase in oil recovery from fines migration could be due to either changes in wettability or diversion of flow. Since clay particles are naturally oil-wet, the stripping of these particles from the pore walls could result in an alteration towards

more water wet conditions, yielding increased recovery. Mobilization of fines could also cause blocking of pores channels. This could lead to sweeping of new pore space, resulting in increased oil recovery. The latter theory was supported by the fact that Tang and Morrow observed a reduction in permeability after injecting low salinity brine.

Some studies indicate that fines migration is not a necessity for increased recovery by low salinity injection. In a coreflooding study, Lager et al [33] reported of increased oil recovery at decreased salinity without any indication of fines migration or significant reduction in permeability. The same observations were made on the reservoir scale [28]. Increased recovery at decreased salinity has also been reported for carbonate cores [34], which are clay free.

#### 3.1.3.4 Multicomponent Ion Exchange (MIE)

Lager et al [33] performed chemical analyses of low salinity effluents from North Slope cores. The results showed a decrease in  $Mg^{2+}$  and  $Ca^{2+}$  concentration in the effluent compared to that of the injected solution. Similar observations had been made previously by Valocchi et al [35]. As a result, the authors suggested that multicomponent ion exchange was the main mechanism behind the low salinity effect.

On oil wet surfaces, multivalent cations at the clay surface will form bonds with polar compounds (resins, asphaltenes) in the oil phase. This leads to the formation of organo-metallic complexes, which promotes oil-wetness. In addition to this, organic polar compounds may also adsorb onto clay surfaces, increasing oil wetness even further [33].

According to the extended DLVO theory, several different mechanisms of organic matter adsorption onto clay minerals are possible. Four of these mechanisms are strongly affected by the cation exchange that occurs during injection of low salinity brine. These include; cation exchange, cation bridging, ligand bonding and water bridging [33].

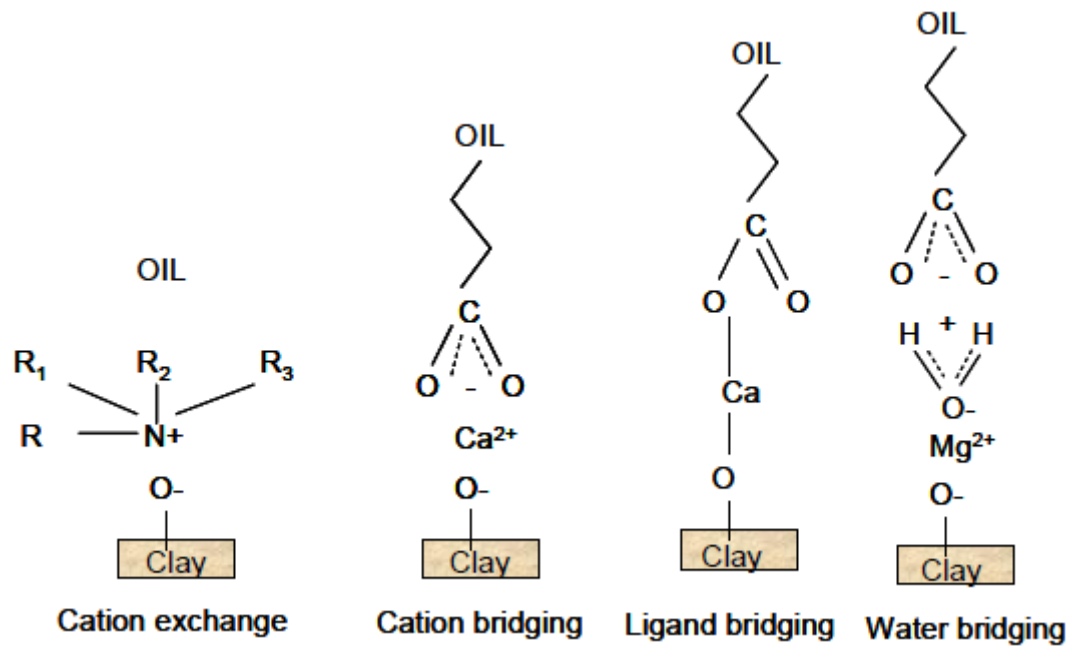


*Figure 3 1: Illustration of oil-wettability mechanisms [36]*

Cation exchange is the exchanging of molecules containing quaternized nitrogen or heterocyclic ring with metal cations bound to the clay surface. Cation bridging is a weak attraction mechanism between polar functional groups and cations on the clay surface. Ligand bonding is the direct bonding between a multivalent cation and a carboxylate group. Water bridging is the exchanging of cations which are strongly solvated ( $Mg^{2+}$ ) [33].

In order to further investigate the influence of MIE on oil recovery, Lager et al [33] performed coreflooding experiments where the multivalent ions  $Mg^{2+}$  and  $Ca^{2+}$  were replaced by  $Na^+$ . By doing so, the formation of organo-metallic complexes were prevented. The cores were subjected to a high salinity NaCl flood, followed by a low salinity NaCl flood. Finally, a tertiary flood of low salinity brine containing  $Mg^{2+}$  and  $Ca^{2+}$  was performed. The results were as expected, with high salinity flooding yielding higher recoveries due to no oil adsorption. The secondary and tertiary floods gave no incremental production due to the absence of organo-metallic complexes. On the basis of these results, the authors concluded that multicomponent ion exchange must be the primary mechanism behind the low salinity effect.

### 3.1.4 Modelling of low salinity waterflooding

Due to the increasing interest in low salinity waterflooding, multiple studies on modelling of the process has been presented. Some of these studies are described in this section.

Jerauld et al [37] presented a low salinity model used to represent both corefloods, single-well tests and field-scale simulations. The model was based on salinity dependent oil/water relative permeability functions resulting from wettability change. The study showed that the model was well suited to describe the benefits of low salinity injection. The relative permeability functions presented in the study has been used in several applications to model low salinity injection. They are given by:

$$k_{rw} = \theta k_{rw}^{HS}(S^*) + (1 - \theta)k_{rw}^{LS}(S^*) \quad (3.2)$$

$$k_{row} = \theta k_{row}^{HS}(S^*) + (1 - \theta)k_{row}^{LS}(S^*) \quad (3.3)$$

$$\theta = (S_{orw} - S_{orw}^{LS}) / (S_{orw}^{HS} - S_{orw}^{LS}) \quad (3.4)$$

$$S^* = (S_o - S_{orw}) / (1 - S_{wr} - S_{orw}) \quad (3.5)$$

Wu & Bai [38] created a general mathematical model for low salinity waterflooding in porous and fractures reservoirs. In this model, salt is treated as an aqueous component and is subject to adsorption onto rock solids. Relative permeability, capillary pressure and residual oil saturation all depend on salinity. According to the authors, the model is applicable to 1D, 2D and 3D simulations.

Omekeh et al [39] presented further development of a one-dimensional mathematical model for modelling of coreflooding experiments. The model describes how dissolution/precipitation of carbonate minerals and MIE affect the water/oil flow function. Using the model, pH and ion concentration from multiple corefloods were successfully history matched.

Dang et al [40] presented a comprehensive ion exchange model with geochemical processes coupled with the compositional simulator GEM from CMG. According to the authors, the model “captures the most important physical and chemical phenomena that occur in low salinity waterflooding, including intra-aqueous reactions, mineral dissolution/precipitation, ion exchange and wettability alteration”. The model was tested for several coreflooding experiments, with results showing excellent agreement for effluent ion concentration, effluent pH, and oil recovery.

## 3.2 Surfactant flooding

The purpose of surfactant flooding is to mobilize capillary trapped oil by reducing the interfacial tension between oil and water [3]. Mobilizing the residual oil increases the microscopic displacement efficiency ( $E_D$ ) and thus enhances oil recovery.

Several studies have indicated that there is a correlation between the residual oil saturation ( $S_{or}$ ) and the capillary number ( $N_{vc}$ ). This correlation is illustrated in a capillary desaturation curve (CDC), which can be seen in figure 2.8. The correlation suggests that by increasing the capillary number by several orders of magnitude, a lower residual oil saturation can be reached. This can be achieved by reducing the interfacial tension between oil and water through surfactant flooding.

### 3.2.1 Surfactants

Surfactants are amphiphilic compounds active at the interface between two immiscible fluids [3]. They consist of a hydrophilic (“water-loving”) head and a hydrophobic (“water hating”) tail. Due to limited solubility in both oil and water, surfactant molecules adsorb at the interface between the fluids and reduces the interfacial tension. Figure 3.2 shows an illustration of a surfactant molecule.

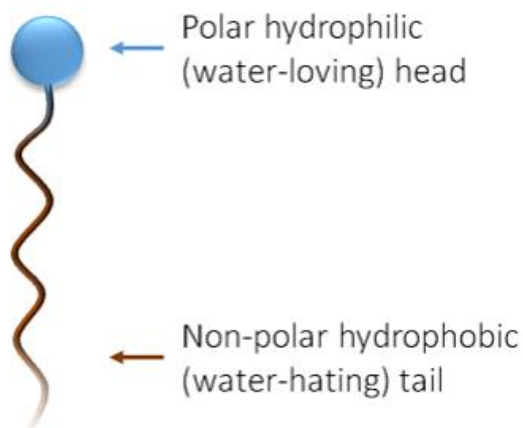


*Figure 3 2: Illustration of a surfactant molecule.*

Surfactants are classified into four main groups based on their polar moieties. These include; anionics, cationics, non-ionics and amphoteric.

Anionics	Cationics	Nonionics	Amphoterics
Sulfonates Sulfates Carboxylates Phosphates	Quaternary ammonium organics, pyridinium, imidazolinium, piperidinium, and sulfonium compounds	Alkyl-, Alkyl-aryl-, acyl-, acylamido-, acyl-aminepolyglycol, and polyol ethers Alkanolamides	Aminocarboxylic acids

Figure 3 3: Classification of surfactant molecules [2]

In this thesis, an anionic surfactant is used to model the low salinity surfactant flooding. Anionics are the most commonly used surfactants in oil recovery due to their ability to efficiently reduce IFT, and their resistance to retention. They are also chosen due to their stability and low cost [3].

When an anionic surfactants are dissolved in the aqueous phase, the molecules will dissociate into a cations ( $\text{Na}^+$ ) and anionic monomers. As the surfactant concentration increases, the monomers aggregate into micelles with hydrophilic heads outwards and hydrophobic tails inwards. At some critical value, further addition of surfactant will only increase the micelle concentration, not the monomer concentration. This value is called the *critical micelle concentration* (CMC) [3]

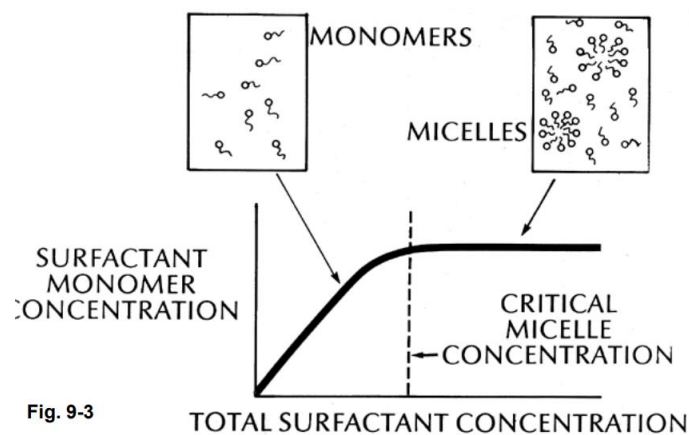


Fig. 9-3

Figure 3 4: Illustration of the critical micelle concentration (CMC) [3]

Due to the critical micelle concentration generally being very low, surfactants are predominantly in micelle form at all practical concentrations. Hence, all surfactant floods will be at concentrations above CMC [3].

### 3.2.2 Phase behavior

Brine salinity is reported to be the most important factor affecting the surfactant-oil-brine (SOB) behavior [4]. Depending on brine salinity, three different phase systems can be distinguished.

At low brine salinity, the surfactant usually shows good solubility in the aqueous phase and poor solubility in the oil phase. As a result, the overall composition near the interface is split into an excess oil phase containing pure oil, and an external micro emulsion phase containing brine, surfactant and some solubilized oil. This is called a type II(-) or Windsor type I system.

At high brine salinity, the electrostatic forces of the brine causes the surfactant to lose most of its solubility in the aqueous phase. The overall composition near the interface at these conditions consist of an excess water phase containing brine, and an external micro emulsion phase containing oil, surfactant and some solubilized brine. This is called a type II(+) or Windsor type II system.

At salinities between that of type II(-) and type II(+) systems, a third phase system is formed. An overall composition in the three phase region consist of both excess oil and excess brine phases, along with a micro emulsion phase. The micro emulsion phase contains two IFTs; between the excess oil and micro emulsion and between the micro emulsion and excess brine. This system is referred to as a type III or Windsor type III system.

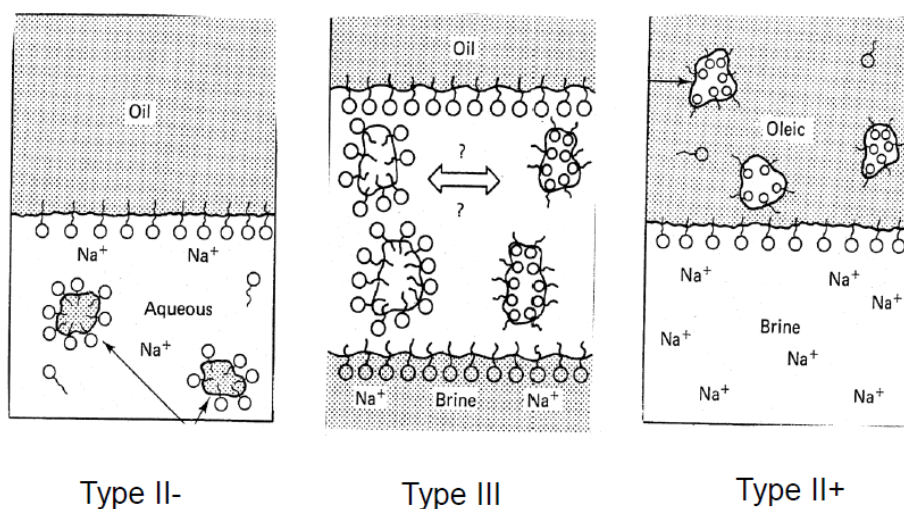


Figure 3 5: Illustration of surfactant – oil – brine (SOB) phase behavior systems [2].

Healy and Reed [41] proposed a relationship between brine salinity and interfacial tension, which was later confirmed experimentally by Huh [42]. It shows the lowest interfacial tension is found in salinities typical for type III systems. This is called the optimum salinity.

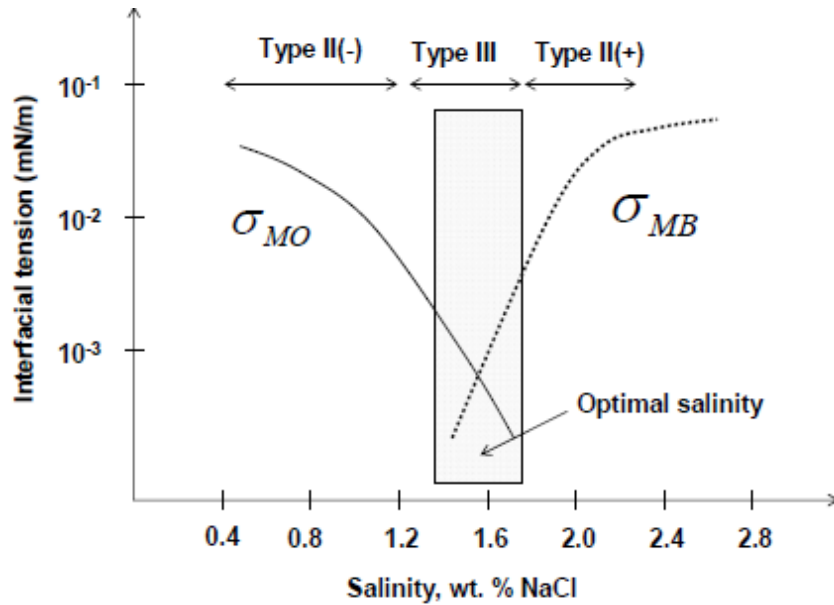


Figure 3 6: Relationship between interfacial tension and salinity [3].

Spildo et al [43] presented a systematic study of surfactant solubility, phase behavior, interfacial tension and retention as a function of salinity for a given surfactant solution. The study revealed that at optimum salinity (Windsor type III system), ultralow interfacial tensions were accompanied by turbidity in the aqueous solution, in addition to high retention values. On the other hand, a region in the Windsor type I area was found where interfacial tensions were low, the aqueous solution was clear, and retention was 10 times lower than at optimum salinity. As a result, a Windsor type I phase behavior was proposed to be the best option for surfactant flooding.

In the coreflooding experiment analyzed in this thesis, surfactant was injected in combination with low salinity water (5000 ppm). The salinity of the solution corresponds to a Windsor type I phase behavior, which makes it plausible that swollen micelles of oil may have formed in the surfactant solution, creating a micro emulsion phase. The laboratory data from the experiment did not include any information regarding micro emulsion viscosity, therefore this was treated as a history matching parameter during modelling.

### 3.2.3 Surfactant retention

Surfactant retention is a significant problem in field application as it reduces the concentration of surfactant in the solution. Retention of surfactant may occur due to adsorption, precipitation, ion exchange or phase trapping [3].

In the laboratory data of the studied experiment, no information on retention values were provided. The retention is however thought to be low, due to the surfactant solution corresponding to a Winsor type I system [43].

When modelling surfactant flooding in this thesis, adsorption was the only retention mechanism considered. Adsorption of surfactants happen when surfactant monomers adsorb to cationic surface sites [3]. Below the critical micelle concentration, the adsorption increases with surfactant concentration, while above CMC, the adsorption remains constant.

### 3.2.4 Laboratory studies on low salinity surfactant (LSS) injection

In this section, previous laboratory studies on the effect of combining low salinity water injection with surfactant flooding is presented.

Alagic & Skauge [44] investigated the effect of combining low salinity brine injection and surfactant flooding in mixed wet sandstone cores. The cores were first pre-flushed with either high or low salinity brine, before being flooded with low salinity surfactant brine in tertiary mode. The results showed a 30-33% increase in oil production when the cores were pre-flushed with low salinity water compared to when pre-flushed with high salinity water. This was attributed to the low salinity water altering the wettability towards more water-wet conditions. Also, divalent ions ( $Mg^{2+}$  and  $Ca^{2+}$ ) in the high salinity water made the subsequent surfactant flooding less effective due to extensive retention. The authors also noticed that the residual oil saturation was reduced by more than expected based on the capillary number increase. This was attributed to the destabilization of oil films due to changes in brine salinity, which in combination with oil mobilization from surfactants yielded a significant reduction in  $S_{or}$ .

Alagic et al [45] presented a study on the effect of crude oil ageing on low salinity and low salinity surfactant flooding. Four Berea cores were investigated, in which two were subjected to aging and two were of natural state. The results showed higher oil recovery from aged cores for both low salinity and low salinity surfactant injection. The authors suggested that this was

due to less water wet cores obtaining more unstable oil layers with larger degree of continuous oil.

Spildo et al [46] presented a study on low salinity waterflooding at reduced capillarity. The purpose was to explore to which extent capillary forces have to be reduced to take advantage of the incremental recovery obtained by low salinity surfactant flooding. Two Berea cores were investigated in the study, in which one was homogenous and one was heterogeneous. The cores were first flooded with high salinity water, before being injected with low salinity brine. Finally, a low salinity surfactant solution was injected at increasing surfactant concentrations. Both cores showed little response to low salinity waterflooding. The following low salinity surfactant flooding yielded higher incremental production than what was expected based on capillary number increase. It was proposed that COBR-interactions during the first low salinity injection had caused redistribution of oil, which may have promoted increased mobilization at reduced capillarity.

### **3.2.5 Modeling of low salinity surfactant (LSS) injection**

Skauge et al [47] presented a simulation study on combined low salinity brine and surfactant flooding. The two simulators UTCHEM and ECLIPSE were used to model the coreflooding experiments. The simulators represented different approaches to modelling, with UTCHEM using a salinity based wettability alteration model and ECLIPSE using a low salinity option model. However, both approaches modeled the incremental production as a result of a shift in relative permeability due to wettability alterations. Oil production and differential pressure from two Berea cores were history matched using both simulators. ECLIPSE was found to have a more flexible interpolation scheme, while UTCHEM could be more easily upscaled. Both models proved to be able to successfully represent laboratory coreflooding experiments.

### 3.3 Polymer flooding

Polymer flooding is an established EOR method in which polymers are added to the injection water to increase the water viscosity. The overall purpose is to achieve a more favorable mobility ratio and increase the volumetric displacement efficiency ( $E_{vol}$ ) [3].

From equation 2.18, it can be seen that an increase in water viscosity would yield a higher capillary number, which according to figure 2.8 could result in a lower residual oil saturation after waterflooding. However, in order to significantly affect  $S_{orw}$ , the capillary number would have to be increased by several orders of magnitude. The viscosity increase from adding polymers to the injection water is not sufficient to do this. Therefore, polymer floods are more to accelerate oil recovery than to enhance it [3].

Polymer flooding is favorable in reservoirs with high oil viscosities or large heterogeneities. It is also useful for near-well treatment to block high-permeable zones to gain better water-cut development [3].

#### 3.3.1 Polymers

Polymers are macromolecules consisting of long chains of monomers lined together by covalent bonds [4]. The types of polymers used for EOR purposes are either biopolymers or synthetic polymers.

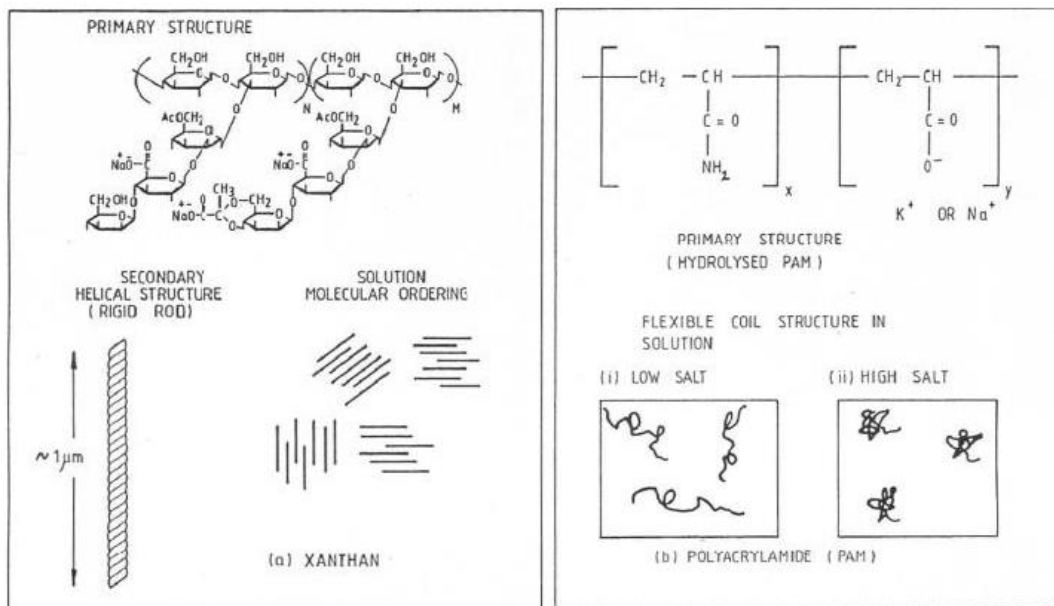


Figure 3.7: Structure and composition of Xanthan, PAM and HPAM [48]

Biopolymers are characterized by their low molecular weight and high viscosity, which is favorable for oil recovery. It also has a high tolerance to mechanical degradation and salt, in addition to being considered environmentally friendly. However, biopolymers are expensive, production capacity is limited, and it's tolerance to bacteria is low [3]. The most commonly used biopolymer in EOR is Xhantan, whose structure and composition can be seen in figure 3.7.

Synthetic polymers have high molecular weight and high viscosity. In contrast to biopolymers, they are relatively cheap, and production capacity is high. They are however susceptible to mechanical degradation, and tend to be unstable at high salinities. In addition to this, synthetic polymers are considered environmentally unfriendly. The most commonly used synthetic polymers for EOR purposes are polyacrylamide (PAM) and hydrolyzed polyacrylamide (HPAM) [3]. These are both described in figure 3.7. In the coreflood experiment analyzed in this thesis, the synthetic polymer HPAM3230S is used.

### 3.3.2 Viscosity of polymer solutions

Polymers are non-Newtonian fluids, which means that their viscosity is dependent on shear rate. The viscosity behavior of polymer solutions in a wide range of shear rates is best described by the Carreau model, which is illustrated in figure 3.8.

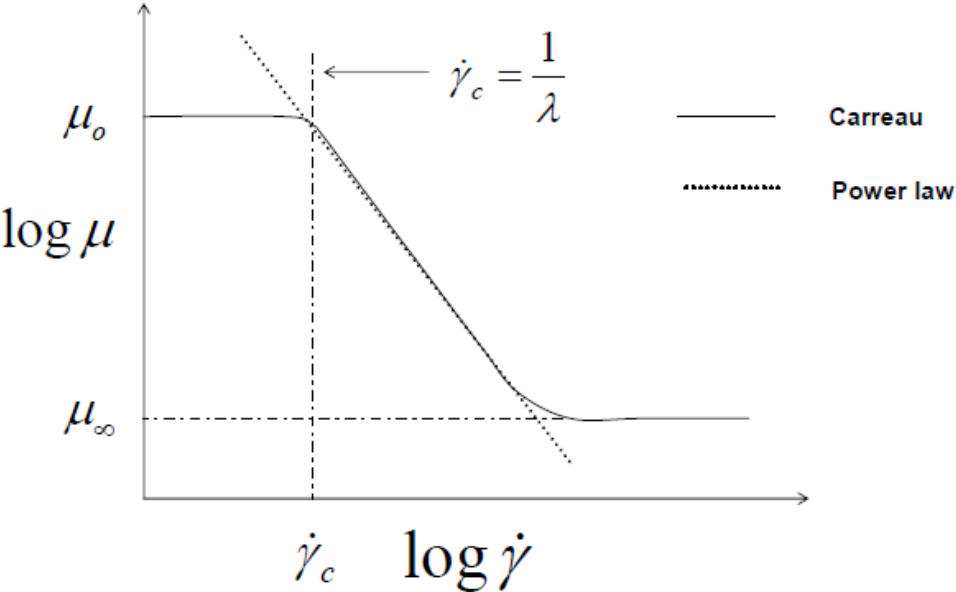


Figure 3 8: The Carreau model for viscosity behavior of polymer solutions [3].

Figure 3.8 shows a constant, Newtonian regime at low shear rates. This is due to the polymer macromolecules rotating at a constant angular velocity, hindering any conformation change. At increasing shear rates, the macromolecules start to deform and orient themselves in the flow direction. This causes a gradual reduction in the viscosity of the solution. At very high shear rates, the macromolecules are oriented in the flow direction and do not affect the viscosity. The regime is Newtonian again, but at a lower viscosity [4].

In the coreflood experiment modelled in this thesis, the low salinity polymer solution was injected at a constant rate of  $0.1 \text{ cm}^3/\text{min}$ . As a result, the shear interval during flooding was assumed to be constant. The viscosity of the polymer solution was therefore defined in the simulation model to be a function of polymer concentration only.

Another factor when evaluating viscosity behavior of polymer solutions is brine salinity. At high salinity concentrations, HPAM molecules tend to contract, which reduces the viscosity effect of the polymer solution. At lower salinities the molecules remain uncoiled and the viscosity of the solution remains unaffected [48]. In coreflooding experiment simulated in this thesis, the polymer is injected in combination with low salinity brine. As a result, it is assumed that coiling of polymer molecules did not affect the polymer viscosity significantly.

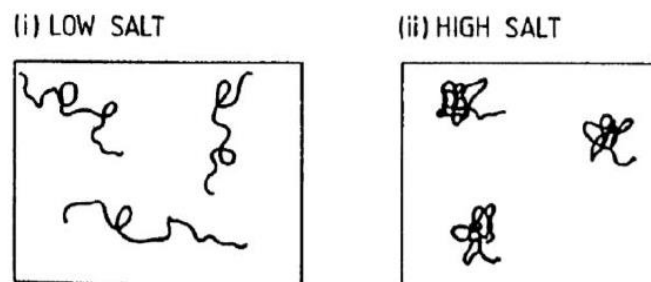


Figure 3 9: Effect of increasing salinity concentration on HPAM molecules [48].

### 3.3.3 Polymer retention and inaccessible pore volume (IPV)

Polymer retention is caused by adsorption, mechanical trapping, or precipitation of polymer molecules. It causes a loss in polymer concentration which reduces the viscosity of the solution. In addition, adsorbed polymer can block passageways and thus reduce the permeability of the porous medium [3].

Due to the large size of polymer molecules, smaller pores may not be invaded by polymer. The fraction of pore space which is not accessible for the polymer is called inaccessible pore volume (IPV). Due to IPV, the velocity of the polymer solution will be increased compared to that of a normal water flood [3].

In the simulation performed in this thesis, polymer is represented by the inclusion of adsorption and inaccessible pore volume in the simulation model.

### 3.3.4 Laboratory studies on low salinity polymer (LSP) injection

As mentioned, the viscosity behavior of polymer solutions is affected by the salinity of the polymer solution. Recently, several studies on the combined effect of low salinity water injection and polymer flooding have been conducted. Some of these are presented in this section.

Ayirala et al [49] compared the economic effects of combining polymer with low salinity water and with high salinity water. The results showed that the low salinity option was more beneficial. Using low salinity water significantly reduced the amount of chemicals needed to reach a target polymer solution viscosity. In fact, the polymer consumption was found to be 5-10 times lower when using low salinity water than when using high salinity water. The authors also found that the incremental desalination costs associated with low salinity waterflooding could be paid off in 1-4 years due to large savings in chemicals and polymer facilities costs. In addition, the added recovery effects of low salinity water injection combined with polymer flooding could result in incremental oil recovery.

Shiran and Skauge [50] presented a study on low salinity water injection and the added effect of polymer flooding. Secondary low salinity and high salinity waterfloods were followed by tertiary low salinity polymer floods in sandstone Berea Cores. The results showed that the recoveries from low salinity polymer flooding were higher in the cores that had first been flooded with low salinity water. This was attributed to the low salinity polymer flood being more stable in the cores with a low salinity environment at  $S_{wi}$ .

Vermolen et al [51] analyzed the recovery effects, associated risks, and economic benefits of using low salinity water for polymer flooding. The study showed that even when there were no incremental recovery it was still beneficial to use low salinity water since the required polymer concentration decreased by a factor of two to four compared to when using high salinity water. In addition, low salinity water allowed for the use of cheaper polymers that would not have been stable in high salinity water. The authors also highlighted that low salinity polymer flooding has lower sensitivity to mechanical shear, less production chemistry issues, and could result in incremental production due to the added recovery mechanisms of low salinity flooding.

In 2014, Rotondi et al [52] presented Eni's experience with low salinity waterflooding, which included the assessment of several different EOR techniques at field scale. Low salinity polymer flooding was identified as the most efficient and cost-effective process for viscous oil fields.

### **3.3.5 Modeling of low salinity polymer (LSP) flooding**

Mohammadi and Jerauld [53] presented a study on mechanistic modelling of combined low salinity water and polymer flooding. 1D simulations were conducted using the reservoir simulator VIP. The low salinity model used in the simulations was based on the model presented in Jerauld et al [37] (equations 3.2-5). The polymer model was similar to that used in early versions of the UTCHEM model, with the polymer viscosity being a function of polymer concentration, shear rate and salinity. Transport parameters such as adsorption, permeability reduction, cation exchange, and inaccessible pore volume were also considered. Relative permeability input was given for high and low salinity water only, not for the polymer solution. Additional 3D simulations were run using the chemical simulator STARS by CMG. The simulated results indicated that both secondary and tertiary low salinity polymer injections were effective, but secondary injections gave better timing of oil recovery.

## 4 CMG STARS – Reservoir Simulator

In this thesis, the reservoir simulator STARS by CMG (Computer Modelling Group) was used to simulate low salinity surfactant polymer (LSSP) flooding. STARS is a three-phase multi-component simulator used for modelling of recovery processes involving chemicals, steam, solvents, and air. The simulator is particularly suited for simulation of LSSP flooding due to its capabilities in managing flow, dispersion and chemical composition of floods [55].

To successfully run a simulation, STARS require an input data file where the most important parameters related to the reservoir, fluids, and recovery processes are defined. When the simulation is run, STARS uses the initial data set to create three new files; a text output file, SR2 index file (IRF), and a SR2 main file (MRF) [55]. This process is illustrated in figure 4.1.

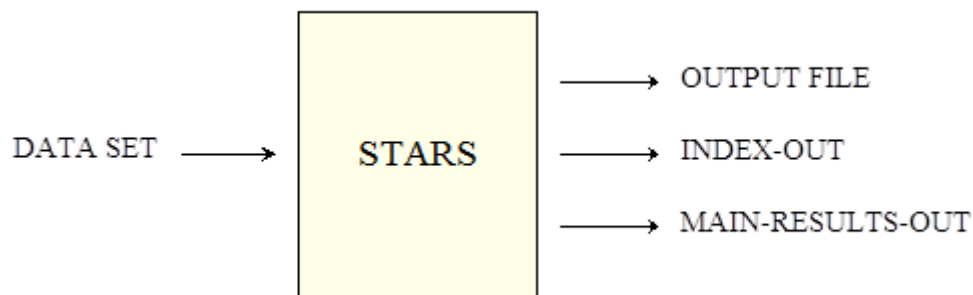


*Figure 4 1: Overview of data files in STARS simulation [55].*

When the simulation run is completed, the results are ready for analysis using the features “Results Graph” and “Results 3D”. “Results Graph” enables plotting of various well data as a function of time, in addition to plotting of special history parameters defined in the input data set. In “Results 3D” the reservoir simulation grid can be viewed in 3D and 2D, and grid properties can be displayed for any output time. It also allows for analysis of properties at individual grid blocks [56].

## 4.1 Relative permeability interpolation

When modelling low salinity waterflooding in this thesis, it was assumed that the injection of low salinity water caused a wettability alteration, which resulted in a change in relative permeability. This was represented in the simulation model by assigning two separate sets of relative permeability curves for high salinity (synthetic seawater) and low salinity water.

Interpolation between high salinity and low salinity relative permeability curves were based on salinity concentration. To activate the interpolation, an interpolation parameter had to be defined through the keyword `INTCOMP`. In this thesis, sodium ( $\text{Na}^+$ ) and chloride ( $\text{Cl}^-$ ) were modelled as individual components in the aqueous phase.  $\text{Na}^+$  was chosen as the interpolation parameter, which meant that the relative permeability interpolation was based on  $\text{Na}^+$  concentration in the water phase. For interpolation to occur, water phase interpolation parameter values had to be defined through the keyword `DTRAPW`. This corresponded to the mole fraction of  $\text{Na}^+$  for the given solution [55].

For the surfactant flooding process, interfacial tension was implemented in the model through the keyword `IFTTABLE`. This is a table consisting of surfactant concentration and its corresponding interfacial tensions. When an `IFTTABLE` is present, the interpolation parameter values defined in `DTRAPW` corresponds to the logarithm of the capillary number [55].

$$DTRAPW = \log_{10}(N_C) \quad (4.1)$$

This meant that the interpolation of relative permeability during surfactant flooding was based on capillary number rather than  $\text{Na}^+$  concentration. The capillary number is in STARS calculated by substituting the Darcy velocity [55]:

$$N_C = \frac{K \cdot \Delta P}{\sigma \cdot \Delta x} \quad (4.2)$$

To calculate relative permeability of water and oil in STARS, relative permeability functions analogous to those presented by Jerauld et al [37] (equations 3.2 – 3.5) are used:

$$k_{rw} = k_{rwA} \cdot (1 - wtr) + k_{rwB} \cdot wtr \quad (4.3)$$

$$k_{ro} = k_{roA} \cdot (1 - oil) + k_{roB} \cdot oil \quad (4.4)$$

*A* and *B* denote rock fluids sets A and B, while *wtr* and *oil* is defined by:

$$wtr = ratw^{WCRV} \quad (4.5)$$

$$oil = ratn^{OCRv} \quad (4.6)$$

$ratw$  and  $ratn$  are normalized current values of dimensionless interpolation parameters, and these are set to a value of 1 for salinity based interpolation [55]. For capillary based interpolation, they are defined by:

$$ratw = \frac{\log_{10}(N_c) - DTRAPWA}{DTRAPWB - DTRAPWA} \quad (4.7)$$

$$ratn = \frac{\log_{10}(N_c) - DTRAPNA}{DTRAPNB - DTRAPNA} \quad (4.8)$$

## 4.2 Dispersion

In STARS, the keywords \*DISPI\*/DISPJ/DISPK are used to define the total dispersion coefficient in all three dimensions for the desired component and phase. The total dispersion includes both effective molecular diffusion and mechanical dispersion. The effective molecular diffusion depends on component and phase, while the mechanical dispersion is a result of rock properties [55]. The total dispersive flux of component  $i$  in phase  $j$  in direction  $k$  is defined by:

$$J_{ijk} = -D_{ijk} \nabla_k (\rho_j x_{i,j}) \quad (4.9)$$

Where  $D_{ijk}$  is the total dispersion coefficient of component  $i$  in phase  $j$  in direction  $k$ , and  $\nabla_{ijk}$  is the concentration gradient of component  $i$  in phase  $j$  in direction  $k$ .

### 4.3 Adsorption

When modelling surfactant and polymer flooding, adsorption of components onto the rock surface must be considered. In STARS, adsorption can be defined either in tabular form or in terms of the Langmuir isotherm correlation [55]. In this thesis, the latter option was chosen. The Langmuir adsorption isotherm gives the adsorbed moles of the chosen component per unit pore volume as:

$$ad = \frac{(tad1 + tad2 \cdot xnacl) \cdot ca}{(1 + tad3 \cdot ca)} \quad (4.10)$$

Where  $xnacl$  is the salinity of the brine,  $ca$  is the mole fraction of the chosen component, and  $tad1$ ,  $tad2$  and  $tad3$  are the Langmuir isotherm coefficients.

Adsorption is included in the model through the keywords ADSCOMP, ADSLANG, ADMAXT, and ADRT. ADSCOMP defines the component and phase for which adsorption is activated. ADSLANG denotes that composition dependence is specified via Langmuir isotherm coefficients. ADMAXT specifies the maximum adsorption capacity, given in  $\text{gmol}/\text{cm}^3$ . ADRT defines the residual adsorption level, where  $ADRT = ADTMAXT$  represents completely irreversible adsorption and  $ADRT = 0$  represents completely reversible adsorption [55].

## 4.4 Multiple interpolation

In the coreflood modelled in this thesis, slug injections of low salinity surfactant and polymer was conducted. Figure 4.2 shows the concentration in block 50 for the simulation yielding the best match in section 7.

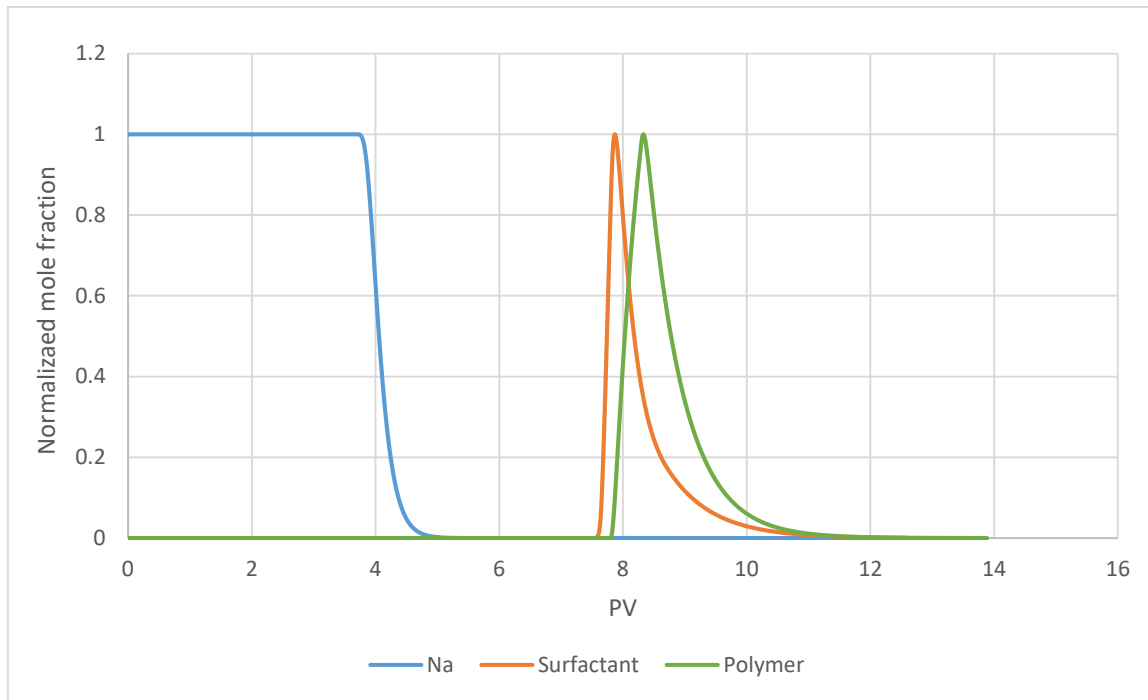


*Figure 4 2: Normalized mole fractions of components in block 50,1,1.*

The concentration profile shows that both surfactant and polymer is present in the core at the same time. This is due to the polymer slug being injected directly after the surfactant slug, which means that the surfactant concentration has not yet reached zero when the polymer is injected. Such cases presents certain challenges when it comes to modelling. Due to the presence of several solutions with different flow characteristic, interpolation between multiple relative permeability curves is required in the model.

When modelling LSSP floods, it is desirable to represent both the low salinity water, surfactant, and polymer solution with its own set of relative permeability curves. Previous studies have at UniResearch CIPR have found this to be challenging when using STARS. In a thesis from 2015, Drønen [57] concluded that STARS was not able to properly model LSSP floods using three interpolation routines. However, good results were achieved with two interpolation routines. Multiple interpolation setups were attempted for the history matching in this thesis, however, in the end, a similar model to that of Drønen was utilized.

#### 4.4.1 Multiple interpolation scheme – core R14

In this section, a detailed description of the interpolation setup used to history match the coreflooding of core R14 is presented. The setup is adopted from the setups used in the previous studies presented in section 5. An overview of the interpolation setup can be seen in figure 4.3.

```
** Rock type 1 - Surfactant curves

RPT 1 WATWET

INTCOMP 'SURF' WATER
IFTTABLE

KRINTRP 1      }
DTRAPW -12.5   } Synthetic seawater,
SWT             } no surfactant

KRINTRP 2      }
DTRAPW -9.5    } Low salinity water,
SWT             } max surfactant

** Rock type 2 - Salinity curves

RPT 2 WATWET

RPT_INTRP      }
COMP 'Na' WATER }
LOWER_BOUND 0.00155 }
UPPER_BOUND 0.00885 } Allows for interpolation
UPPERB_RPT 1      } between rock type 1 and 2

INTCOMP 'Na' WATER

KRINTRP 1      }
DTRAPW 0.00885 } Synthetic seawater,
SWT             } no surfactant

KRINTRP 2      }
DTRAPW 0.00155 } Low salinity water,
SWT             } no surfactant

KRTYPE CON 2
```

Figure 4 3: Interpolation setup used in history matching of core R14.

The experimental coreflooding of core R14 started with an initial synthetic seawater (SSW) injection, followed by injections of low salinity water (LS), low salinity surfactant (LSS), low salinity polymer (LSP), and then chase water.

The first three injection sequences (SSW, LS and LSS) were modelled by including two different interpolation routines containing two separate sets of relative permeability curves. The fourth sequence (LSP) was modelled as a viscosity effect only.

The implementation of two interpolation routines required the definition of two separate rock types, specified by keywords RPT1 and RPT2. Rock type 1 was defined for interpolation purposes only, as this was an requirement for interpolation between rock types in STARS [55]. By using this setup, interpolation was based on salinity concentration between SSW and LS in rock type 2, and on logarithm of capillary number in rock type 1. Logically, the relative permeability curves should have followed the same order as the injection sequences, meaning that rock type 1 should have contained the salinity curves, and rock type 2 should have contained the surfactant curves. However, this was found to not work properly.

In order for interpolation between rock type 1 and 2 to occur, the section directly after RPT 2 WATWET in figure 4.3 had to be included. Interpolation between rock types is activated through the keyword RPT\_INTRP. COMP defines the interpolation parameter and the phase of the parameter. LOWER\_BOUND specifies the lower bound of the interpolation parameter, while UPPER\_BOUND specifies the upper bound. UPPERB\_RPT specifies the rock type number which is used as the upper bound for the interpolation between the rock types.

Two relative permeability sets are highlighted for each rock type in figure 4.3. For each set, KRINTRP specifies the interpolation set number, local to the current rock type. DTRAPW denotes the value of the water phase interpolation parameter. In this case, the interpolation parameter is mole fraction of 'Na' in rock type 2, and  $\log_{10}(N_{vc})$  for rock type 1. SWT defines the water-oil relative permeability table for the interpolation set.

The keyword KRATYPE assigns a rock type number to each grid block. In this case, rock type 2 was assigned to the grid blocks, while rock type 1 was for interpolation purposes only.

## 5 Previous Studies at UniResearch CIPR

Several experimental studies on low salinity surfactant polymer (LSSP) flooding have been conducted at UniResearch CIPR. Some of these experiments have also been subjected to modelling. In this section, a selection of simulation studies where LSSP floods have been modelled are presented. These studies have been used as a basis for the simulation work in this thesis.

### 5.1 Simulation study of core R3 and R4 by Drønen

In a master thesis from 2015, Drønen [57] presented a simulation study on modelling of low salinity waterflooding and hybrid EOR methods in multiple Berea outcrop sandstone cores. From the cores studied, cores R3 and R4 were subjected to LSSP flooding, and the results from these are presented in this section.

R3 and R4 are Berea outcrop sandstone cores, originating from the same Berea outcrop as core R14 studied in this thesis. Coreflooding experiments were performed on the cores at UniResearch CIPR's laboratories in 2013. The purpose of the experiments were to study the effect of combined low salinity surfactant and low salinity polymer slug injections on oil recovery.

The cores were first flooded with synthetic seawater (SSW), before an  $S_{wi}$  was obtained by draining the cores with highly viscous Marcol 152 oil. Next, the Marcol 152 was replaced by Heidrun crude oil before the cores were placed in core holders for aging. After aging, the cores were reaged with Total crude oil. Next,  $k_o(S_{wi})$  was measured by draining the cores with Brage crude oil, before aging again at high temperatures.

After extensive aging, coreflooding experiments were initiated. Similar flooding sequences were run for both cores, starting with an initial synthetic seawater (SSW) injection, followed by injection of low salinity water (LS), low salinity surfactant (LSS), low salinity polymer (LSP), and chase water in the end. A more detailed overview of the flooding sequences can be seen in figure 5.1.

	Core R3	Core R4
Initial Conditions	$S_{wi(SSW)}$ $S_{oi}$	$S_{wi(SSW)}$ $S_{oi}$
Step 1	36000 ppm SSW 2.1 PV	36000 ppm SSW 2.3 PV
	↓	↓
Step 2	5000 ppm NaCl 1 PV	4500 ppm NaCl 1 PV
	↓	↓
Step 3	5000 ppm NaCl 10 000 ppm Surf 0.5 PV	4500 ppm NaCl 10 000 ppm Surf 0.5 PV
	↓	↓
Step 4	5000 ppm NaCl 1500 ppm Poly 0.5 PV	4500 ppm NaCl 1500 ppm Poly 0.5 PV
	↓	↓
Step 5	5000 ppm NaCl 2.3 PV	4500 ppm NaCl 8 PV

Figure 5 1: Summary of coreflooding sequences of core R3 and R4 [57].

Initial SSW injection yielded a recovery of 68% for both core R3 and R4. The following LS injection showed a moderate increase in recovery from 68% to 72% for R3, while no incremental production was observed for R4. The final recovery after LSS, LSP and second LS injection was 88% for core R3 and 97.5% for core R4. The oil recovery and water cut curves for all flooding sequences can be seen figure 5.2 and 5.3.

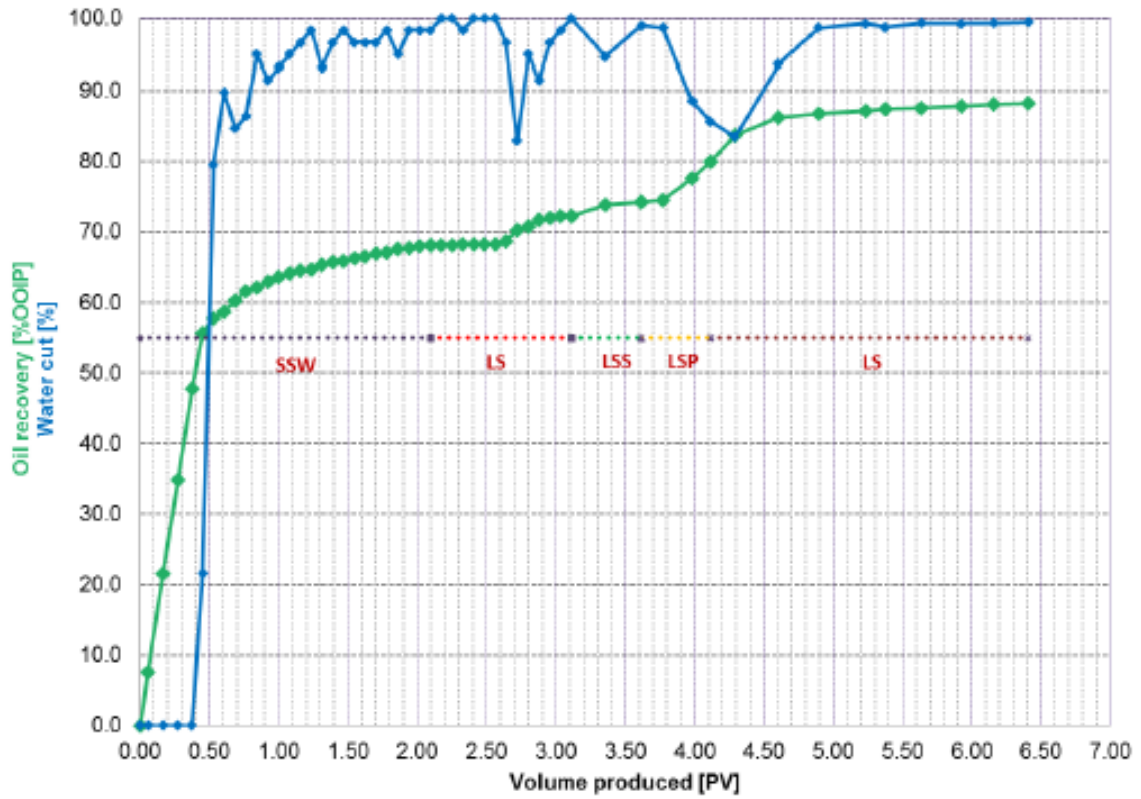


Figure 5 2: Oil recovery and water cut during LSSP flooding of core R3 [57].

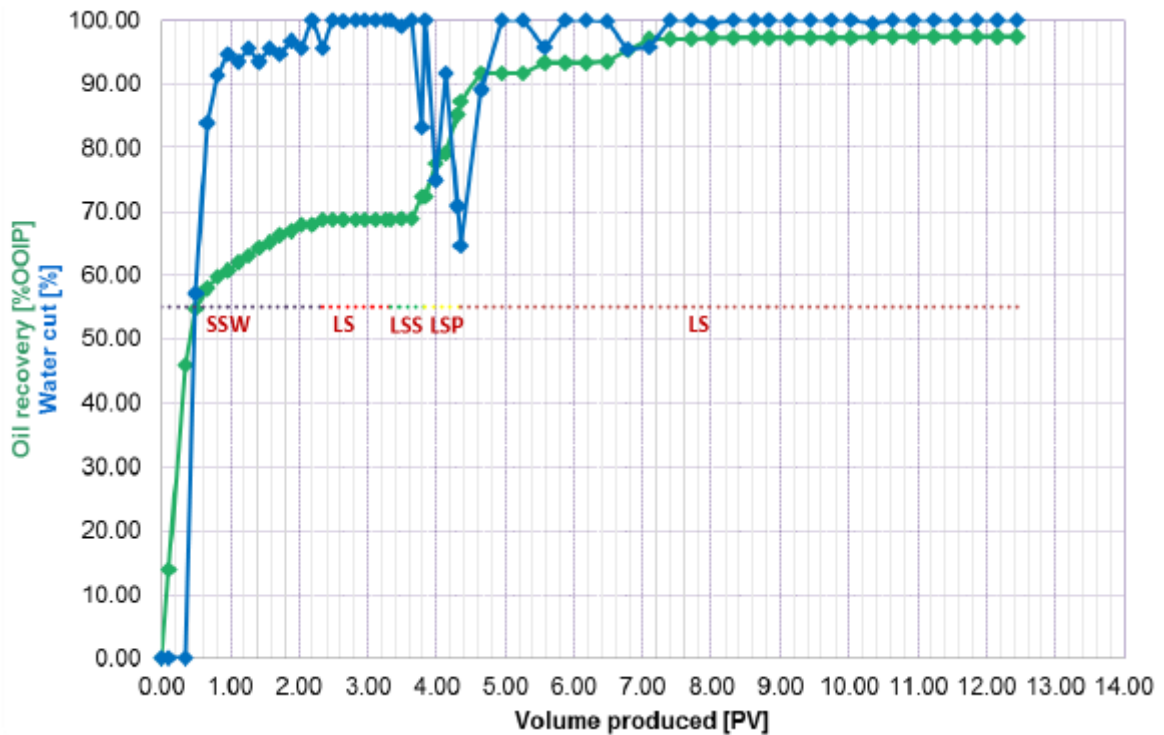


Figure 5 3: Oil recovery and water cut during LSSP flooding of core R4 [57].

In order to history match the flooding sequences of cores R3 and R4, Drønen built a simulation model based on the petrophysical data from the coreflooding experiments. The interpolation setup was similar to that used in the history matching in this thesis. SSW, LS, and LSS floods were modelled by including two interpolation routines in two separate rock types. The LSP flood was modelled as a viscosity effect only. An overview of the setup can be seen in figure 5.4.

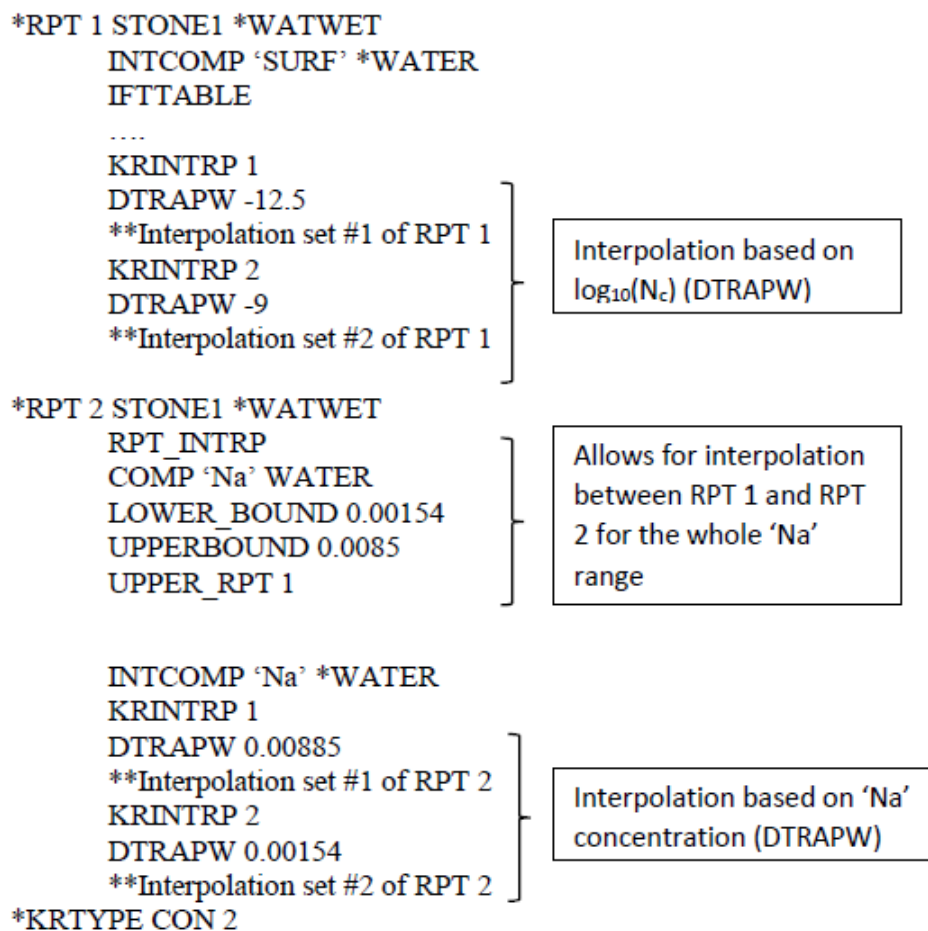


Figure 5 4: Interpolation setup in Drønen's modelling of flooding sequences in R3 and R4.

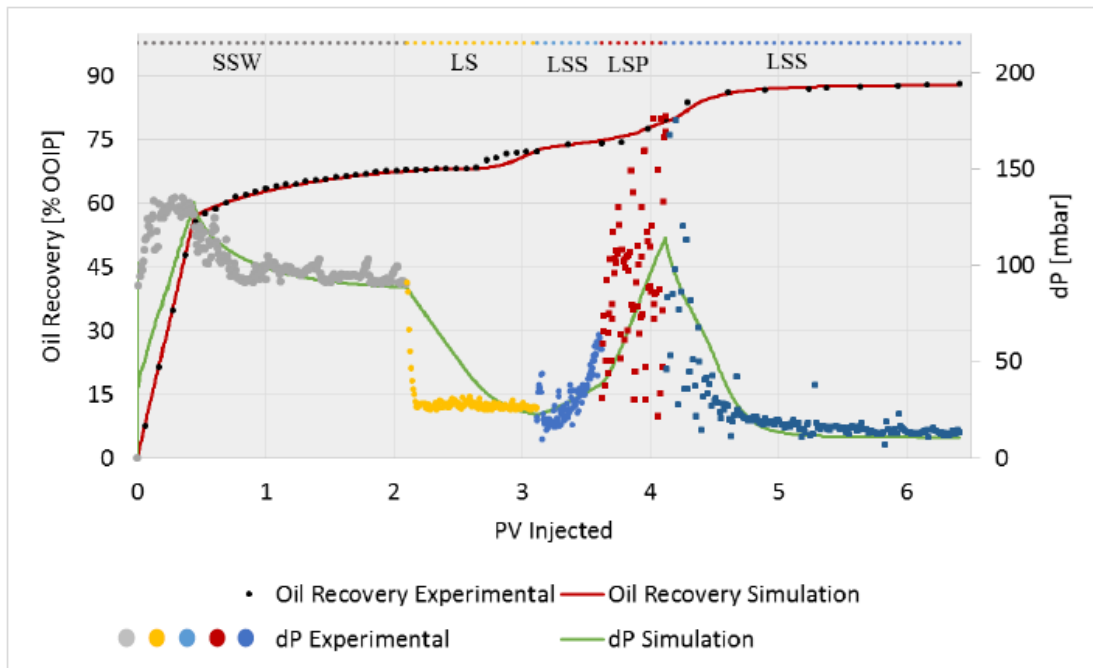


Figure 5.5: History match of oil production and differential pressure for core R3.

Figure 5.5 shows the history match of oil production and differential pressure from core R3 by Drønen. The simulated oil recovery for SSW was found to match the experimental data well, while the simulated differential pressure showed a delay for the initial pressure build-up. Despite this, the pressure curve followed the usual trend of increasing until water breakthrough, before declining afterwards.

For the LS flood, the simulation model successfully captured the increased recovery from low salinity injection. The response was however slightly delayed. For the differential pressure, the experimental data showed a sharp decline in pressure when transitioning from SSW to LS. Drønen attributed this to a redistribution of fluids, since no oil production was observed in that period. The simulation model was not able to accurately match the abrupt decline in experimental differential pressure when transitioning from SSW to LS. According to Drønen, this was because of the salinity based interpolation implemented in the model.

For the LSS and LSP flooding, the simulated and experimental oil recovery matched reasonably well. The differential pressure peak during polymer injection was not fully captured in the simulation. This was attributed to polymer not being represented with its own set of relative permeability curves.

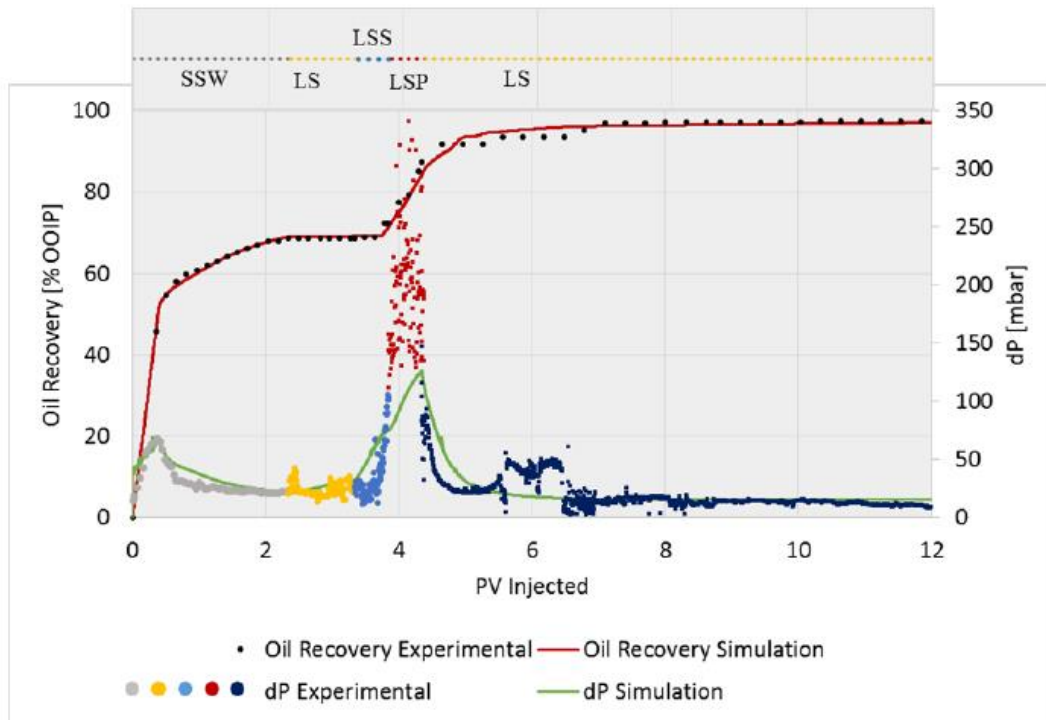


Figure 5.6: History match of oil production and differential pressure for core R4.

Figure 5.6 shows the history match of all flooding sequences for core R4. A good match was achieved for oil recovery and differential pressure for synthetic seawater and low salinity water flooding. An increase in differential pressure was observed during the LS flood, with no incremental oil recovery being registered. The reason for this was first thought to be permeability damage due to salinity contrast, however this was discarded in further investigations. In the end, no conclusions were made on the increase in differential pressure.

For the LSS and LSP floods, the simulated oil recovery matched the experimental data. For the differential pressure, the pressure peak during LSP was significantly lower than experimental values. According to Drønen, the pressure peak could have been increased by decreasing the polymer dispersion, but this would have increased the width of the peak. A decision was made that matching the shape of the peak was more important than matching the height.

## 5.2 Simulation study of core R10 by Jarlsby

In 2018, Jarlsby [58] presented a master thesis on mechanistic modelling of combined low salinity surfactant polymer flooding. In this thesis, Jarlsby performed an extensive study on interpolation routines, in addition to presenting a history match of core R10.

Core R10 is a Berea outcrop sandstone core from the same outcrop as cores R3, R4 and R14. Like the other cores, R10 was subjected to LSSP flooding in an experimental study at UniResearch CIPR's laboratories.

R10 was initially saturated with synthetic seawater (SSW), before being drained with Peregrino crude oil and then aged. After aging, the Peregrino crude oil was exchanged with Brage stock tank oil, and then aged again.

The coreflooding sequences were similar to that of core R3, R4 and R14, with an initial synthetic seawater (SSW) injection, followed by injection of low salinity water (LS), low salinity surfactant (LSS), low salinity polymer (LSP), and chase water in the end. The flooding sequences can be viewed in more detail in figure 5.7

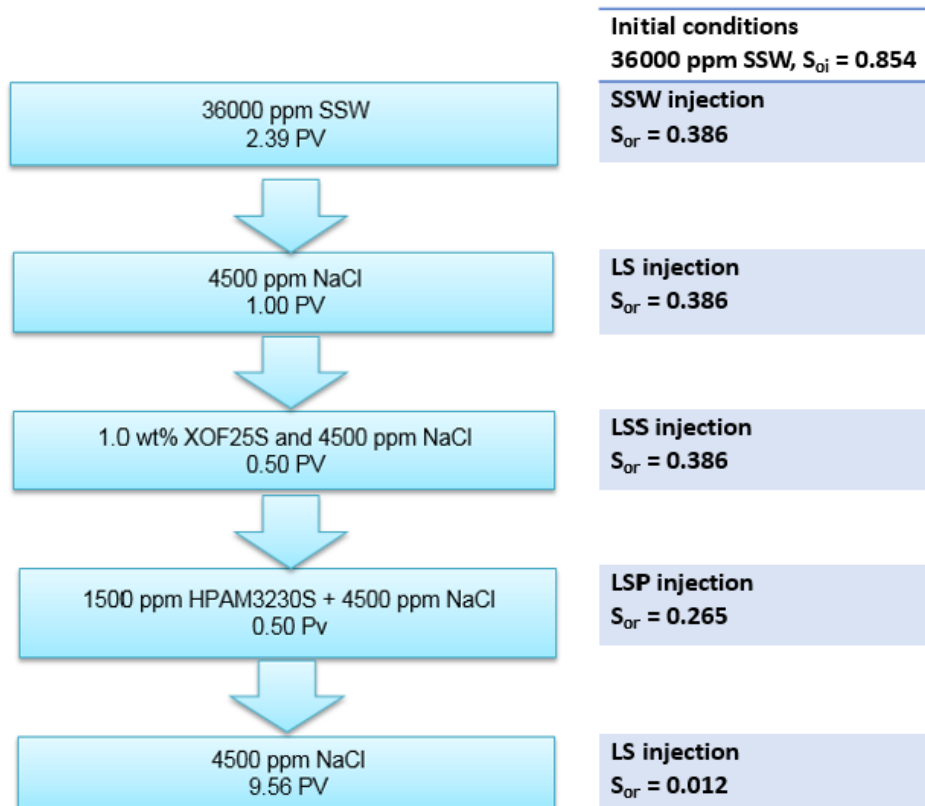


Figure 5 7: Summary of coreflooding sequences in core R10 [58].

After experimenting with different interpolation setups, Jarlsby decided to use a setup similar to that used by Drønen. This included two different interpolation routines in two separate rock types, in which interpolation was based on salinity concentration between SSW and LS in rock type 2, and on logarithm of capillary number between SSW and LSS in rock type 1. The polymer was only modelled as a viscosity effect. In figure 5.8, a description of Jarlsby's relative permeability and interpolation setup can be seen. The history match oil recovery and differential pressure in R10 can be seen in figure 5.9.

- Rock type 1: Surfactant curves**
- Set 1: High salinity, no surfactant  
DTRAPW =  $\text{Log}(N_c)$
  - Set 2: Low salinity, max surfactant  
DTRAPW =  $\text{Log}(N_c)$
- Rock type 2: Salinity curves**
- Set 1: High salinity, no surfactant  
DTRAPW =  $x_{\text{Na}^+, \text{high}}$
  - Set 2: Low salinity, no surfactant  
DTRAPW =  $x_{\text{Na}^+, \text{low}}$

Figure 5 8: Interpolation setup in Jarlsby's modelling of core R10 [58].

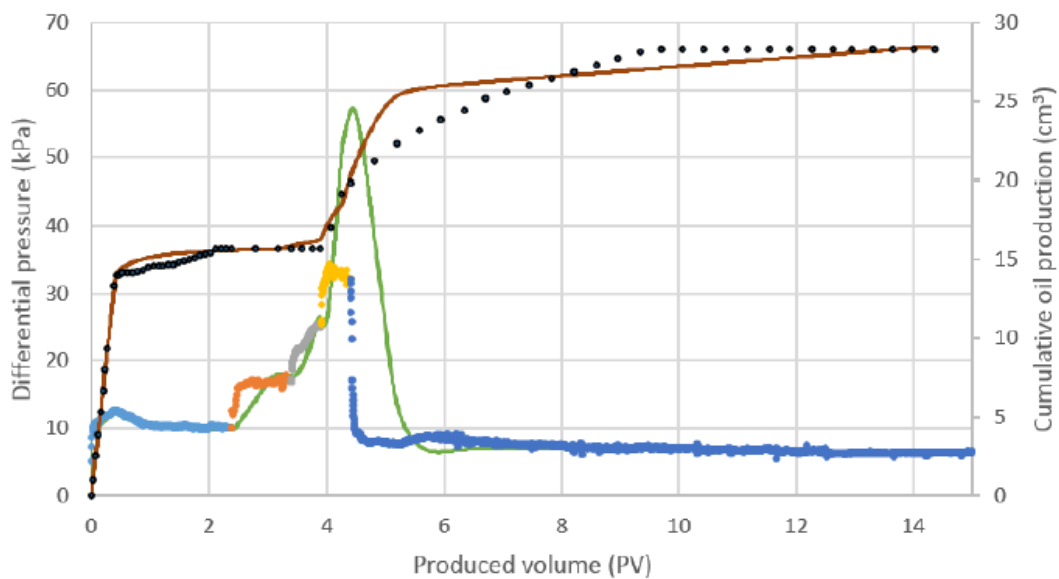


Figure 5 9: History match of oil production and differential pressure for core R10 [58]

The simulated oil recovery for the SSW and LS floods matched reasonably well, with a slight mismatch in the shape of the curve in the tail production during the SSW flood. No incremental production was observed during LS, however an increase in differential pressure was registered. The simulation was not able to capture the abrupt rise in experimental differential pressure during the LS flood, and Jarlsby attributed this to the salinity based interpolation implemented in the model.

For LSS and LSP flooding, there was a mismatch in the shape of the simulated oil recovery curve compared to the experimental. However, the end-point values were found to match well. The differential pressure peak during polymer flooding was slightly delayed and too high. Jarlsby suggested this was due to the polymer not being represented with its own set of relative permeability curves.

## 6 Sensitivity and Verification Studies

In order to understand how different parameters affect the simulation results, several sensitivity and verification studies were performed. The results from the studies were used to verify the simulator's capabilities of modelling coreflood experiments, as well as to history match the experimental coreflooding of core R14 in section 7.

The parameters evaluated in this section include:

- Corey relative permeability parameters
- Dispersion
- Viscosity
- Interfacial tension and capillary number
- Adsorption

### 6.1 Corey relative permeability parameters

In this section, the effect of altering Corey relative permeability parameters is investigated. This was done by modelling waterflooding in an arbitrary core whilst systematically altering the wettability of the core. To adjust the wettability, relative permeability curves were altered by changing the Corey parameters  $n_o$ ,  $n_w$ ,  $K_{rw}(S_{orw})$  and  $S_{or}$ . The results from the study were later used in the history matching of core R14.

An arbitrary core of 100x1x1 cm in i, j and k directions was modelled in the study. The porosity and absolute permeability was set to 0.25 and 2000 mD, while the water and oil viscosity was set to 5 and 13.8 cP, respectively. Relative permeability curves were created from the Corey functions presented in section 2.1.3 (equations 2.6-2.8).

In order to compare the effects of varying Corey parameters, base case relative permeability curves were established. The Corey parameters for the base case are listed in table 6.1, while the base case relative permeability curves can be seen in figure 6.1

*Table 6 1: Corey parameters used in calculation of base case relative permeability.*

$S_{wi}$	$S_{or}$	$k_{rw}(S_{or})$	$k_{ro}(S_{wi})$	$n_w$	$n_o$
0.2	0.3	0.3	1	2	2

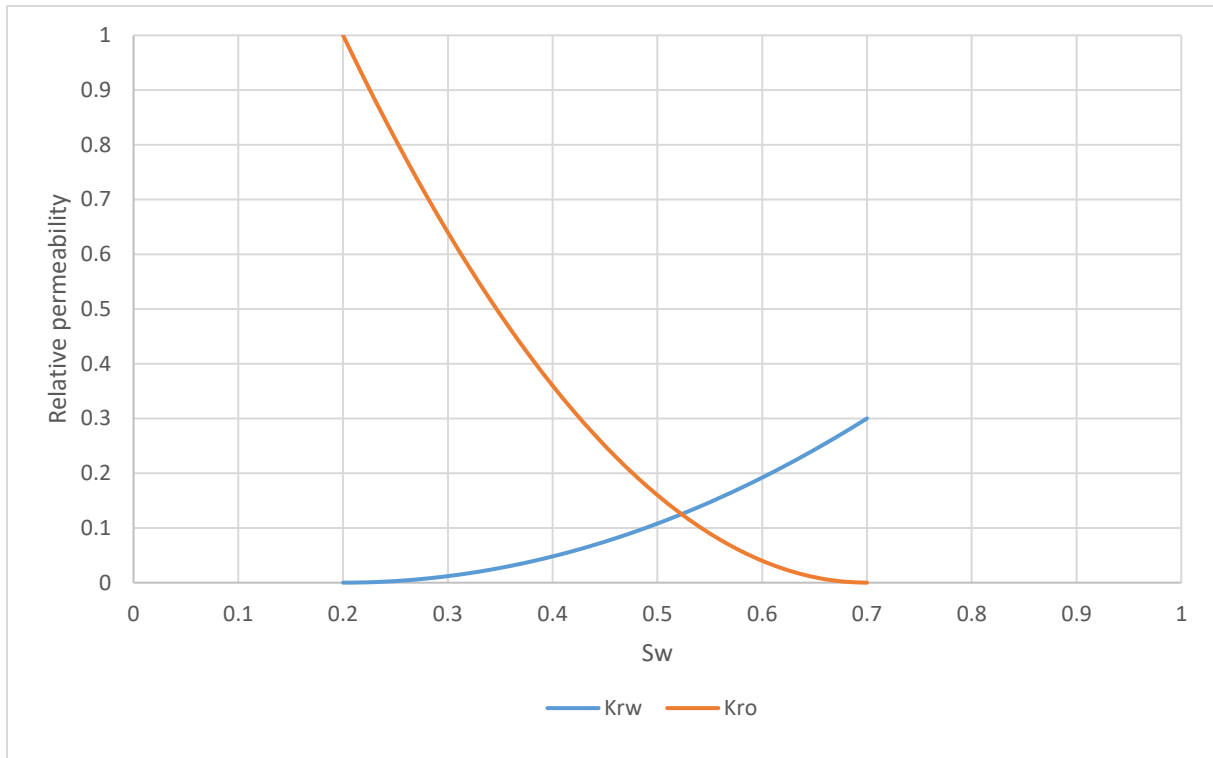


Figure 6 1: Base case relative permeability curves.

### 6.1.1 Sensitivity - varying $n_o$

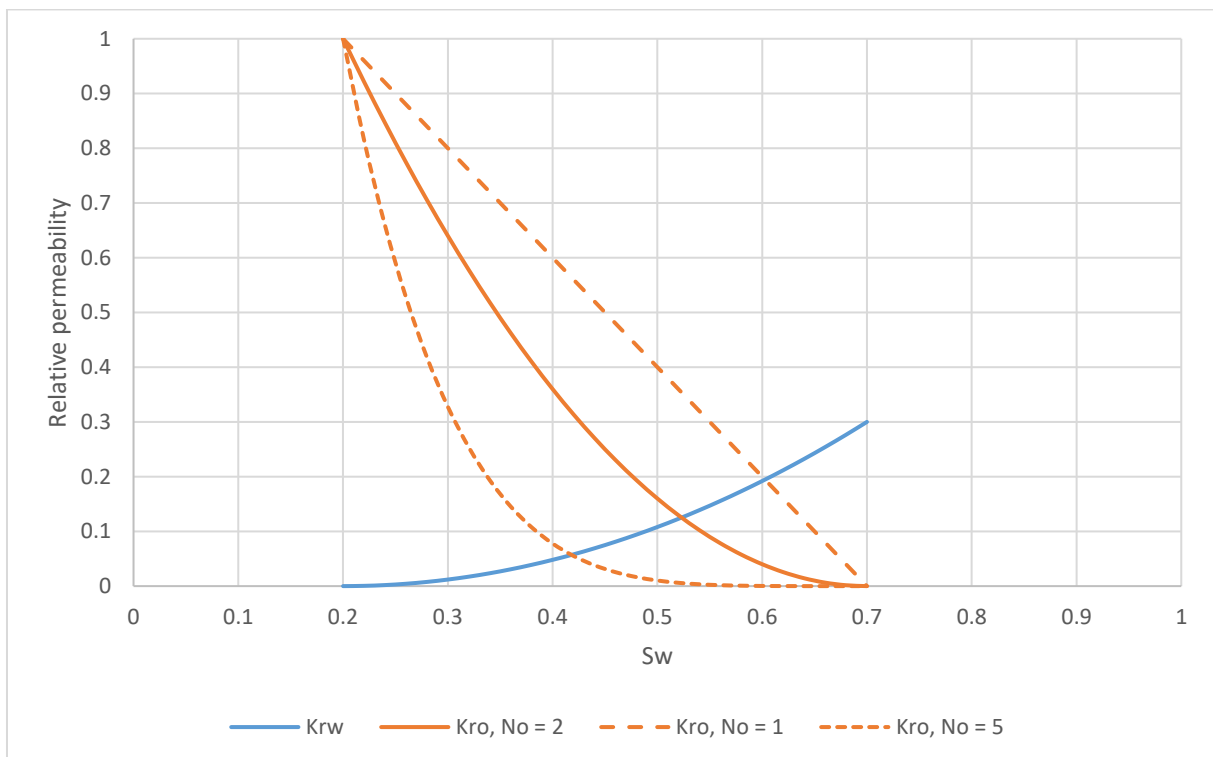


Figure 6 2: Relative permeability curves for varying  $n_o$ .

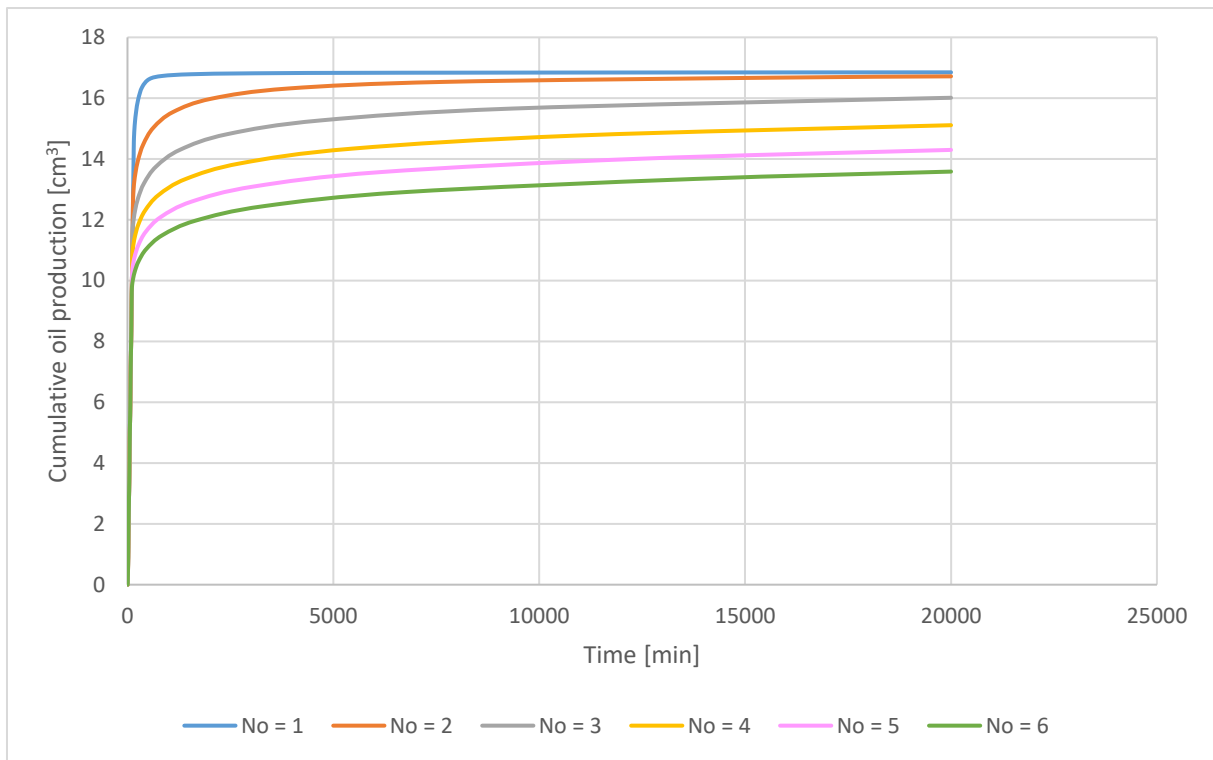


Figure 6 3: Cumulative oil production for varying  $n_o$ .

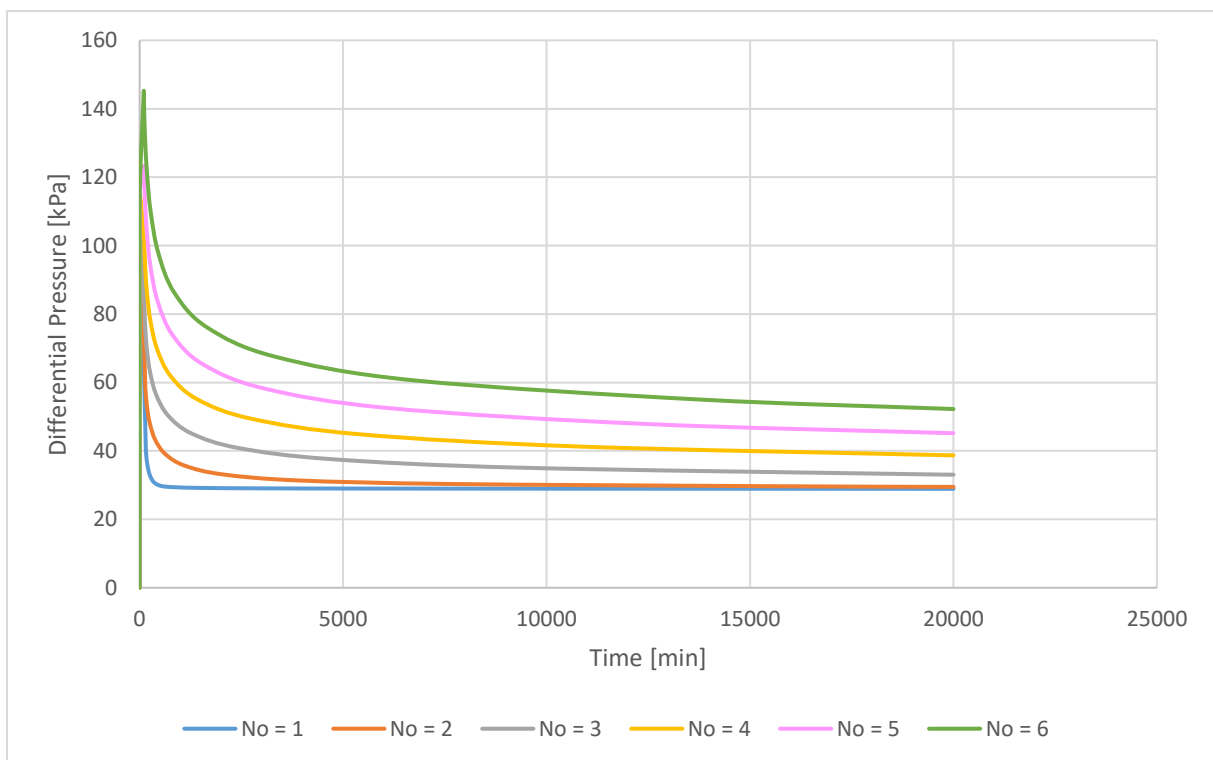
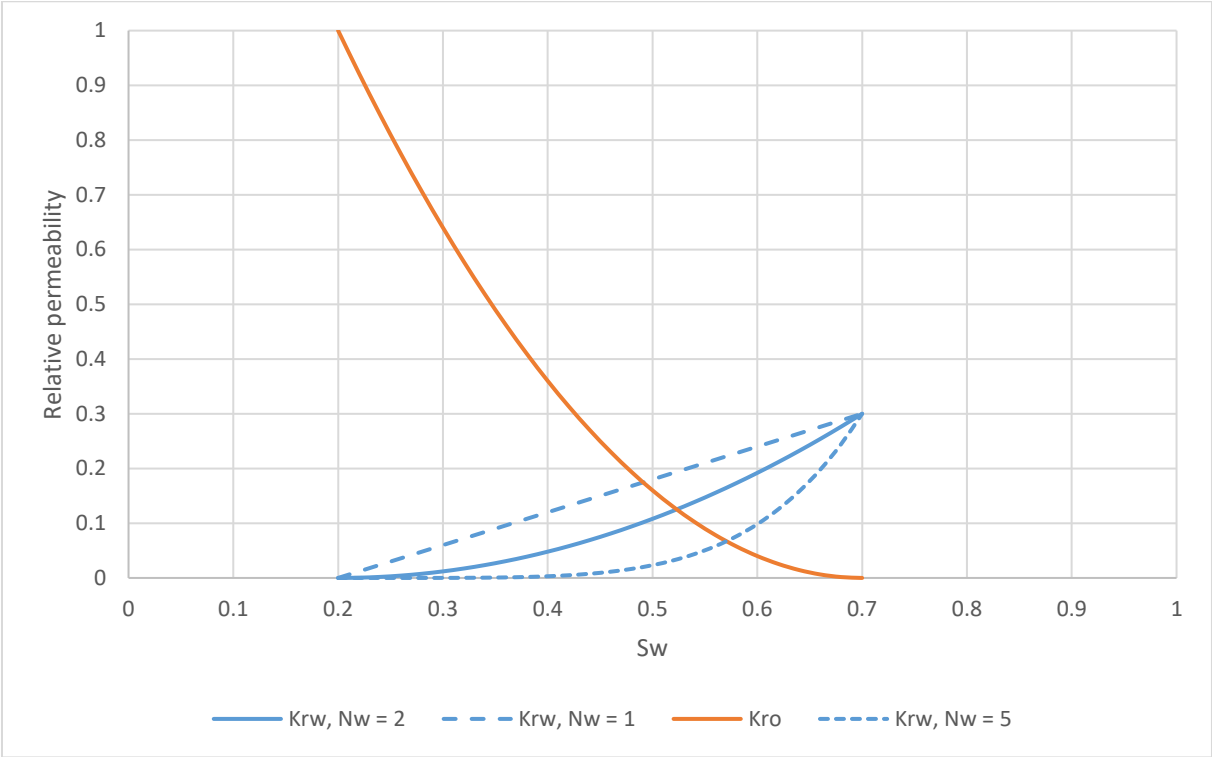


Figure 6 4: Differential pressure for varying  $n_o$ .

As can be seen in figure 6.2, an increase in  $n_o$  enhances the curvature of the oil relative permeability curve, resulting in a decrease in oil relative permeability at all saturations except end-point saturations. This corresponds to a shift in wettability towards more oil-wet conditions, which leads to earlier water breakthrough and lower cumulative oil production. This can be seen in figure 6.3. In addition, the differential pressure increases with increasing  $n_o$  due to flow restrictions as oil relative permeability is reduced. This is seen in figure 6.4.

**6.1.2 Sensitivity - varying  $n_w$**



*Figure 6 5: Relative permeability curves for varying  $n_w$ .*

Figure 6.5 shows that an increase in  $n_w$  enhances the curvature of the water relative permeability, resulting in a decrease in water relative permeability at all saturations except end-point saturations. This causes the wettability to alter towards more water wet conditions. Oil production and differential pressure curves for varying  $n_w$  can be seen in figures 6.6-9.

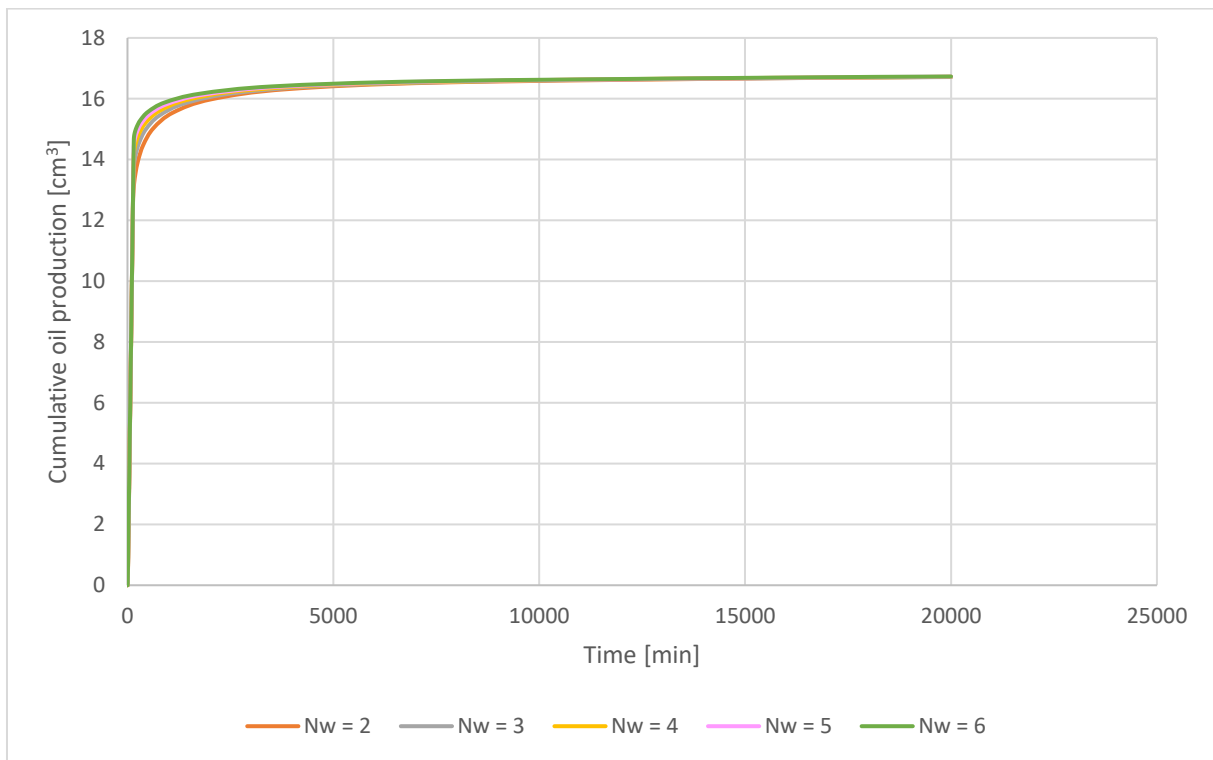


Figure 6 6: Cumulative oil production at varying  $n_w$ .

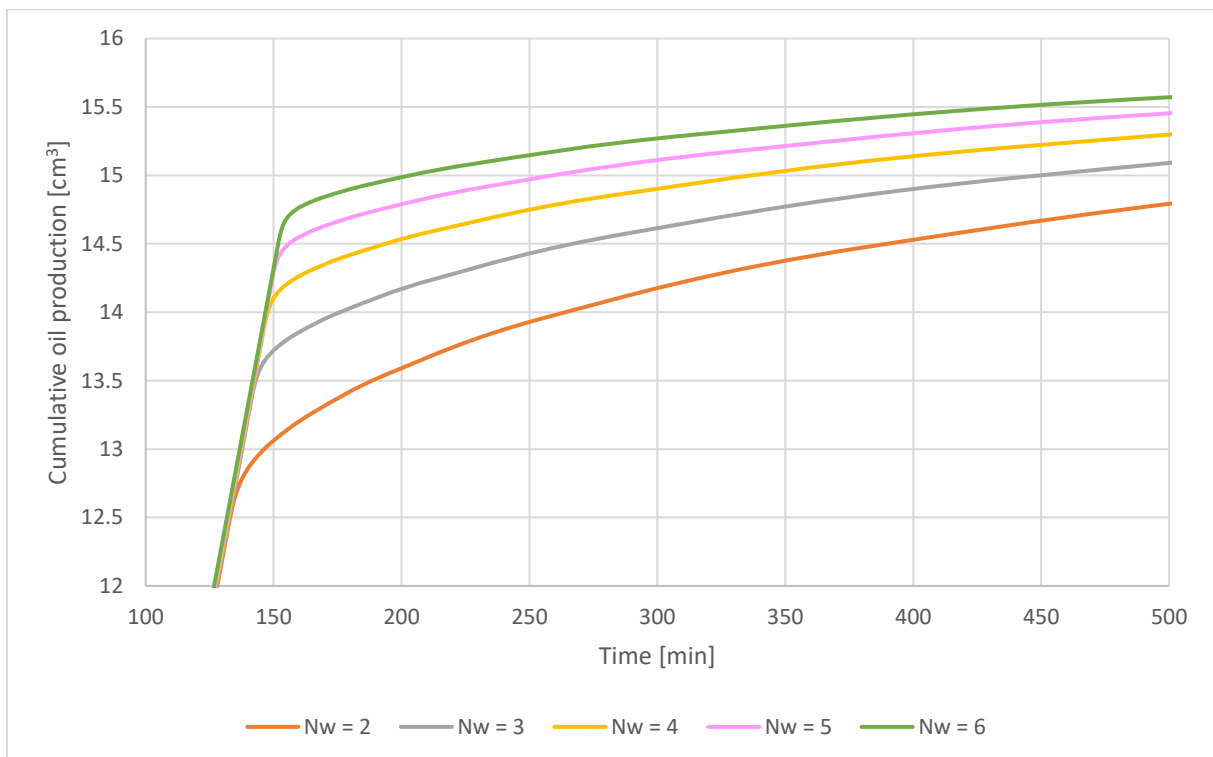


Figure 6 7: Cumulative oil production at varying  $n_w$ , with altered x-axis and y-axis.

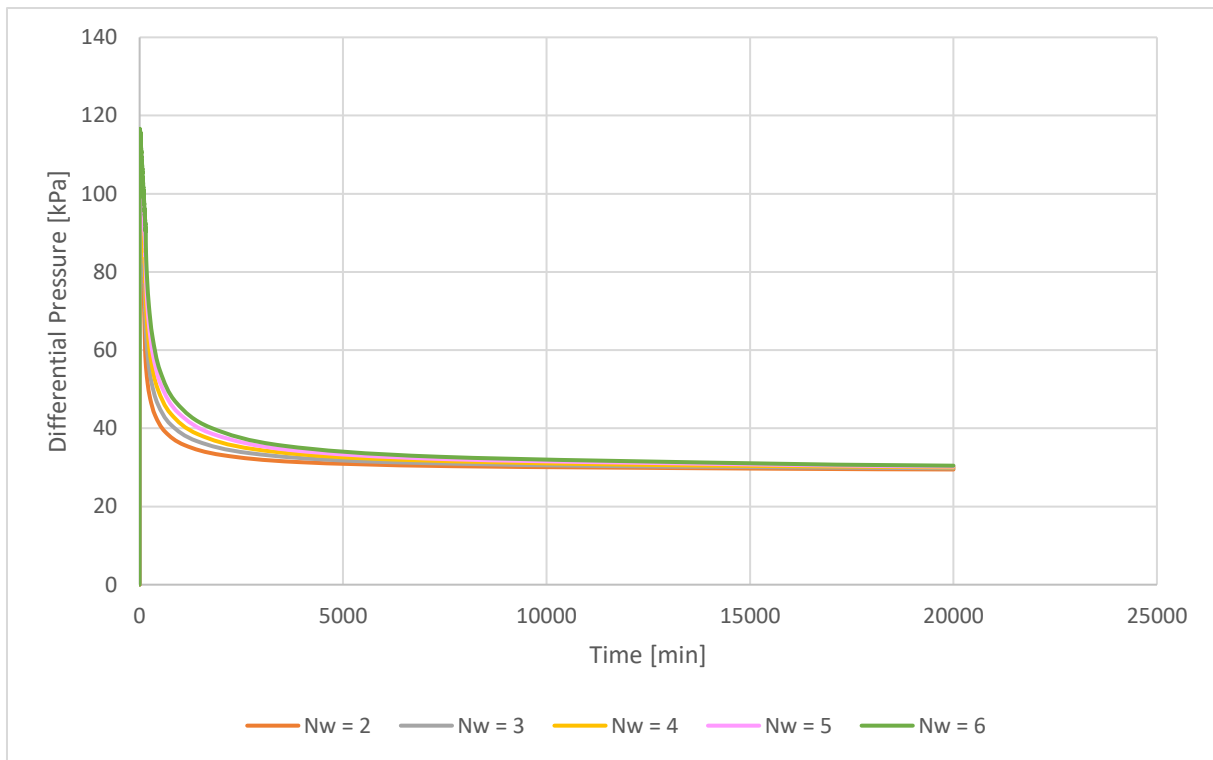


Figure 6 8: Differential pressure for varying  $n_w$ .

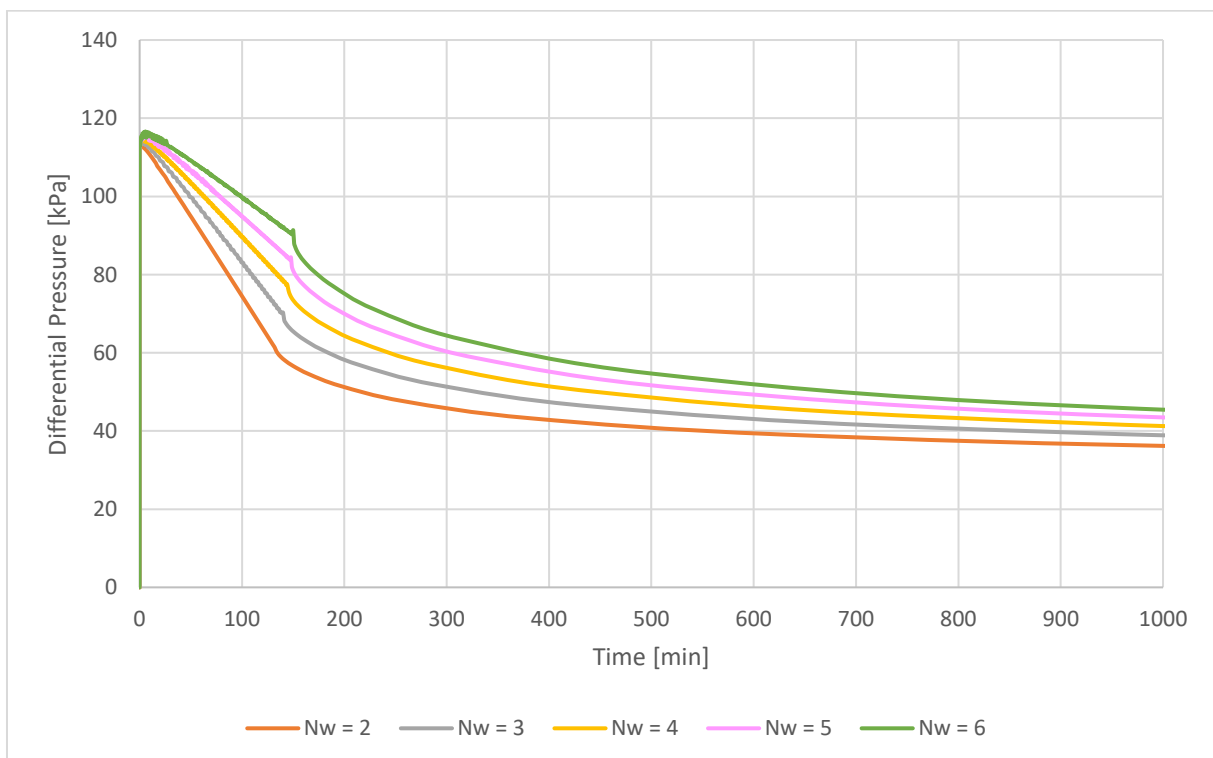
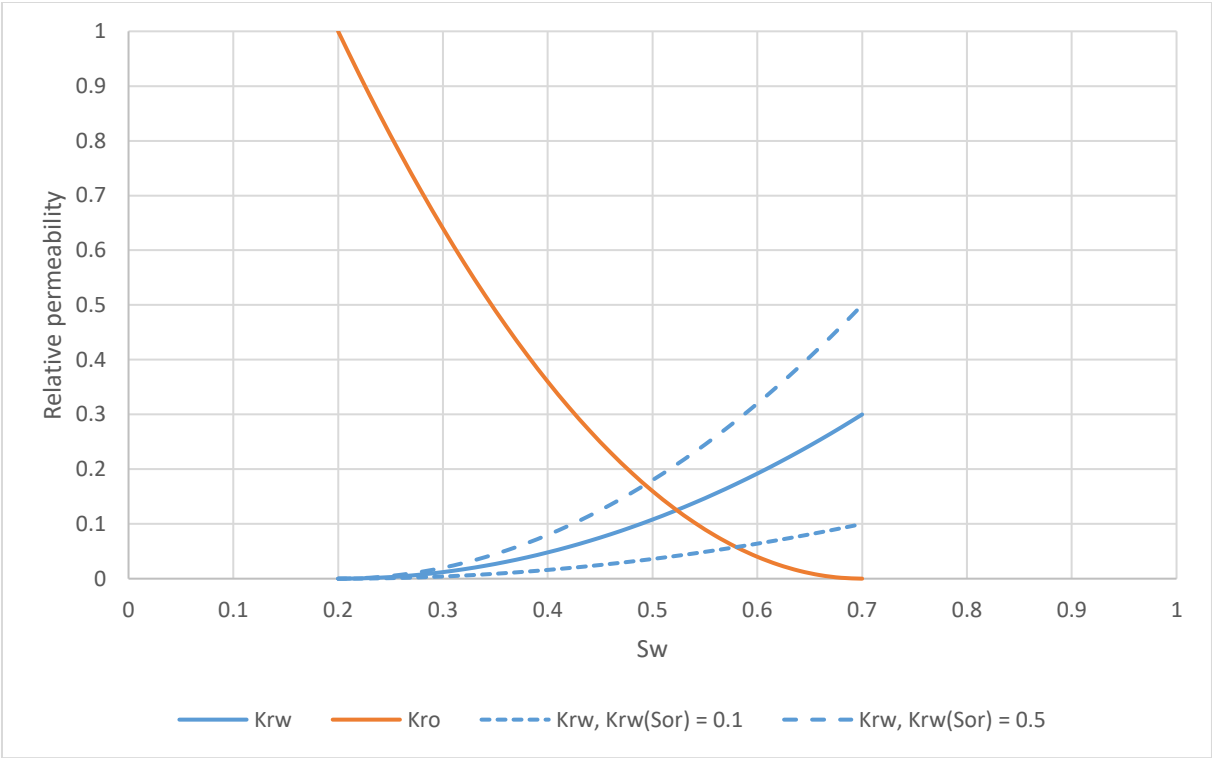


Figure 6 9: Differential pressure at varying  $n_w$ , with altered x-axis.

From figures 6.6-7 it can be seen that an increase in  $n_w$  leads to later water breakthrough and increased cumulative oil production. This is a result of the wettability shifting towards more water wet conditions. Figures 6.8-9 shows that the differential pressure increases with increasing  $n_w$ . The change is however significantly weaker for  $n_w$  than for  $n_o$ . This is due to the difference in viscosity between water and oil. With the oil viscosity being more than ten times as high as the water viscosity, a change in oil relative permeability will have a larger impact on the differential pressure.

**6.1.3 Sensitivity - varying  $k_{rw}(S_{or})$**



*Figure 6 10: Relative permeability curves for varying  $k_{rw}(S_{or})$ .*

Figure 6.10 shows that an increase in  $k_{rw}(S_{or})$  increases the water relative permeability at all saturations except the initial water saturation ( $S_{wi}$ ). This corresponds to a shift in wettability towards more oil wet conditions. Oil production and differential pressure curves for varying  $k_{rw}(S_{or})$  are presented in figures 6.11-13.

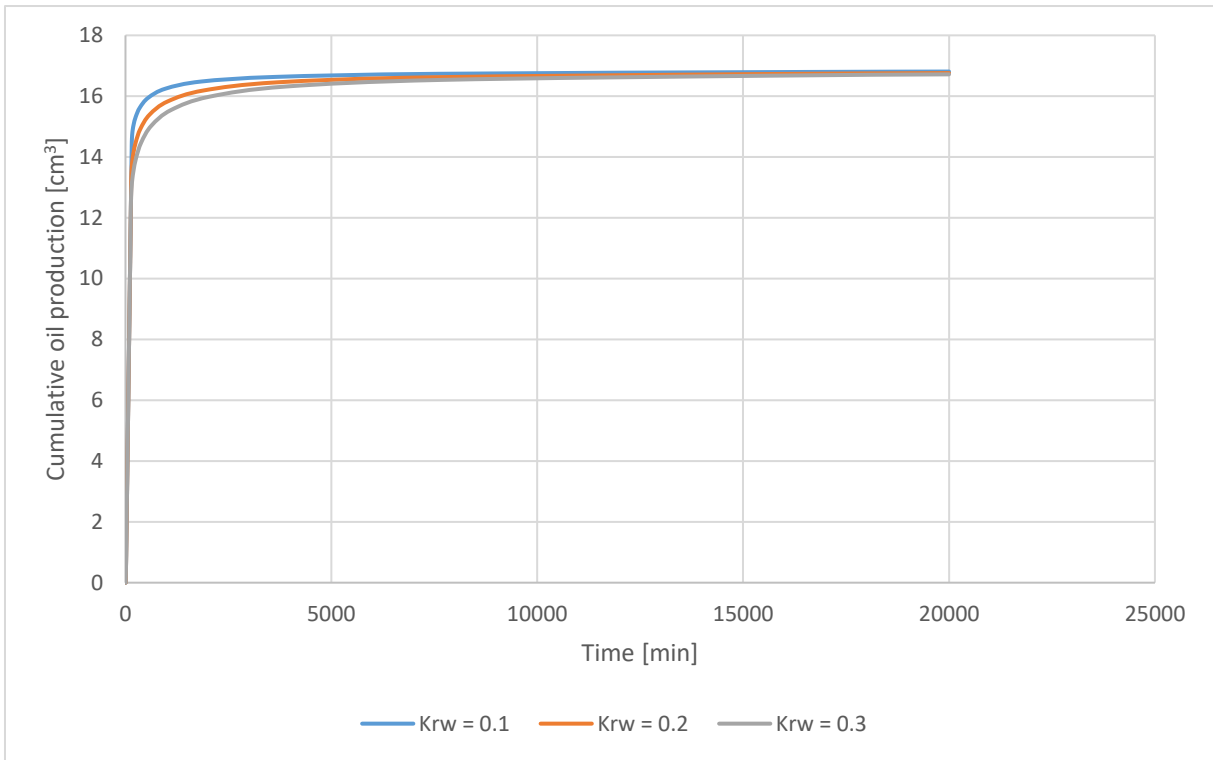


Figure 6 11: Cumulative oil production at varying  $k_{rw}(S_{or})$ .

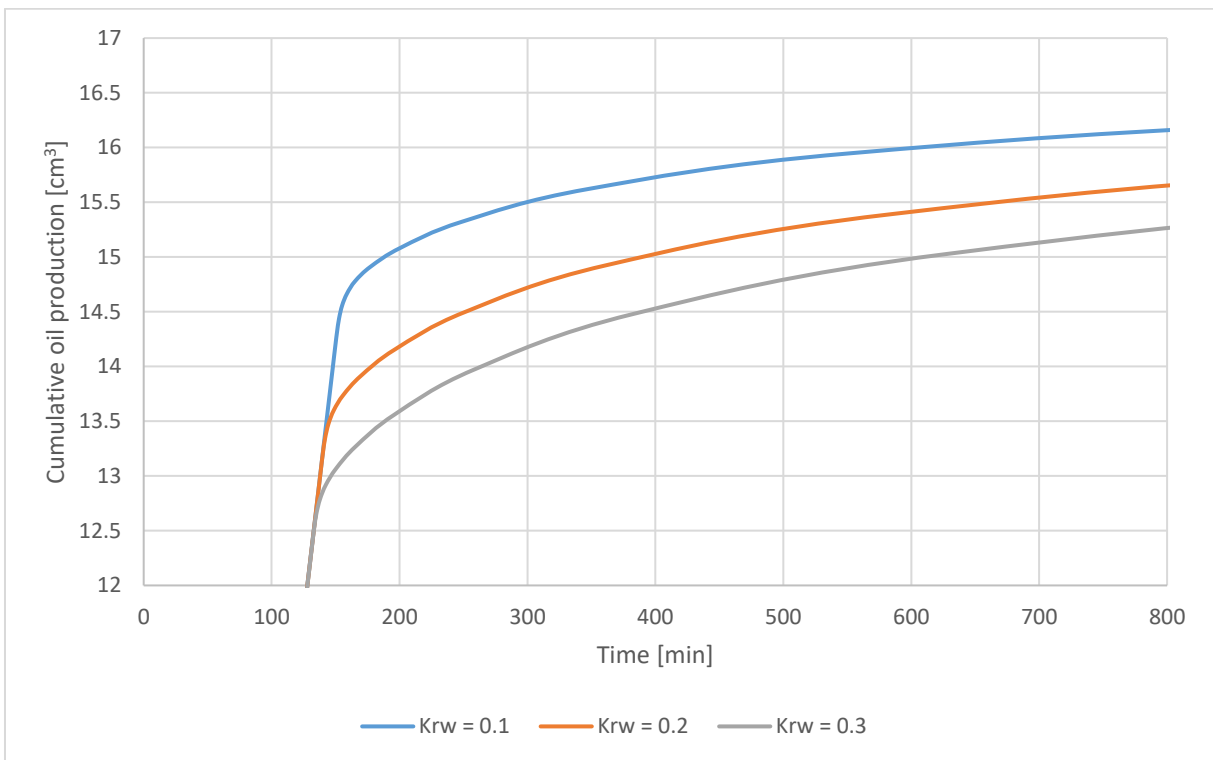


Figure 6 12: Cumulative oil production at varying  $k_{rw}(S_{or})$ , with altered x-axis and y-axis.

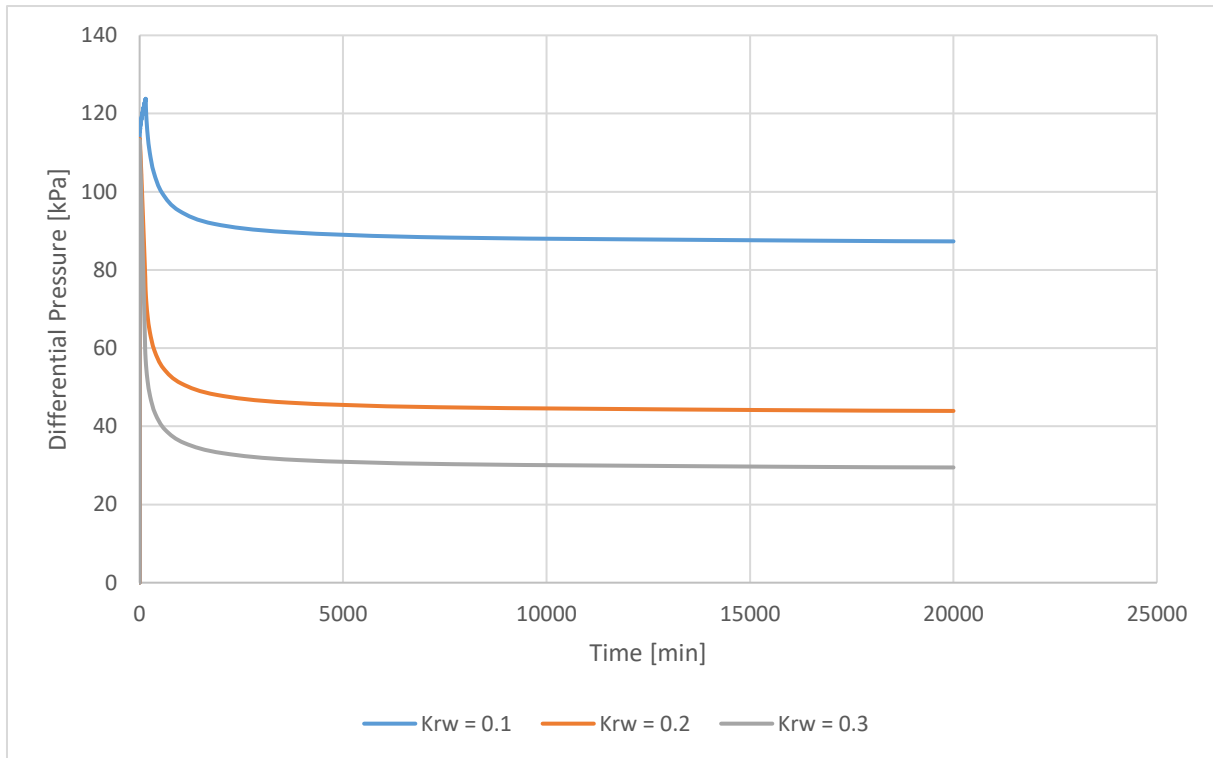


Figure 6.13: Differential pressure at varying  $k_{rw}(S_{or})$ .

Figures 6.11-12 show that an increase in  $k_{rw}(S_{or})$  yields earlier water breakthrough and lower cumulative oil production. This is a result of the wettability conditions shifting towards more oil wet conditions. As can be seen from figure 6.13, the differential pressure decreases with increasing  $k_{rw}(S_{or})$ . This is due to water having less impact on differential pressure compared to oil.

### 6.1.4 Sensitivity - varying $S_{or}$

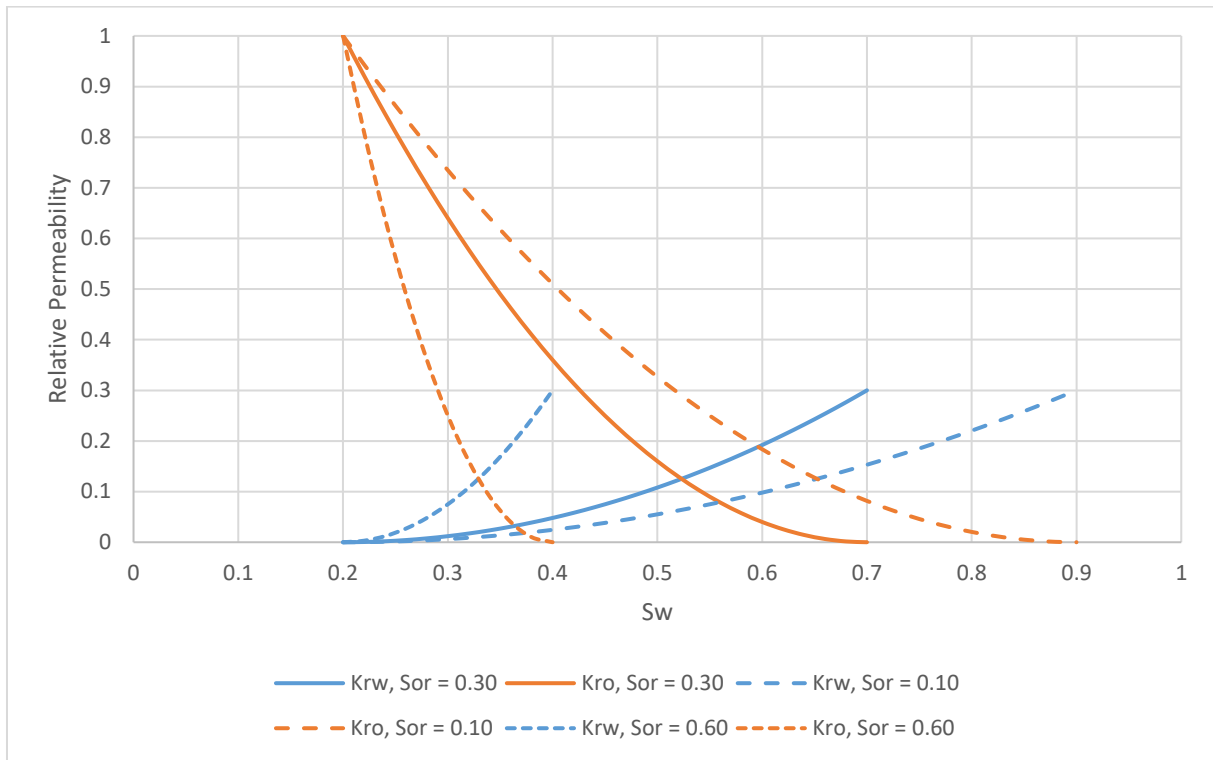


Figure 6.14: Relative permeability curves at varying  $S_{or}$ .

From figure 6.14 it is seen that an increase in  $S_{or}$  increases the water relative permeability and reduces the oil relative permeability at all saturations except end-point saturations. This corresponds to a shift in wettability more oil wet conditions. Plots of cumulative oil production and differential pressure at varying  $S_{or}$  is seen in figures 6.15-17.

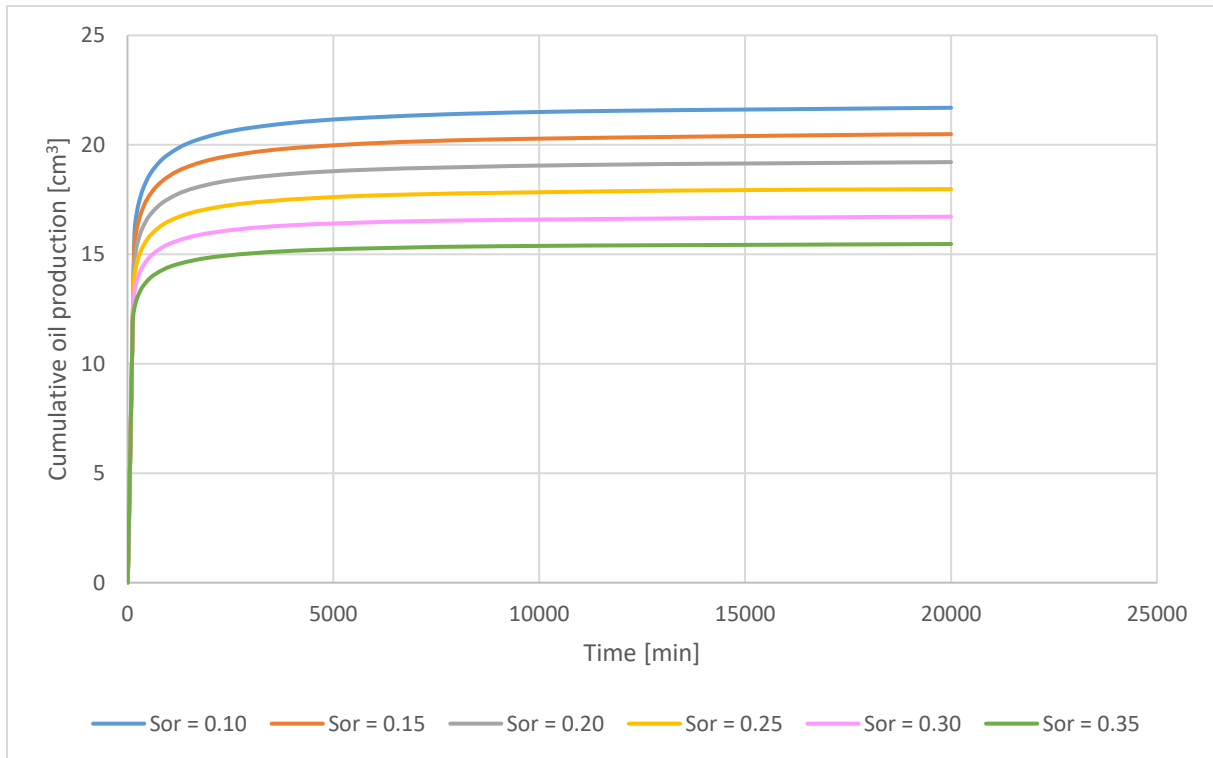


Figure 6 15: Cumulative oil production at varying  $S_{or}$ .

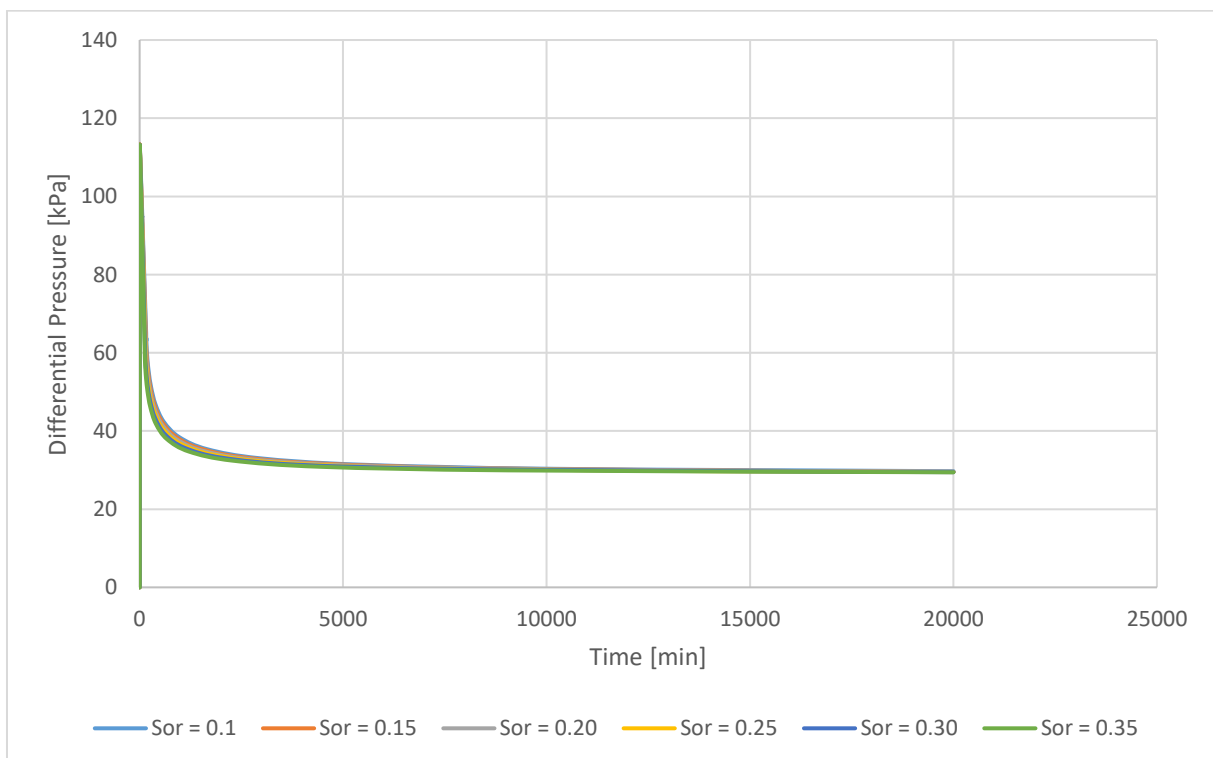


Figure 6 16: Differential pressure at varying  $S_{or}$ .

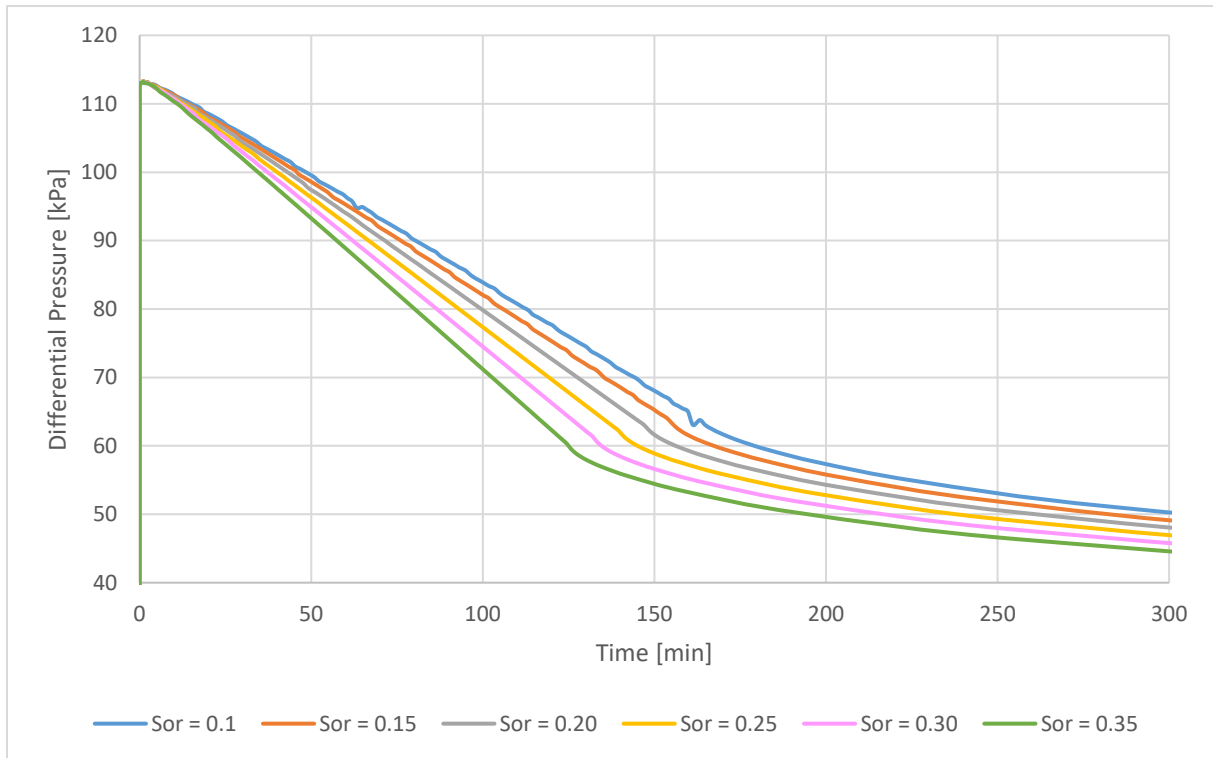


Figure 6 17: Differential pressure at varying  $S_{or}$ , with altered x-axis and y-axis.

Figure 6.15 shows that an increase in  $S_{or}$  results in earlier water breakthrough and lower cumulative oil production. The response in cumulative oil production is likely to be more affected by the residual oil saturation itself than the shift in relative permeability and water breakthrough. As can be seen from figure 6.17, increasing  $S_{or}$  causes a decrease in differential pressure. This due to the high viscosity of the oil, and the fact that less oil means less flow resistance.

Table 6 2: Observations from sensitivity study of Corey parameters.

$n_o$ variation	$\uparrow n_o$	Lower oil relative permeability Lower cumulative oil production Earlier water breakthrough Higher differential pressure
	$\downarrow n_o$	Higher oil relative permeability Higher cumulative oil production Later water breakthrough Lower differential pressure
$n_w$ variation	$\uparrow n_w$	Lower water relative permeability Higher cumulative oil production Later water breakthrough Higher differential pressure
	$\downarrow n_w$	Higher water relative permeability Lower cumulative oil production Earlier water breakthrough Lower differential pressure
$k_{rw}(S_{or})$ variation	$\uparrow k_{rw}(S_{or})$	Higher water relative permeability Lower cumulative oil production Earlier water breakthrough Lower differential pressure
	$\downarrow k_{rw}(S_{or})$	Lower water relative permeability Higher cumulative oil recovery Later water breakthrough Higher differential pressure
$S_{or}$ variation	$\uparrow S_{or}$	Higher water and lower oil relative permeability Lower cumulative oil production Earlier water breakthrough Lower differential pressure
	$\downarrow S_{or}$	Lower water and higher oil relative permeability Higher cumulative oil production Later water breakthrough Higher differential pressure

## 6.2 Dispersion

During waterflooding, the injected water is expected to either displace, mix with, or potentially by-pass the connate water. According to Jerauld [37], most literature on the subject suggest that all of the water in the pore-space is displaced by the injected water, with some degree of mixing between the two.

Dispersion is defined as the mixing of fluids caused by diffusion, local velocity gradients, heterogeneous streamline lengths, and mechanical mixing [2]. An example of dispersion is the mixing of salt in the aqueous phase. During coreflood simulations, two types of dispersion must be considered; numerical dispersion and physical dispersion.

### 6.2.1 Numerical dispersion

Numerical dispersion can be described as a numerical error caused by the calculations performed by the simulator. In the case of salt concentration, it causes smearing of sharp fronts, which leads to the development of mixing zones. This has an effect on the simulation results, and can for example result in a too early calculated water breakthrough [59].

To analyze the numerical dispersion in the simulation model, two separate sensitivity studies were performed. Both included plotting of salinity profiles, with 'Na' being the chosen component. First, simulations were performed using different amount of grid-blocks, thus altering the size of each individual grid-block in the model. Next, simulations were run using different sized time-steps. These analyses were performed in order to determine a setup in which the numerical dispersion in the model was minimized. The results can be seen in figures 6.18-19. Physical dispersion was not included in the analysis of numerical dispersion, since combining the two would make it hard to distinguish their individual effects and determine an optimal setup.

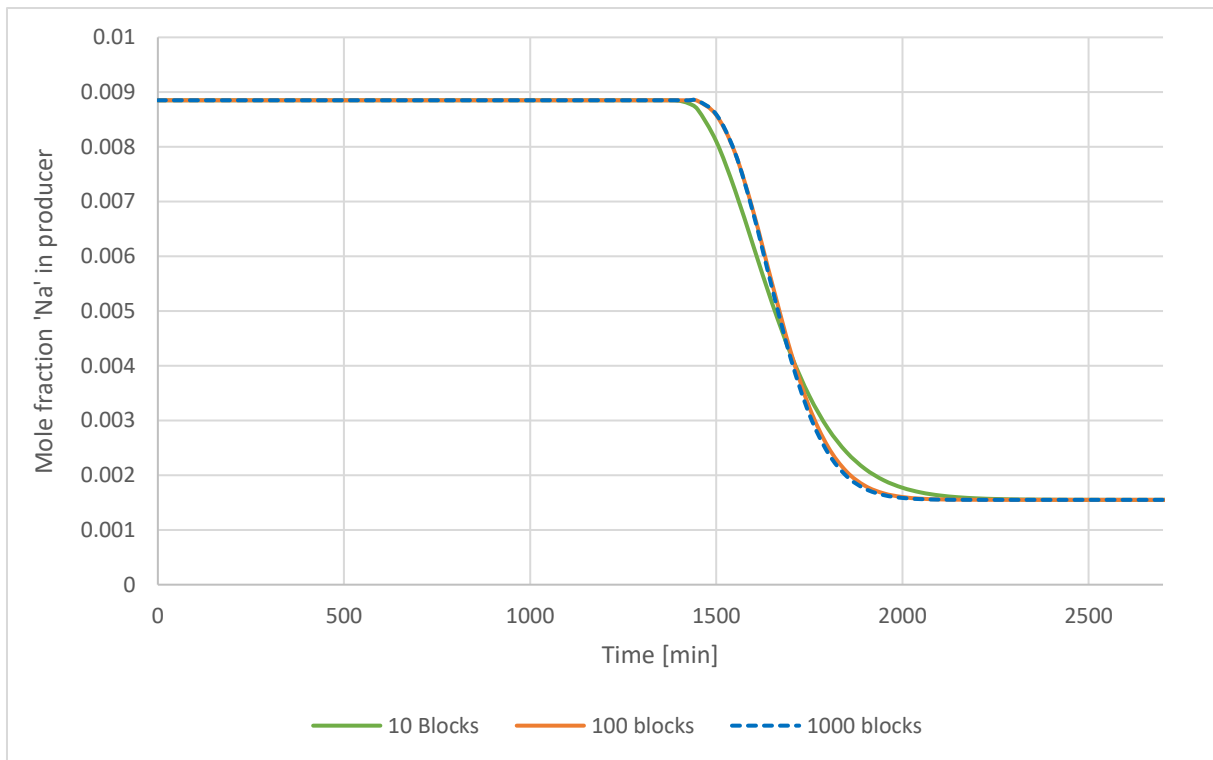


Figure 6 18: Numerical dispersion of salt concentration in the producer for different amount of grid-blocks.

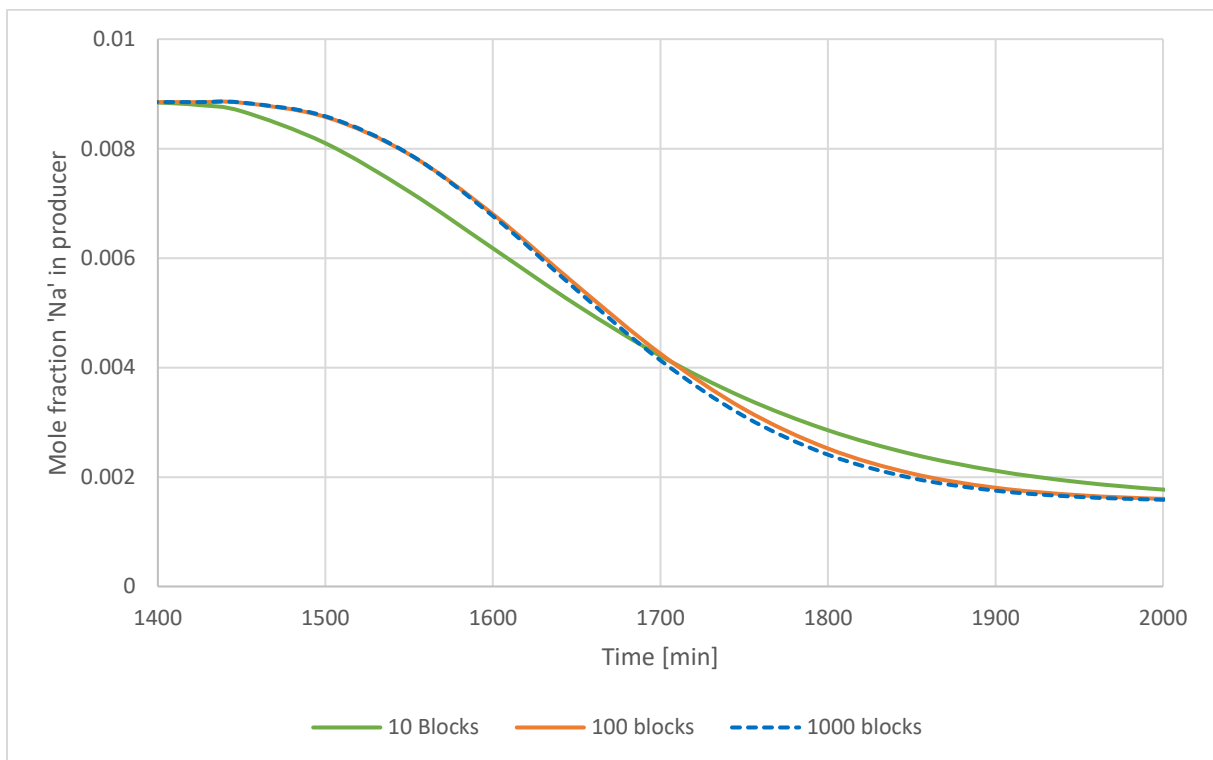


Figure 6 19: Numerical dispersion of salt concentration in the producer for different amount of grid-blocks, with altered x-axis.

Figures 6.18-19 show that the numerical dispersion depends on the size of the grid blocks. By increasing the total amount of blocks, the size of each individual grid block is reduced and the margin of error in the simulators' calculations is minimized. This effectively decreases the mixing zone, and thus the numerical dispersion in the model.

As can be seen from figures 6.18-19, the use of 10 grid blocks resulted in increased smearing of the curve, indicating significant numerical dispersion. The use 100 and 1000 grid blocks showed less smearing, and thus less numerical dispersion. Since the curves for 100 and 1000 grid blocks more or less overlapped, it was assumed that 100 grid blocks was sufficient to minimize the numerical dispersion in the model. As a result, 100 grid blocks were used in the simulation model used to history match core R14 in section 7.

The amount of numerical dispersion in the simulation also depends on size of the time-steps. To analyze this, salinity profiles were plotted for simulations containing different sized time-steps. The time-step sizes were defined through the keyword DTMAX, and the amount of grid blocks were kept constant at 100 for all simulations. The results can be seen in figures 6.20-21. The numerical dispersion was found to be minimized for a time-step size of 1. This was therefore the selected time-step size in the model used to history match core R14 in section 7.

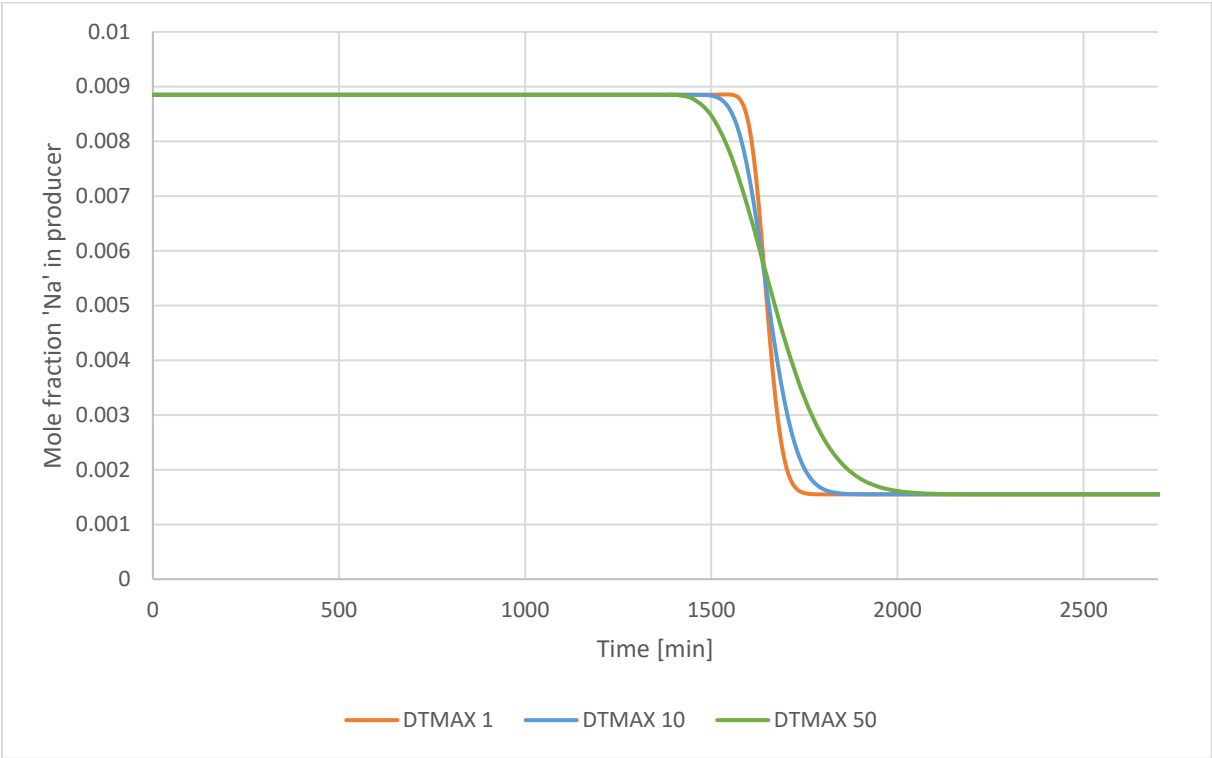
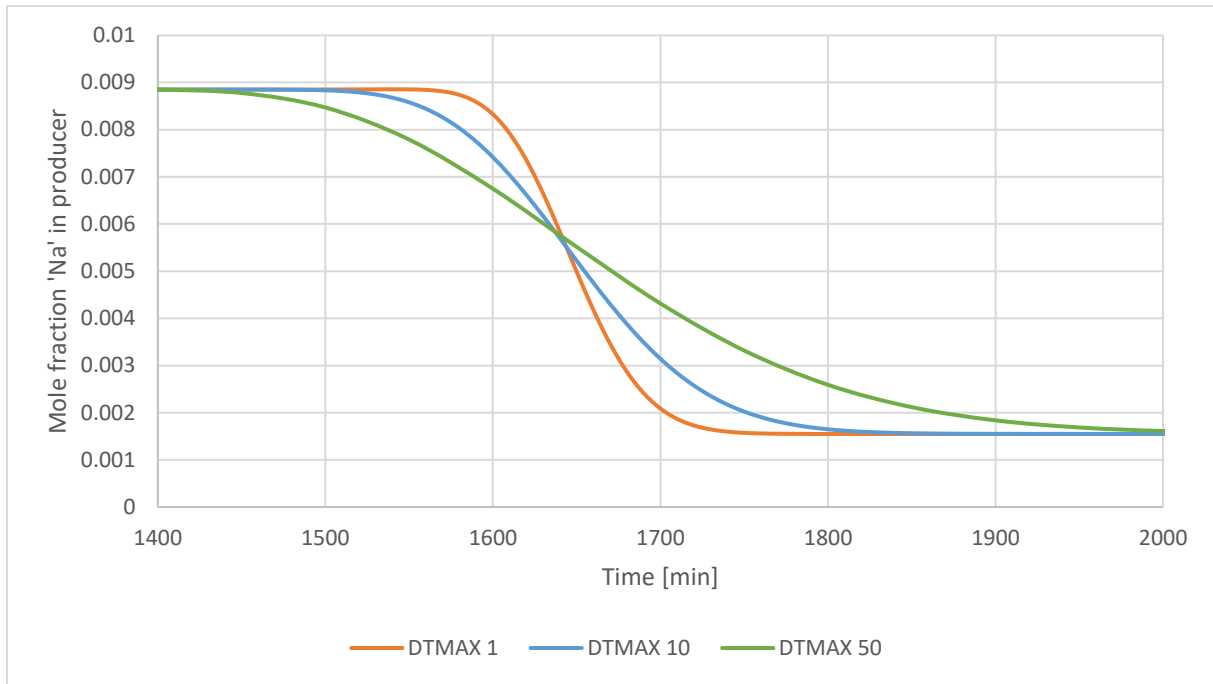


Figure 6 20: Numerical dispersion of salt concentration for different sized time-steps. 100 grid blocks is used.



*Figure 6 21: Numerical dispersion of salt concentration for different sized time-steps, with altered x-axis. 100 grid blocks is used.*

From this sensitivity study on numerical dispersion, it was concluded that the numerical dispersion was minimized by using 100 grid blocks and a maximum time-step size of 1. This information was used when evaluating the physical dispersion in the next section.

## 6.2.2 Physical dispersion

As discussed in section 4.2, the keywords \*DISPI/\*DISPJ/DISPK is used in STARS to define the total dispersion coefficient in all three dimensions [55]. In STARS, the total dispersion coefficient can be seen as the true physical dispersion minus the numerical dispersion [60]. By minimizing the numerical dispersion in the previous section, the total dispersion coefficient could be used to represent physical dispersion only.

In order to evaluate the effect of physical dispersion, salinity profiles for different dispersion coefficients were plotted. These are seen in figure 6.22. The true physical dispersion is estimated in the lab by measuring the salt concentration in the effluent. There was however no such information included in the laboratory data provided for this thesis. Therefore, the physical dispersion was to some degree treated as a history matching parameter.

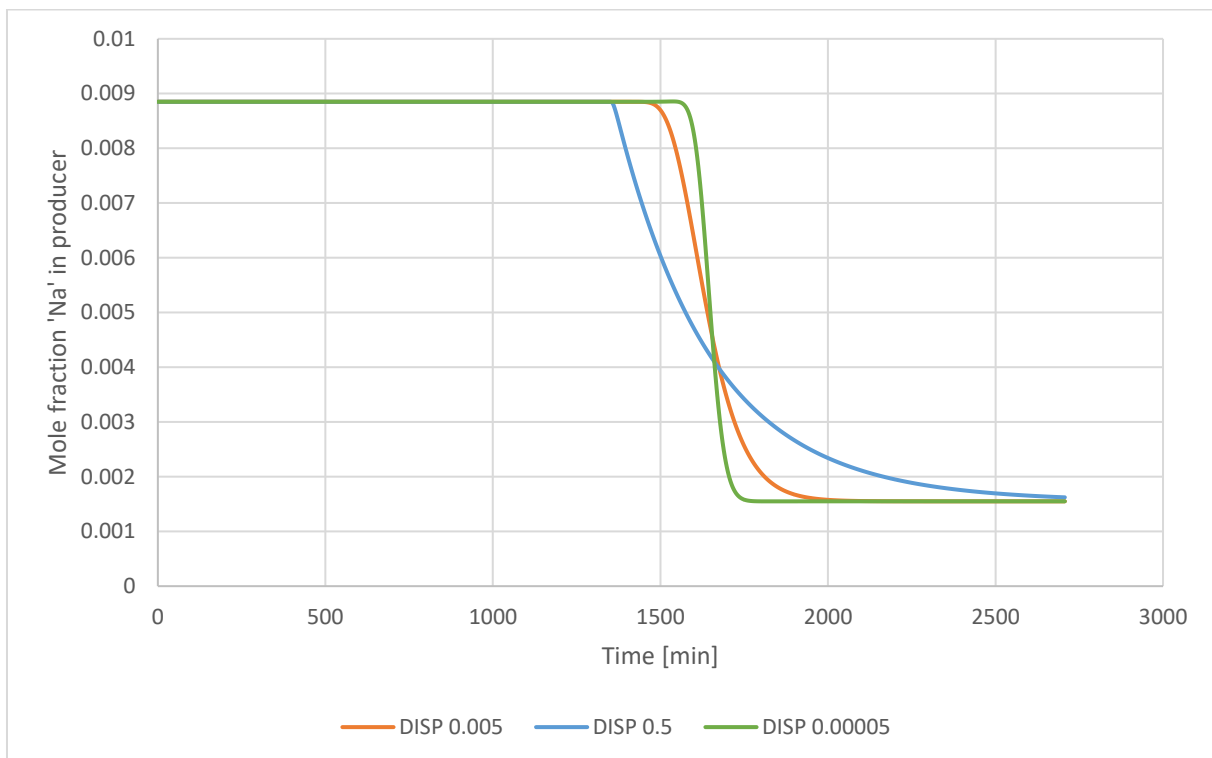


Figure 6 22: Physical dispersion for different dispersion coefficients. 100 grid-blocks and DTMAX 1 is used.

Figure 6.22 shows that a smaller dispersion coefficient yielded less dispersion. The salinity profile for  $\text{DISP} = 0.5 \text{ cm}^2/\text{min}$  indicated that this dispersion value was out of range. For the history matching of core R14, the total dispersion coefficient of 'Na' was set to  $0.005 \text{ cm}^2/\text{min}$ .

### 6.2.3 Dispersion over distance

According to Mahadevan [61], dispersivity appears to grow with distance covered. This was investigated for the physical dispersion by plotting salinity profiles at increasing distances from the injector. The results can be seen in figure 6.23. Both cases showed increased smearing, larger mixing zones and less piston-like displacement at distances further away from the injector. This confirms that the dispersivity increases with distance in the simulation model.

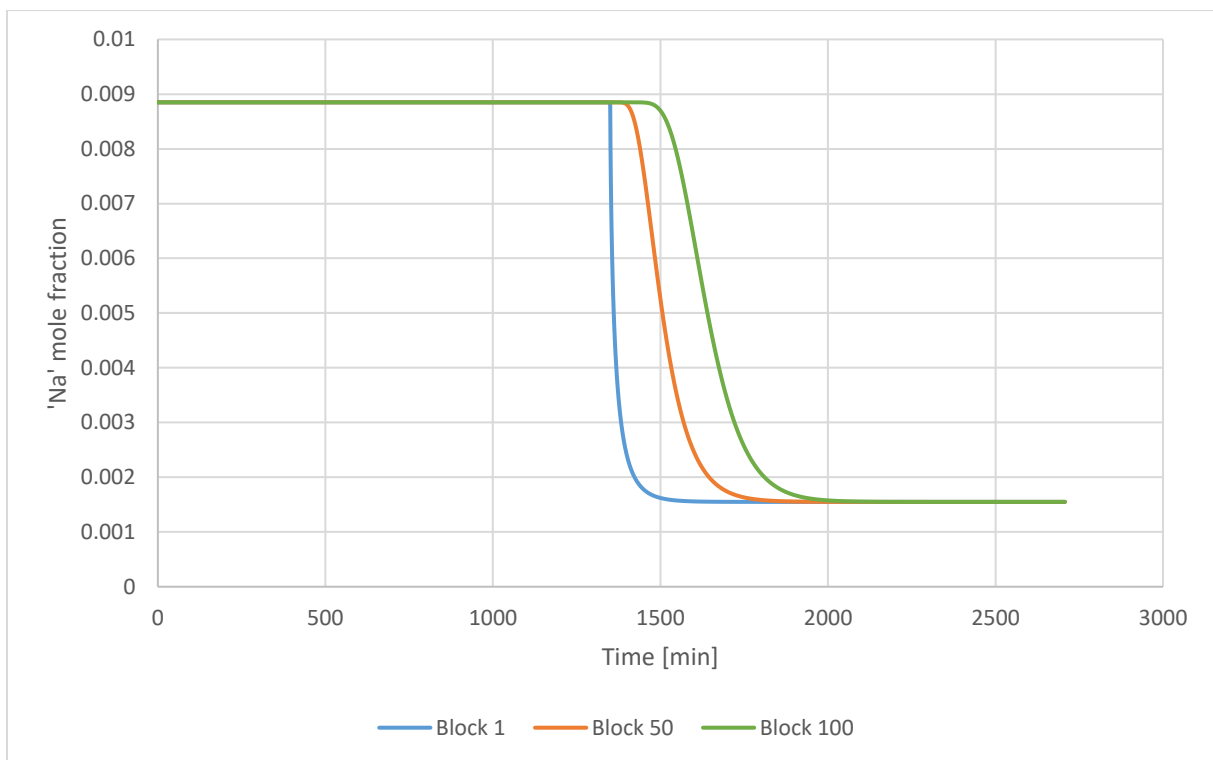


Figure 6 23: Physical dispersion at increasing distance from the injector. A model of 100 grid blocks and DTMAX 1 is used, with dispersion set to  $0.005 \text{ cm}^2/\text{min}$ .

#### 6.2.4 Effect of dispersion on relative permeability

In the history matching of core R14, interpolation between synthetic seawater (SSW) and low salinity water (LS) relative permeability curves is based on salt concentration. As a result, the dispersion of 'Na' will affect the relative permeability in the simulation. This is illustrated in figure 6.24.

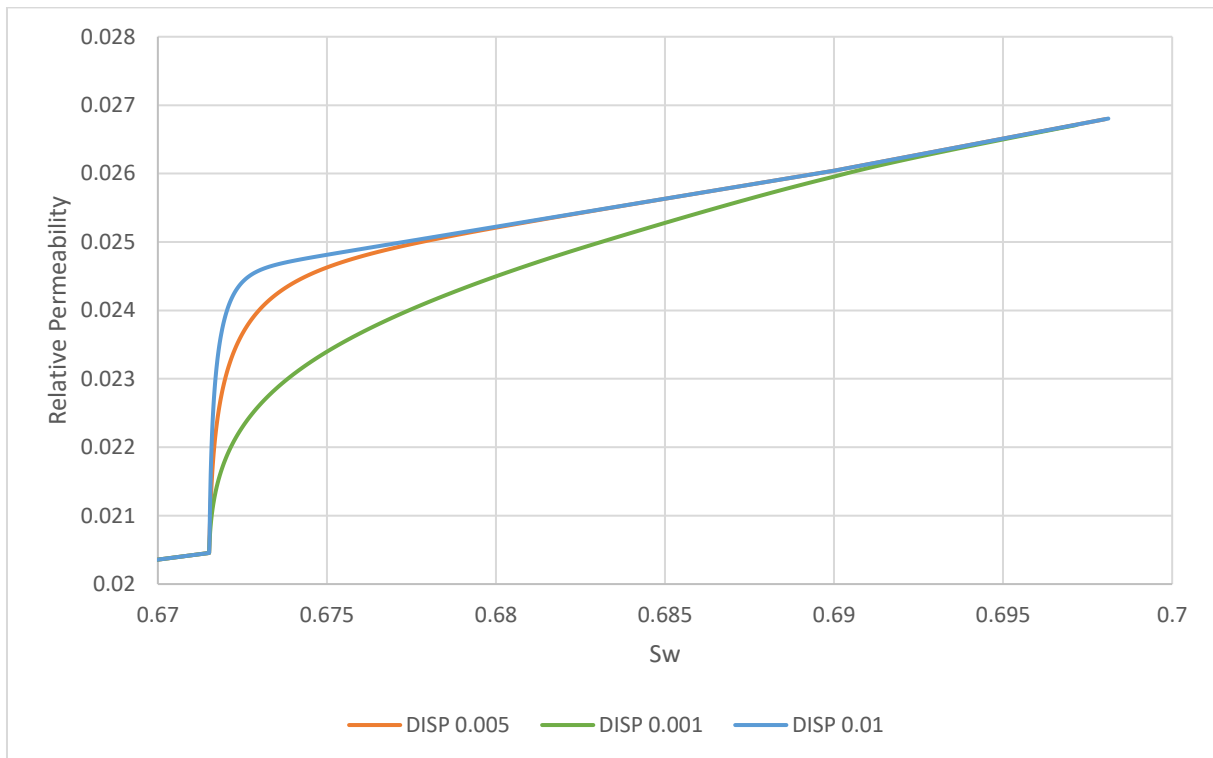


Figure 6 24: Water relative permeability for different dispersion coefficients, with altered x-axis and y-axis.

The results indicate that for lower dispersion coefficients, the switch from high salinity to low salinity relative permeability occurs more rapidly. For higher dispersion coefficients, smearing of the curve is observed. This information is useful for the history matching, as changes in relative permeability influence oil production and differential pressure curves. Alteration of dispersion coefficients could therefore yield a better match between simulated and experimental values.

### 6.3 Surfactant and polymer viscosity

When surfactant is added to the injection water, the viscosity of the water solution is increased compared to that of synthetic seawater and low salinity water. For surfactant solutions, the viscosity is a function of the surfactant concentration. In order to evaluate STARS capabilities of modeling the viscosity of such solutions, a verification study was performed.

In STARS, viscosity of components are defined through the keywords AVISC, VSMIXCOMP, VSMIXENDP and VSMIXFUNC. AVISC defines the liquid viscosity of each specific component. VSMIXCOMP specifies the name of the component for which viscosity mixing is assigned. VSMIXENDP specifies the minimum and maximum mole fractions of the component subjected to mixing, while VSMIXFUNC defines an eleven entry ( $f_1 \dots f_{11}$ ) non-linear mixing rule where the viscosity is dependent on the mole fraction of the component [55].

In the laboratory data from core R14, no information was provided on the relationship between surfactant concentration and water phase viscosity. As a result, an assumption of an ideal system was made, and the relationship between surfactant concentration and water viscosity was assumed to be exponential [57].

In order to achieve an exponential increase in viscosity, VSMIXFUNC was omitted in the model. According to the STARS manual [55], when VSMIXFUNC is omitted, entries  $f_i = (i-1)/10$  for  $i = 1$  to 11 is used. This corresponds to linear spacing from 0 to 1, resulting in a linear-log mixing rule where the mole fractions  $x_i$  act as weighting factors.

$$\ln(\mu) = \sum_i x_i \ln(\mu_i) \quad (6.1)$$

This should result in an exponential increase in viscosity for increasing surfactant concentration. In order to verify this, a simulation of a surfactant flooding sequence was run, and a plot of water viscosity vs. water mole fraction surfactant was made. The input values used in the simulation can be seen in table 6.1, while the plot is shown in figure 6.25.

Table 6 3: Input values used in simulation of surfactant injection

AVISC	VSMIXCOMP	VSMIXENDP
1.5	'SURF'	0.000427

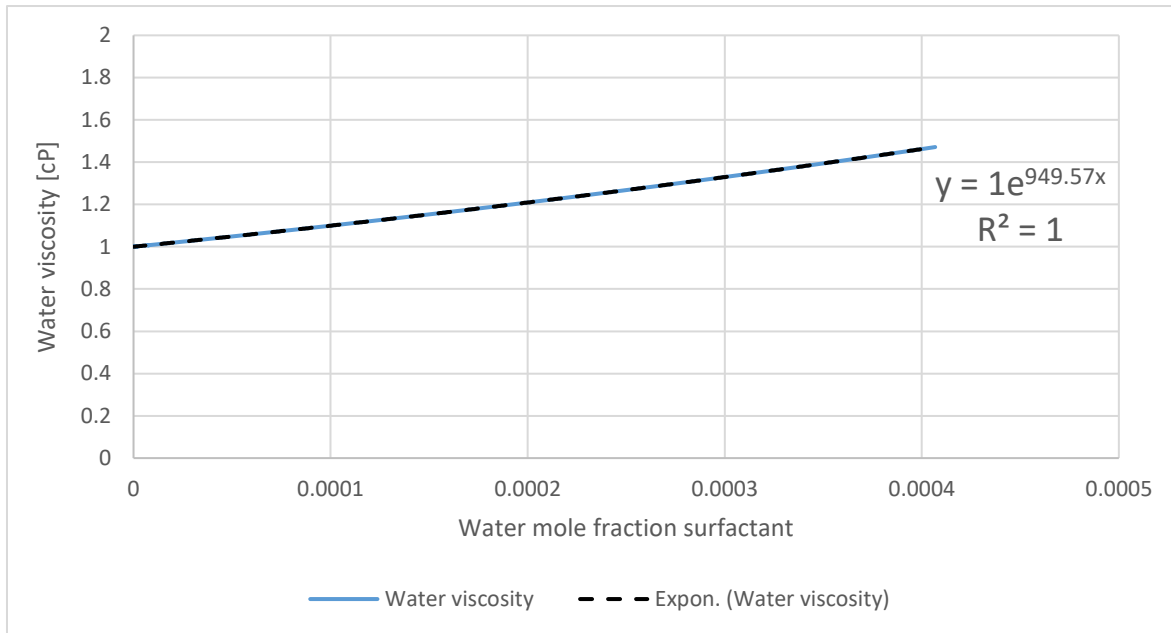


Figure 6 25: Water viscosity as a function of water mole fraction of surfactant (Block 50,1,1)

The plot confirms that the water viscosity increases exponentially with surfactant concentration when VSMIXFUNC is not included in the model. Therefore, VSMIXFUNC was not used when modelling the surfactant flooding of core R14. Polymer viscosity was modelled in the same way as the surfactant, with an exponential increase in viscosity with increasing polymer concentration. In addition, the viscosity was defined to be independent of shear rate, and therefore a function of the polymer concentration only. This is further discussed in section 7.4.

When surfactant solutions are injected into oil-filled mediums, a change in the viscosity of the solution may occur depending on the surfactant-oil-brine (SOB) phase behavior. In the coreflooding of core R14, the surfactant was injected in combination with low salinity brine. As discussed in section 3.2.2, this corresponds to a Winsor type I system, which makes it likely that swollen micelles of oil could have formed and increased the viscosity of the surfactant solution.

The laboratory data from core R14 did not include any information on micro emulsion viscosity. As a result, this was treated as a history matching parameter. The micro emulsion viscosity was modelled by ascribing it to the viscosity of the surfactant component in AVISC.

## 6.4 Interfacial tension and capillary number

In the coreflood experiment performed on core R14, low salinity surfactant solution was injected to reduce the interfacial tension between oil and water. Before modelling this process, it was necessary to investigate how STARS handles the reduction of interfacial tension in the simulations.

For the study, a simulation model was built on the basis of the petrophysical properties of core R14. Two separate relative permeability curves were defined for high salinity water with no surfactant, and high salinity water with maximum surfactant. Interpolation between the sets were activated for concentrations between the two. Interfacial tension was added to the model through the keyword IFTTABLE, and the values used can be seen in table 6.2.

*Table 6 4: Interfacial Tension values used in the verification study*

Water Mole Fraction Surfactant	Interfacial Tension [mN/m]
0	30
0.000427	0.2

The IFTTABLE included two data points representing interfacial tension at zero surfactant concentration and at maximum surfactant concentration. According to the STARS manual [55], the default method for interpolation of IFT is linear interpolation when doing a table lookup. To verify this, a simulation was run, and the interfacial tension from one specific block was plotted as a function of the water mole fraction of surfactant from the same block. The results can be seen in figure 6.26.

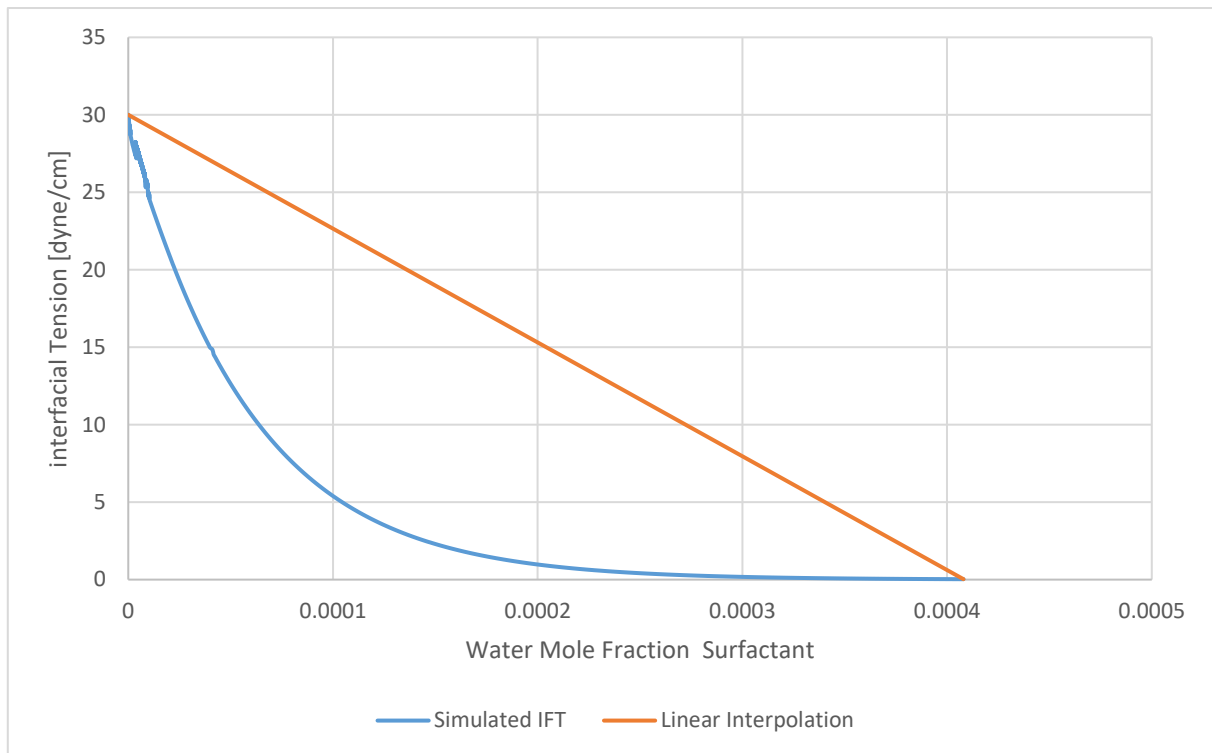


*Figure 6 26: Simulated interpolation between interfacial tension entries compared to the expected linear interpolation from the STARS manual.*

The figure shows that interpolation was not linear as expected from what was stated in the STARS manual. Instead, the IFT reduction appears to have been more rapid at low surfactant concentrations compared to at high concentrations. Despite not being in accordance with the STARS manual, this behavior is similar to that described in literature. According to Sheng [62], interfacial tension between oil and water changes significantly when surfactant is added at concentrations below critical micelle concentration (CMC). At concentrations above CMC, further addition of surfactant were reported to have no effect on IFT.

In conclusion, STARS does not seem to handle IFT reduction in the manner which is stated in the manual. However, the simulated IFT behavior is similar to that reported in literature, and therefore the modelling of IFT in STARS is considered adequate.

Another verification study was conducted to investigate how STARS handles modelling of capillary number. In order to ensure that STARS estimated capillary numbers correctly, simulated and manually calculated capillary number values were compared. According to the STARS manual [55], the simulator calculates the capillary number by substituting the velocity in equation 2.18 for Darcy's law, resulting in the following equation:

$$N_c = \frac{K_{abs} \cdot \Delta P}{\sigma_{ow} \Delta x} \quad (6.2)$$

To verify that this is the equation used by STARS, a simulation of a surfactant flood was run and the capillary numbers from one specific block was extracted. At the same time, interfacial tension and differential pressure values were extracted from the same block to be used for manual calculations. The comparison between the simulated and calculated values can be seen in figure 6.27. The results show little difference between the simulated and calculated values, which confirms that STARS uses equation 6.2 to calculate the capillary number.

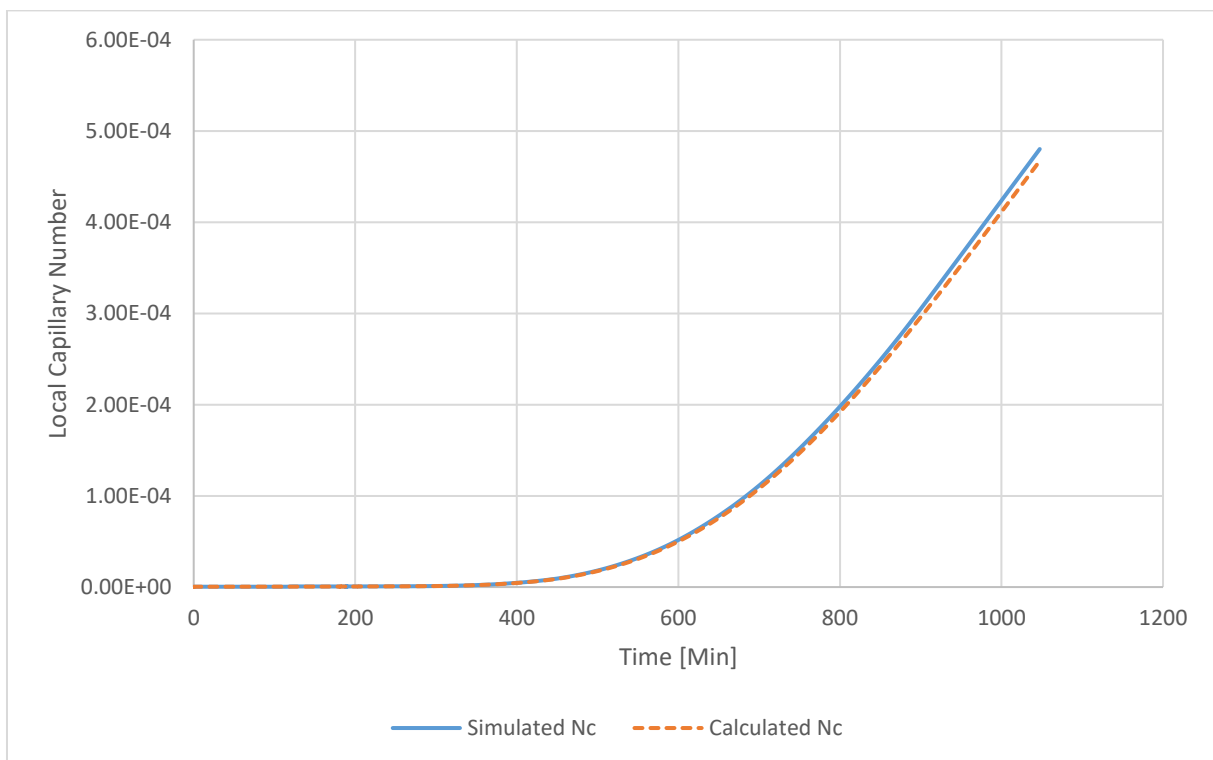


Figure 6 27: Comparison of simulated and calculated capillary numbers.

## 6.5 Surfactant and polymer adsorption

When modelling surfactant and polymer flooding, adsorption of components onto the rock surface must be considered. In the simulation model used in this thesis, adsorption follows the Langmuir isotherm correlation defined in equation 4.10. In order to verify that STARS calculates adsorption correctly, a verification study was performed.

The verification study consisted of comparing simulated adsorption to manually calculated adsorption. The calculated values were found using equation 4.10. The simulated values were obtained by simulating a surfactant flood with a surfactant adsorption of 0.2 mg/g. In STARS, adsorption is given in mol/cm<sup>3</sup>, and therefore a conversion from mg/g to mol/cm<sup>3</sup> had to be made. This was achieved by using the following equation [55]:

$$Ad_i \left( \frac{\text{mol}}{\text{cm}^3} \right) = Ad_i \left( \frac{\text{mg}}{\text{g}} \right) \cdot 10^{-3} \cdot \frac{(1 - \phi) \rho_{rock} \left( \frac{\text{g}}{\text{cm}^3} \right)}{\phi} \cdot \frac{1}{M_{W_i} \left( \frac{\text{g}}{\text{mol}} \right)} \quad (6.3)$$

Where  $Ad_i$  is the adsorption of component  $i$ ,  $\phi$  is porosity,  $\rho_{rock}$  is the density of the rock, and  $M_{W_i}$  is the molecular weight of component  $i$ .

The comparison between the simulated and calculated adsorption can be seen in figure 6.28.

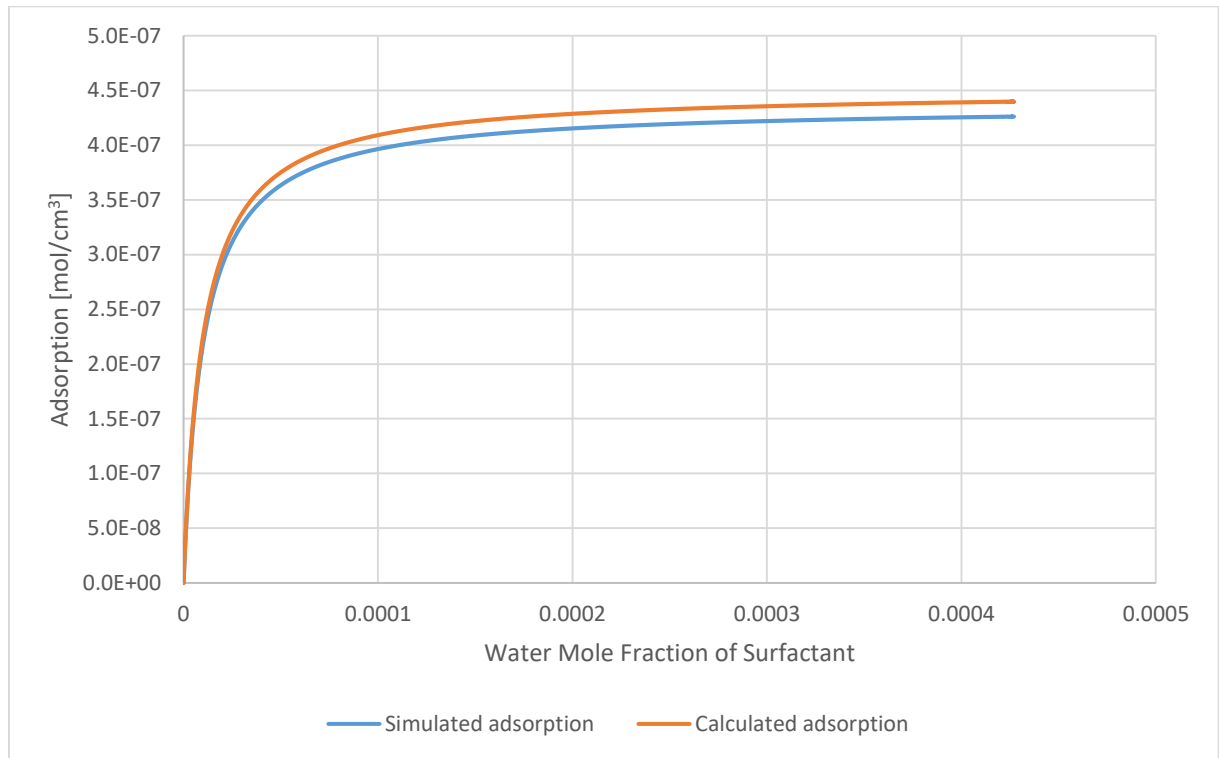
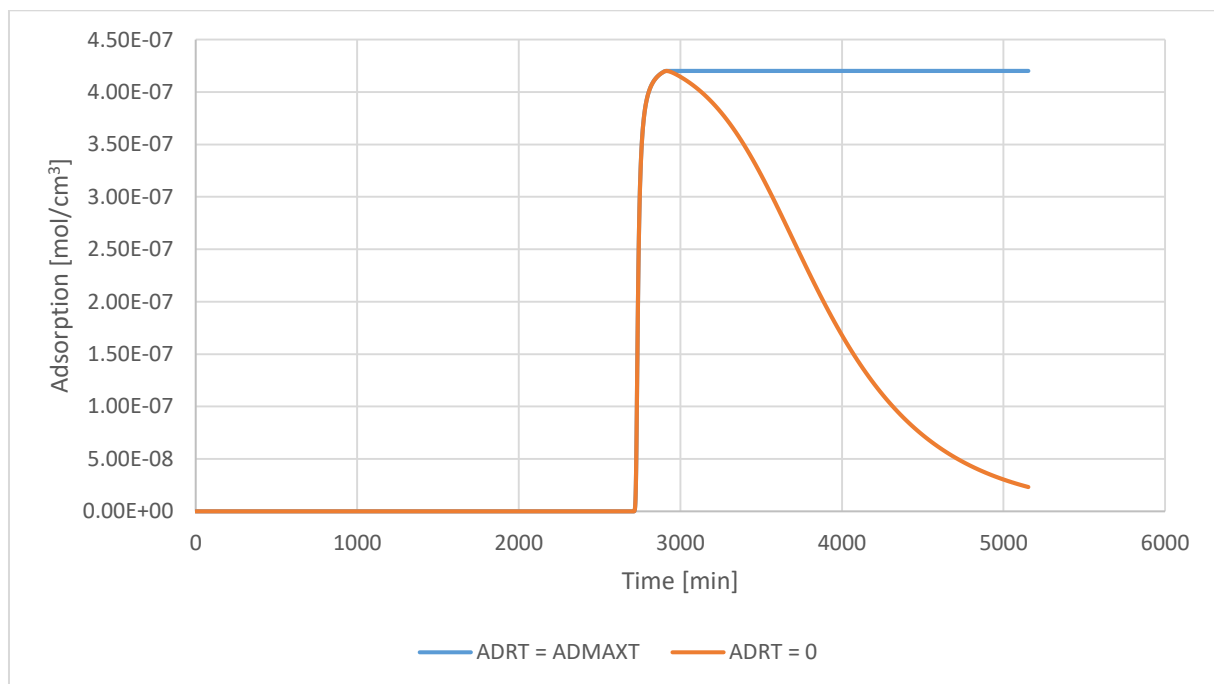


Figure 6.28: Comparison of simulated and calculated adsorption

The results show that there is little difference between the simulated and calculated adsorptions. This confirms that STARS calculates the adsorption as described in the STARS manual [55]. This verification is also applicable for the polymer adsorption, as it is also defined to follow the Langmuir isotherm correlation.

According to literature [62], adsorption is considered irreversible with concentration. As a result, surfactant and polymer adsorption was defined to be irreversible in the simulations performed in this thesis. This was achieved by defining the residual adsorption capacity (ADRT) to be equal to the maximum adsorption capacity (ADMAXT). In order to investigate if irreversible and reversible adsorption is modelled correctly in STARS, another verification study was performed. Using a model similar to that used in the history matching of core R14, two simulations were run; one with irreversible (ADRT = ADMAXT) adsorption and one with reversible (ADRT = 0) adsorption. The results can be seen in figure 6.29.



*Figure 6 29: Reversible and irreversible adsorption of surfactant*

The plot clearly indicates that STARS distinguishes between irreversible and reversible adsorption, and that the adsorption in the history matching model is in fact irreversible.

## 7 History Matching of Core R14

In this section, history matching of the low salinity surfactant polymer (LSSP) coreflooding of core R14 is presented. The section includes analyses of the individual flooding sequences, as well as a description of how a best match of the experimental results was achieved. The simulation model used to obtain a best match is included in the appendix.

Core R14 is one of several Berea sandstone outcrops that have been subjected to hybrid EOR experiments by UniResearch CIPR. The core has a measured porosity of 22.19%, and absolute permeability of 525 mD. Additional properties can be seen in table 7.1.

*Table 7 1: Properties of core R14*

Length [cm]	Diameter [cm]	Areal [cm <sup>2</sup> ]	Measured Vp [ml]	Porosity [%]	Permeability [mD]
14.83	3.79	11.28	37.13	22.19	525

LSSP slug injections was conducted on core R14 to investigate the effect combining low salinity water injection with surfactant and polymer flooding. Initially, the core was flooded with synthetic seawater, and absolute permeability was measured. The core was then drained with Peregrino crude oil at 60 °C for 3 days, and then aged. After aging, the Peregrino oil was exchanged with Brage stock tank oil. This was done at a temperature of 70 °C and at very slow injection rates. 2 weeks later, the effective oil permeability was measured and the coreflooding experiments were initiated. All experiments were performed at temperatures of 70 °C with a BPR of 12 bars. An overview of the coreflooding sequences can be seen in figure 7.1.

For the history matching, a one-dimensional simulation model was used. The block distribution was set to 100,1,1 in  $i$ ,  $j$  and  $k$  directions respectively, and the maximum time-step was limited to 1. These configurations were chosen based on the sensitivity study presented in section 6.2. In addition to this, a linear flow between the injector and the producer was defined through the use of the keyword TUBE-END under 'recurrent data'. This was considered a suitable model for inflow and outflow simulation.

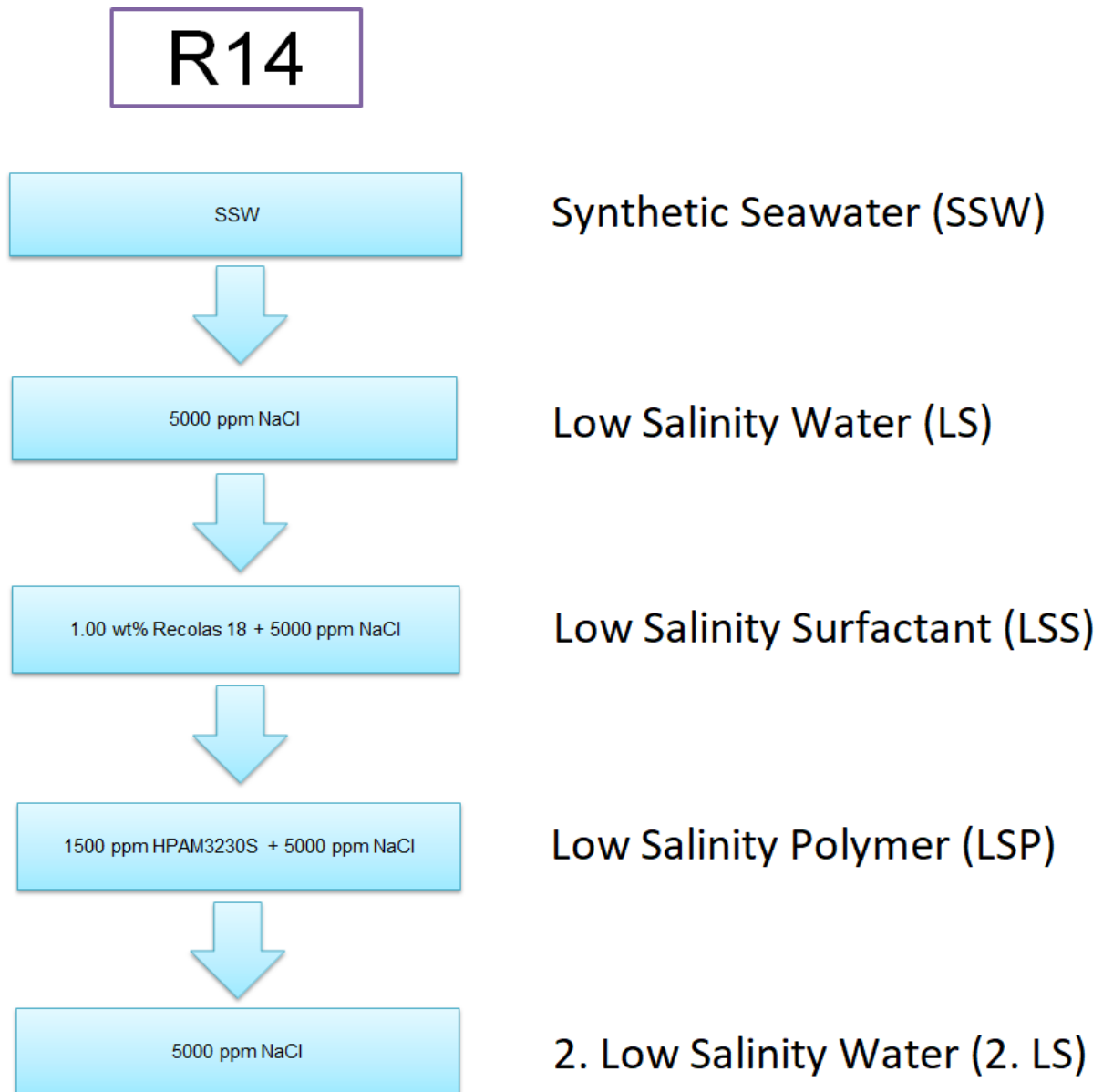


*Figure 7 1: Coreflooding sequences performed on core R14.*

Laboratory data from the experiment was provided in order to history match the coreflood. It contained the petrophysical properties of the core, the properties of the injected fluids, and data related to the individual flooding sequences. Key figures from the laboratory data can be seen under “Experimental data” in the Appendix. The experimental results from the coreflood can be seen in figures 7.2 and 7.3.

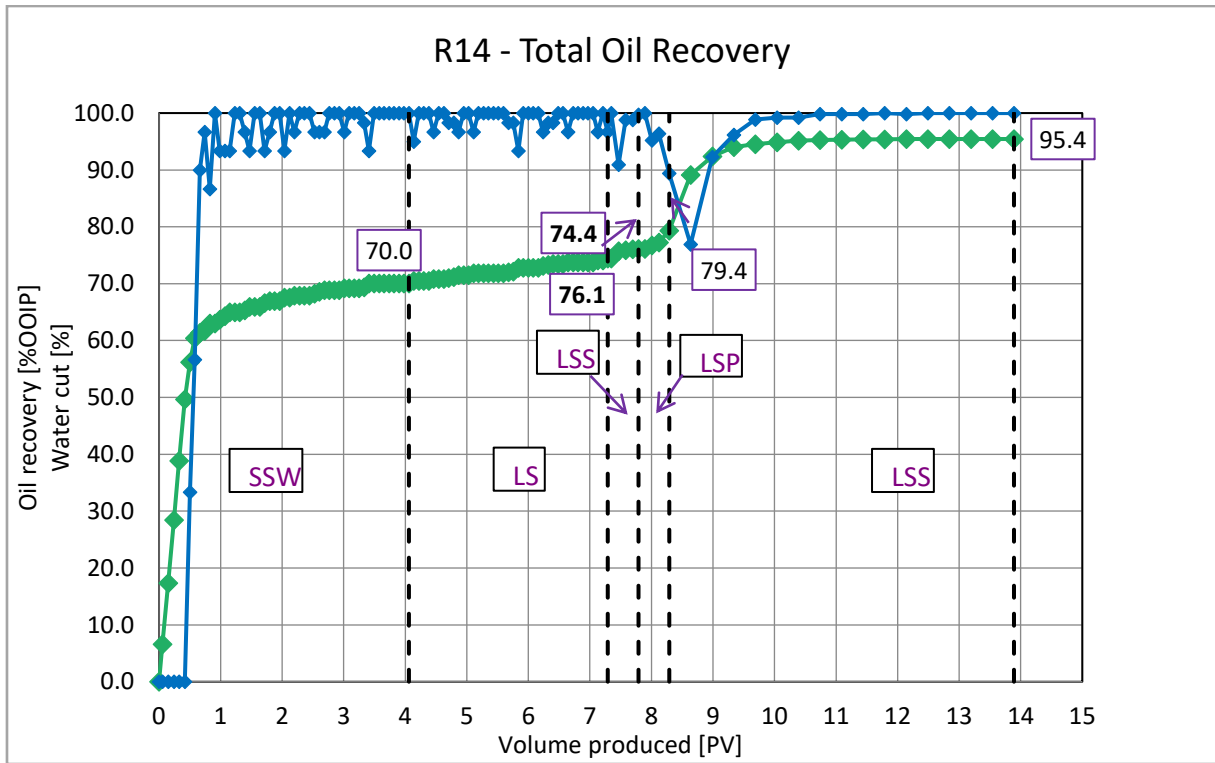


Figure 7 2: Experimental oil recovery and water cut for core R14. Plot is taken from laboratory data sheet.

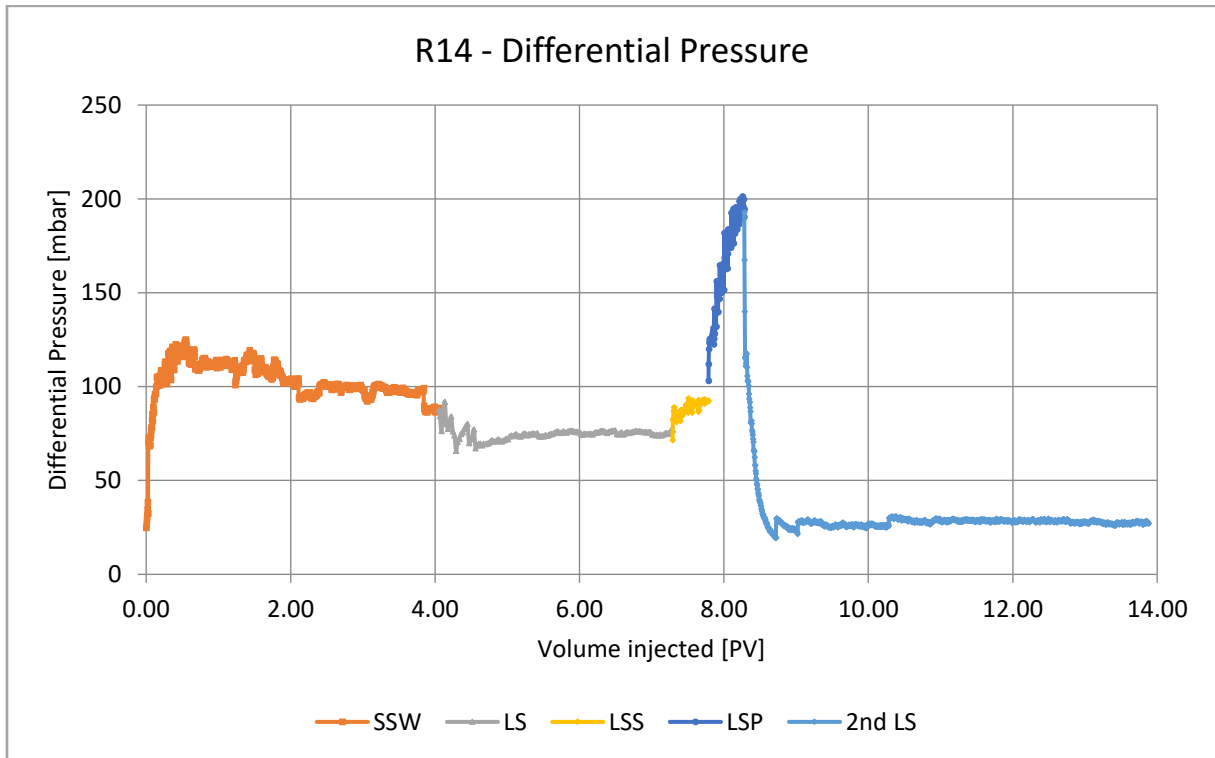


Figure 7 3: Experimental differential pressure for core 14. Plot is taken from laboratory data sheet.

## 7.1 R14 – synthetic seawater (SSW) flooding

In order to model the injection of synthetic seawater (SSW), relative permeability curves and salt composition was implemented in the model. The seawater composition was simplified for the simulation model, with salt being defined through the components  $\text{Na}^+$  and  $\text{Cl}^-$  only. The actual composition of the synthetic seawater can be seen in table 7.2.

Table 7 2: Chemical composition of the synthetic seawater used in coreflooding experiments.

Ion	$\text{Na}^+$	$\text{Ca}^{2+}$	$\text{Mg}^{2+}$	$\text{Cl}^-$	$\text{HCO}_3^-$	$\text{SO}_4^{2-}$	$\text{K}^+$
C (ppm)	11 159	471	1 329	20 130	142	2 740	349

The simulation of the synthetic seawater injection was run for 4 PV at an injection rate of 0.1  $\text{cm}^3/\text{min}$ . The viscosity of the synthetic seawater and Brage stock tank oil were set to experimental values of 0.5 and 3.0 cP.

Before history matching the process, a sensitivity study was performed in order to evaluate the wettability of the core.

### 7.1.1 Wettability evaluation

Since the composition of the connate water and the injected water were identical during synthetic seawater flooding, a wettability alteration did most likely not occur.

Due to extensive aging, the wettability of core R14 before SSW injection was assumed to be either intermediate wet or slightly water-wet. This was supported by the experimental production profile in figure 7.2, which shows two-phase production after water breakthrough.

To evaluate the wettability of the core, three simulations with different relative permeability curves representing different wettability conditions were run. The simulated results were then compared to the experimental data from the synthetic seawater flood to see which wettability conditions showed the best match.

The Corey functions presented in chapter 2.1.3 (equations 2.6-8) were used to create the relative permeability curves for the simulations. Experimental values for  $S_{wi}$ ,  $S_{or}$ ,  $k_{rw}(S_{or})$  and  $k_{ro}(S_{wi})$  were used, while Corey exponents  $n_w$  and  $n_o$  were altered to define the wettability conditions. The Corey exponents used in the simulations, along with their corresponding

wettability conditions, can be seen in table 7.3. Simulated relative permeability curves are shown in figure 7.4

Table 7 3: Corey parameters for intermediate wet, more water wet and more oil wet cases

	$n_w$	$n_o$
More oil wet	3	4
Intermediate wet	2	5
More water wet	1	6

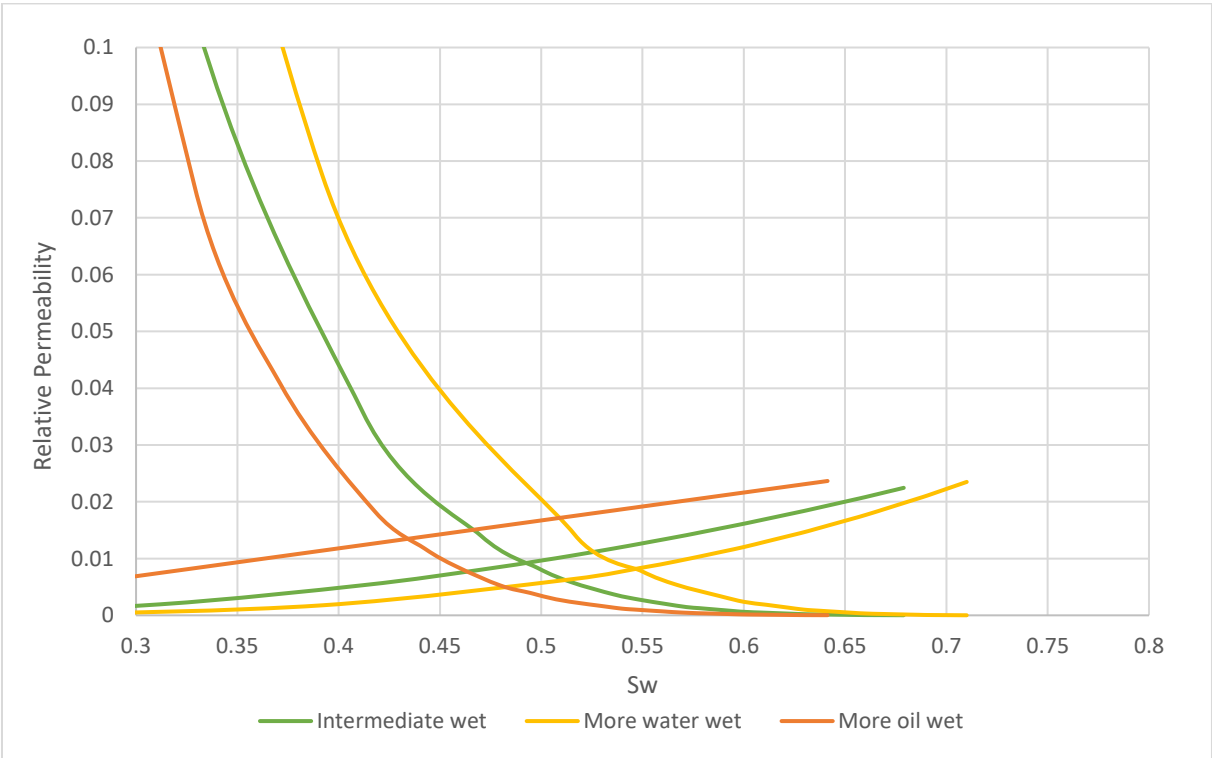


Figure 7 4: Simulated relative permeability curves for different wettability conditions, with altered x-axis.

According to Craig’s rules of thumb [13], relative permeability curves should have crossover points at water saturations above 50% for water wet conditions and below 50% for oil wet conditions. Intermediate wet conditions should have crossover point at approximately 50%. As can be seen from figure 7.4, the simulated relative permeability curves for the different wettability conditions are consistent with these rules.

In figures 7.5-6, simulated oil recovery and differential pressure for the different wetting conditions is compared to experimental values in order to evaluate the wettability of the core.

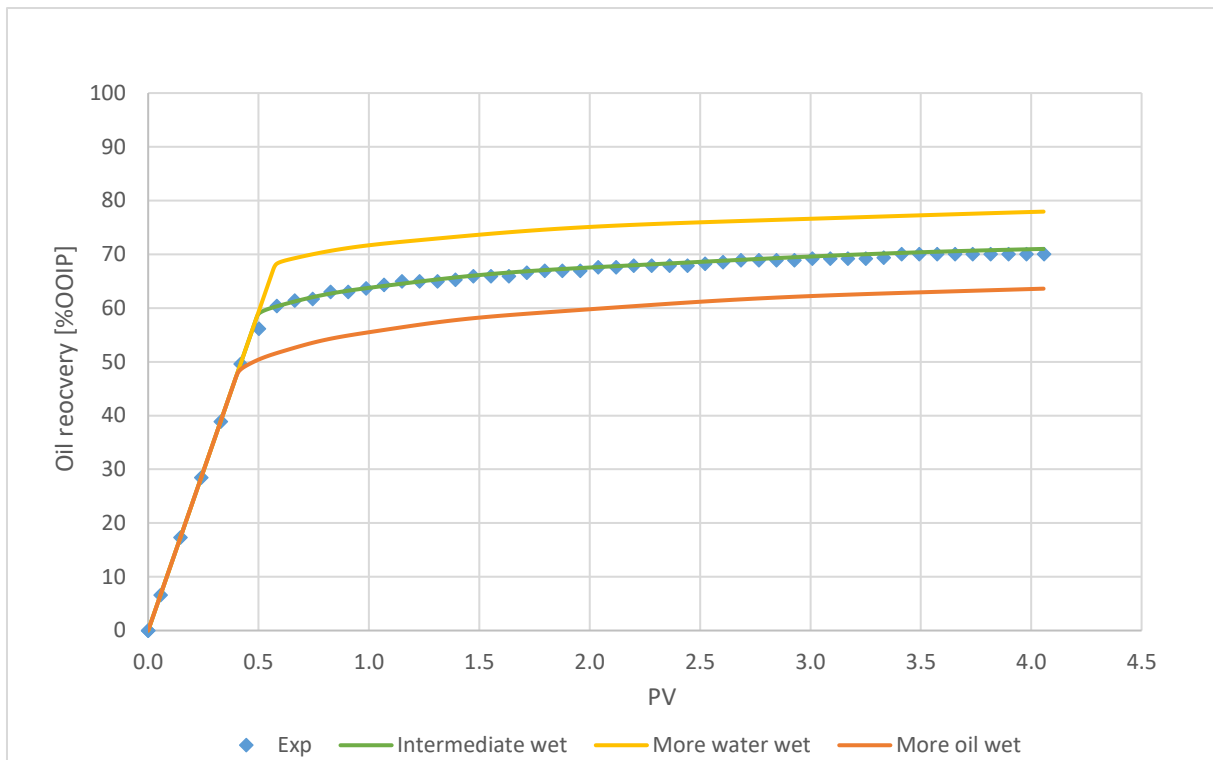


Figure 7 5: Simulated oil recovery for different wettability conditions.

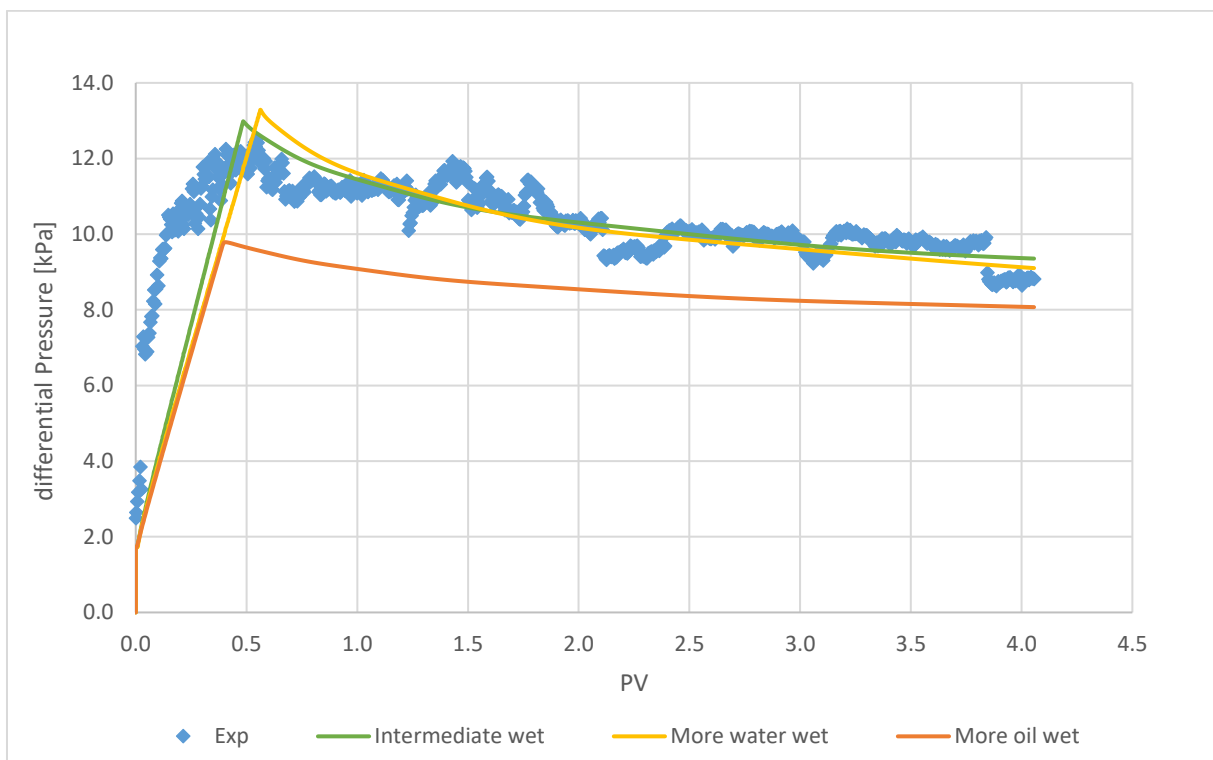


Figure 7 6: Simulated differential pressure for different wettability conditions.

The results show that the oil production and differential pressure is sensitive to changes in wettability. More oil wet conditions results in earlier water breakthrough, lower oil recovery, and lower differential pressure, while more water wet conditions had the opposite effects. This is consisted with the observations made in the sensitivity study in section 6.1.

Figures 7.5-6 show that the intermediate wet conditions gave the closest match to the experimental results. This is particularly evident in the oil recovery curve, which shows an almost complete match. This indicates that the wettability of core R14 is likely to have been intermediate during synthetic seawater injection. However, figure 7.4 shows very low end-point water relative permeabilities. According to Craig’s rules of thumb, this suggest more water wet conditions. As a result, the wettability of the core was thought to be somewhere in the range of intermediate to slightly water wet.

### 7.1.2 History matching

In this section, history matching of the synthetic seawater flood is presented. A best match of oil recovery and differential pressure was achieved by altering the relative permeability curves in the simulation model. First, an initial guess of Corey parameters was made based on experimental values and the observations from the wettability evaluation.

In order to make an initial guess, end-point relative permeabilities of water and oil had to be calculated from experimental permeability values.

Table 7 4: Experimental permeability values

Absolute Permeability [mD]	Water Permeability after SSW [mD]	Water Permeability after LS [mD]	Oil Permeability after aging [mD]
525	15	18	300

$k_{rw}(S_{or})$  and  $k_{ro}(S_{wi})$  were estimated to be 0.029 and 0.571, respectively. These values, along with experimental  $S_{wi}$  and  $S_{or}$  and Corey exponents for intermediate wet conditions, were used in the initial guess. Table 7.5 lists the experimental, initial guess, and best match Corey parameters values used in the history matching.

Table 7 5: Experimental, initial guess and best match values for SSW flooding.

	Experimental	Initial Guess	Best Match
$S_{wi}$	0.16	0.16	0.16
$S_{or}$	0.25	0.25	0.26
$k_{rw}(S_{or})$	0.029	0.029	0.025
$k_{ro}(S_{wi})$	0.571	0.571	0.571
$n_w$	-	5	4.9
$n_o$	-	2	1.6

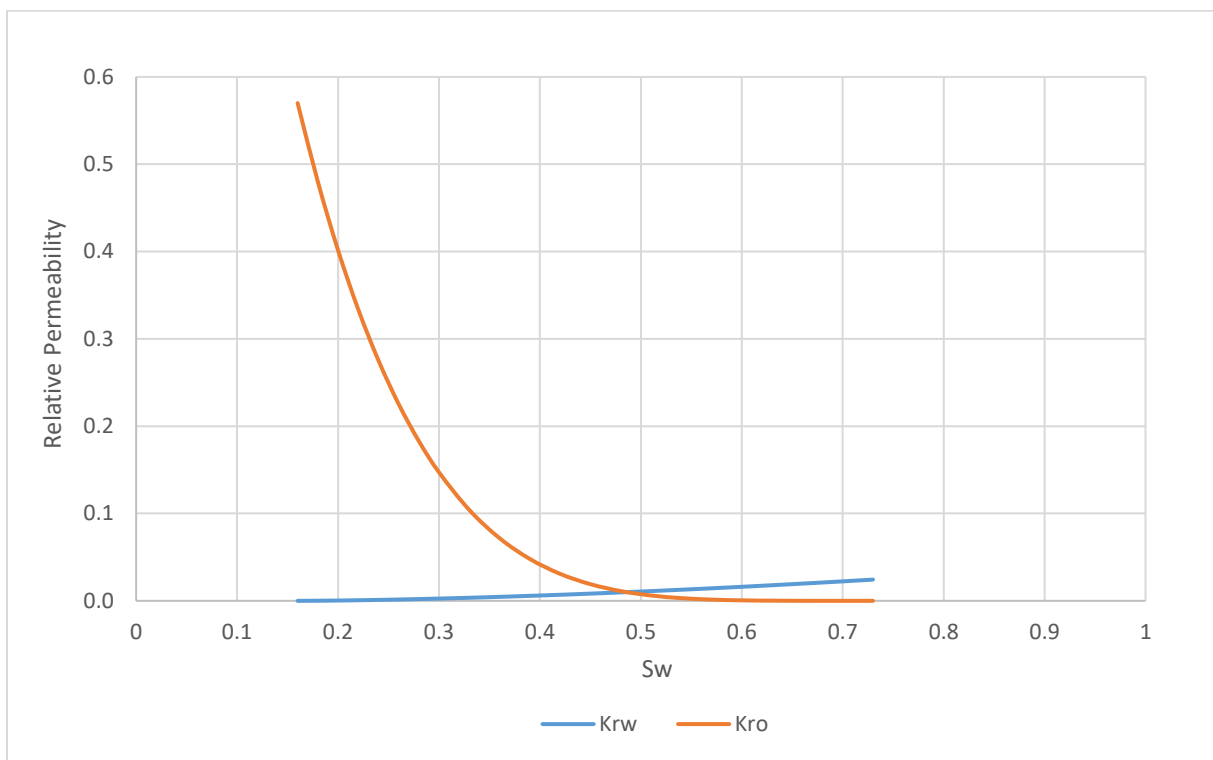


Figure 7 7: Relative permeability curves yielding the best match for SSW flooding.

To achieve a best match of oil recovery and differential pressure, the curvature of the water and oil relative permeability curves were altered. This was done by changing  $n_w$  from 2→1.6 and  $n_o$  from 5→4.9. In addition to this,  $k_{rw}(S_{or})$  was reduced from 0.029→0.025 and  $S_{or}$  was increased from 0.25→0.26. Due to the uncertainties related to laboratory measurements, these alterations were considered to be within an acceptable range. Figures 7.8-9 show the best match of oil recovery and differential pressure for the SSW flood.

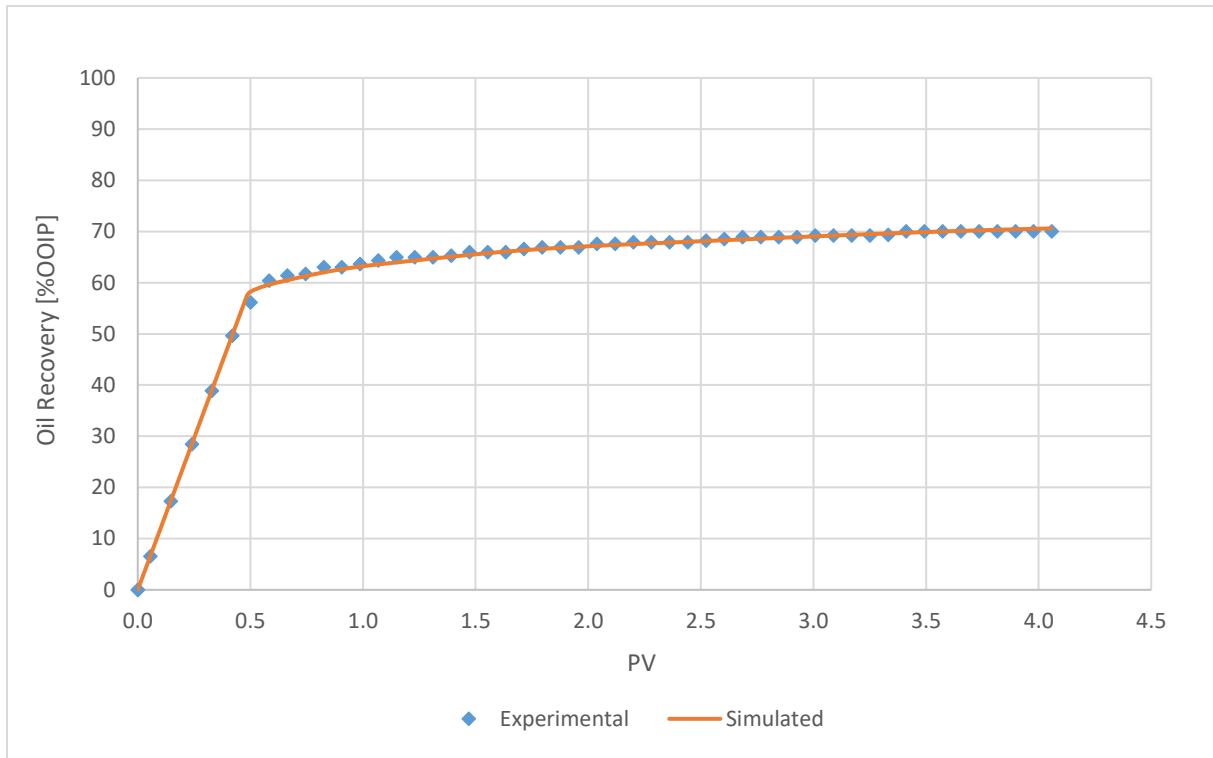


Figure 7 8: History match of oil recovery for the SSW flood.

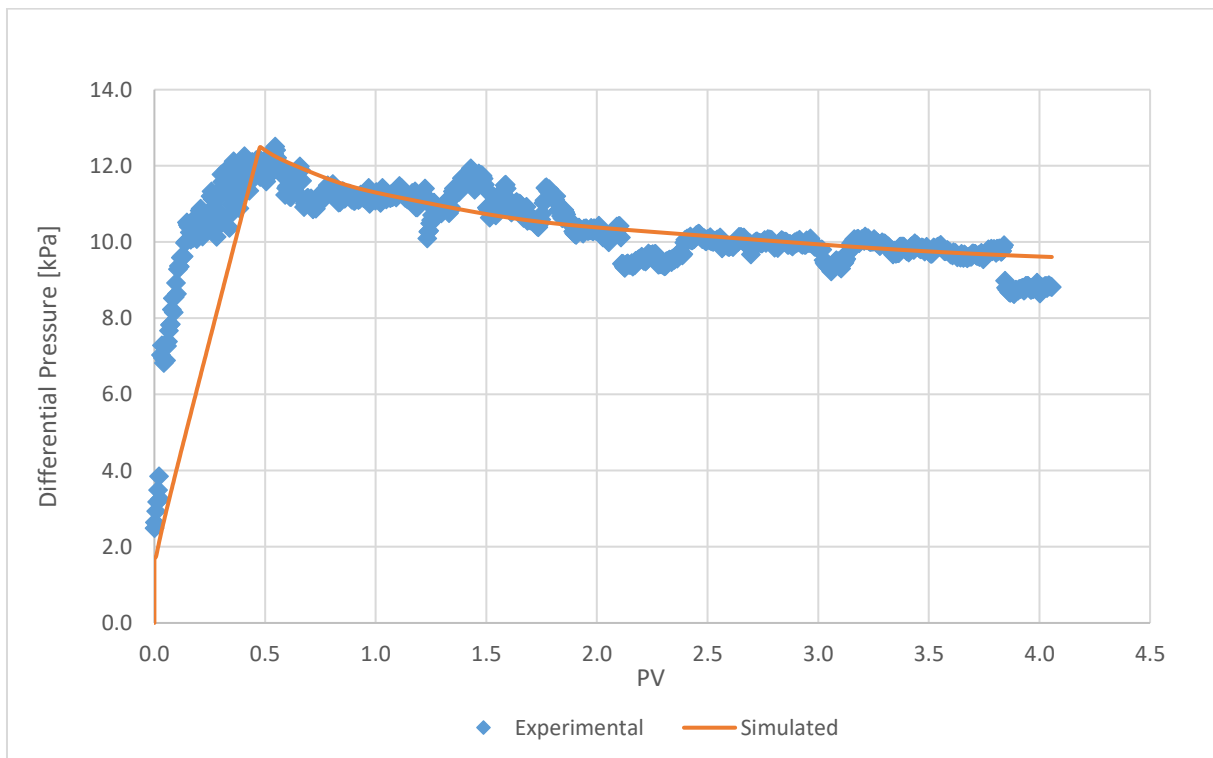


Figure 7 9: History match of differential pressure for the SSW flood.

Figure 7.8 shows that an accurate match of oil recovery was obtained, with water breakthrough occurring at approximately 0.5 PV. Figure 7.9 shows that the simulation model was not able to accurately match the initial pressure build-up before breakthrough. This has been reported in previous studies as well [57] [58], and is likely due to the simulator not being able to generate pressure fast enough. The simulated pressure peak and subsequent pressure decline matches the experimental values well. The exception is around 4.0 PV, where there is a significant drop in the experimental values. This is most likely due to an experimental error when transition from high salinity to low salinity injection.

## **7.2 R14 – Low salinity water (LS) flooding**

According to the experimental results in figures 7.2-3, the injection of low salinity water resulted in a slight increase in oil recovery, in addition to reduced differential pressure. In order to model the process, a new set of relative permeability curves representing the low salinity water was added to the model. To model the synthetic seawater, the relative permeability curves yielding the best match for the SSW flood was used. Salinity based interpolation was activated to model relative permeability when transition from SSW to LS floods.

The simulation of the LS flood was run for 3.2 PV at an injection rate of 0.1 cm<sup>3</sup>/min. The water viscosity was kept at 0.5 cP, equal to that of the synthetic seawater.

### **7.2.1 History matching**

A best match of oil recovery and differential pressure was achieved by altering the relative permeability curves of the low salinity water. First, an initial guess was made based on the experimental values from the LS flood the Corey exponents yielding the best match for the SSW flood. Table 7.6 lists the experimental, initial guess, and best match values for the low salinity flood.

Table 7 6: Experimental, initial guess and best match values for LS flooding.

	Experimental Values	Initial Guess	Best Match
$S_{wi}$	0.16	0.16	0.16
$S_{or}$	0.22	0.22	0.22
$k_{rw}(S_{or})$	0.034	0.034	0.034
$k_{ro}(S_{wi})$	0.571	0.571	0.571
$n_w$	-	1.6	1.7
$n_o$	-	4.9	5.1

To achieve a best match, only minor adjustments of Corey exponents  $n_w$  (1.6→1.7) and  $n_o$  (4.9→5.1) had to be made. The rest of the Corey parameters were kept at experimental values. The relative permeability curves yielding the best match is shown in figure 7.10.

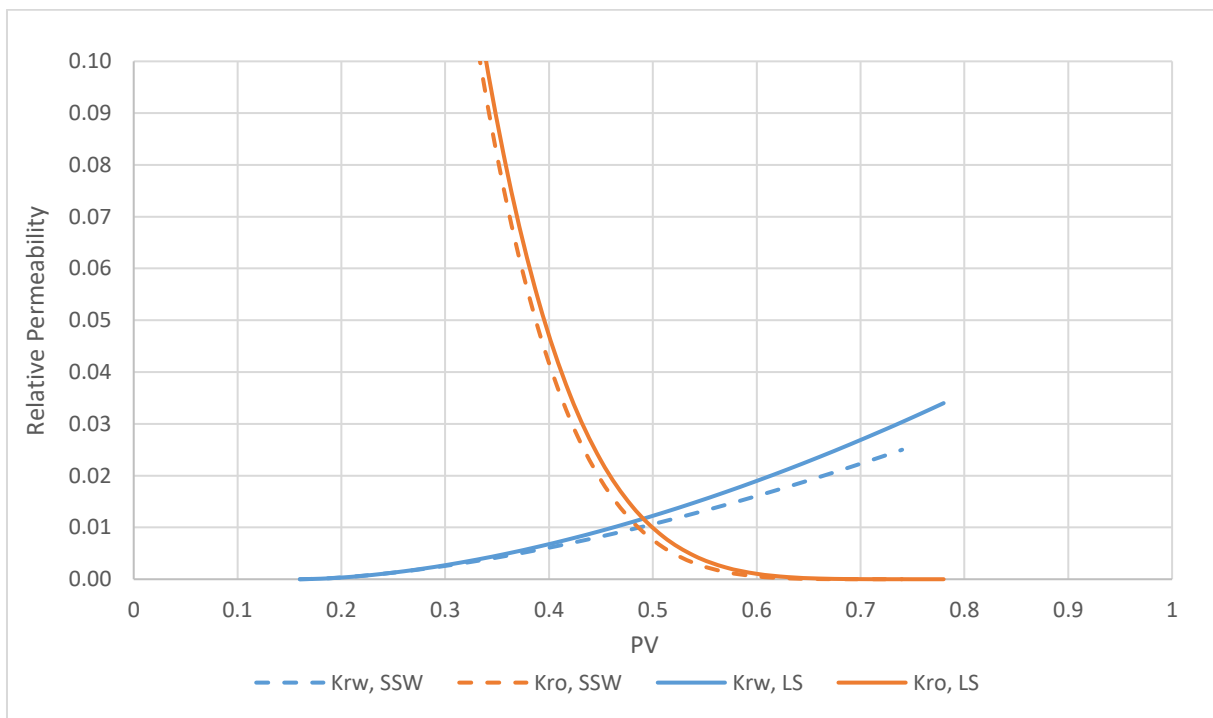


Figure 7 10: Relative permeability curves yielding the best match for the LS flood.

The plot shows an increase in end-point water relative permeability for the LS flood compared to the SSW flood. This indicates a shift towards more oil wet conditions. The best matches of oil recovery and differential pressure can be seen in figures 7.11-12.

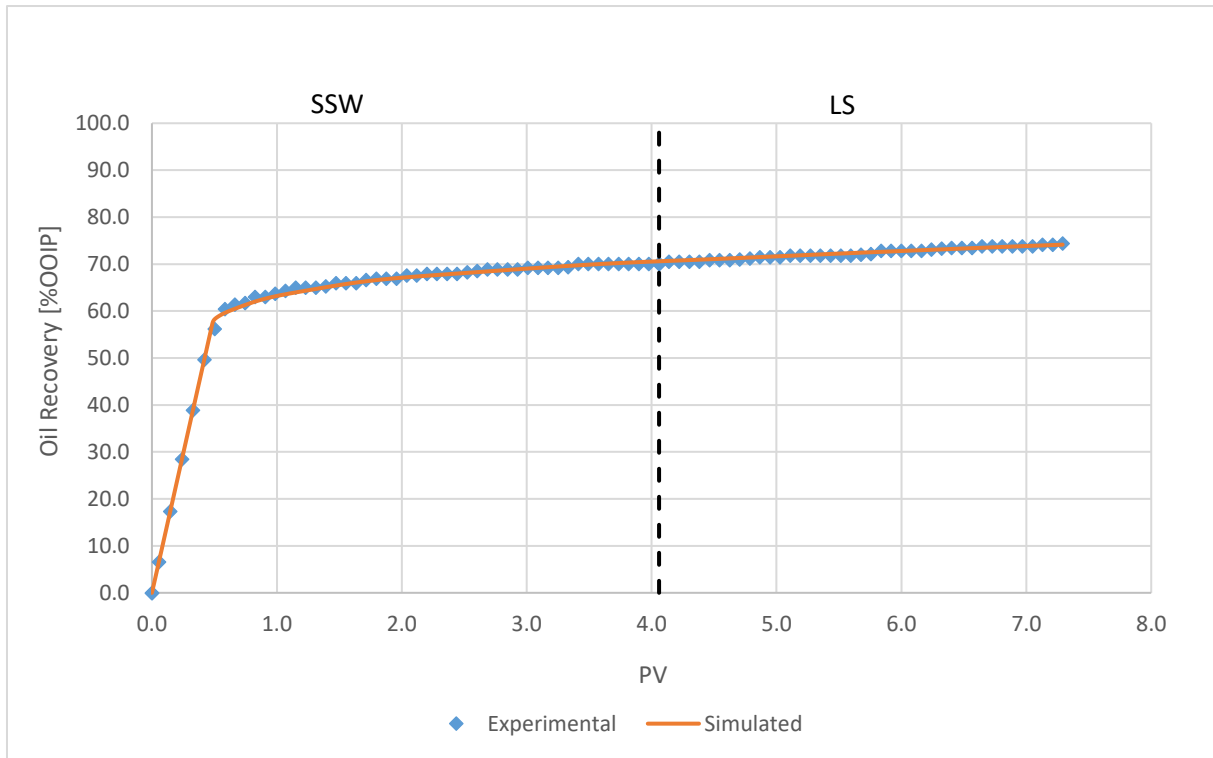


Figure 7 11: History Match of oil recovery for the SSW and LS floods.

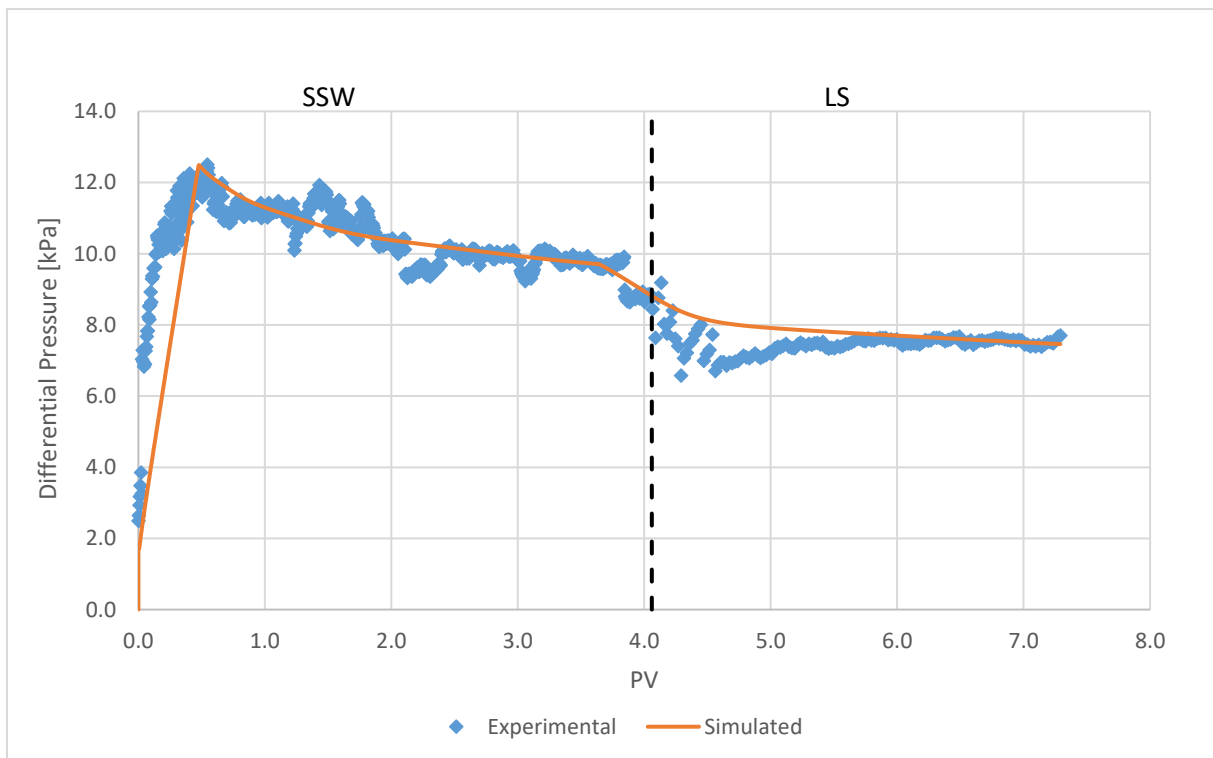


Figure 7 12: History match of differential pressure for the SSW and LS floods.

As can be seen from figure 7.11, there was no significant spike in oil recovery as a result of low salinity injection. Instead, the production increases steadily throughout the process. This indicates that the low salinity injection had little immediate effect on the oil recovery. The incremental production observed is most likely a result of the SSW injection not being continued until an ultimate  $S_{or}$ . As can be seen from figure 7.11, the simulated oil recovery matched the experimental values well.

Figure 7.12 shows that the transition from SSW injection to LS injection resulted in a drop in differential pressure. This is similar to what was observed for core R3 by Drønen [57]. Since no significant spike in oil production is seen, the decline in differential pressure is likely due to a redistribution of phases. This supports the indication of a wettability alteration towards more oil wet conditions during low salinity flooding.

Figure 7.12 shows that a good match between simulated and experimental differential pressure was found for the pressure plateau and end-point values. However, there is a mismatch in the pressure drop when switching to low salinity injection. This could be due to errors in experimental values, too high dispersion, or not enough flexibility in the relative permeability functions. Drønen [57] encountered similar problems when history matching core R3, and suggested that the mismatch could be due to the salinity based interpolation implemented in the model.

### 7.3 R14 - Low salinity surfactant (LSS) flooding

A slug of low salinity surfactant (LSS) solution was injected into the core after approximately 7.3 PV. In order to simulate the process, a new rock type was added to the model, in which two new sets of relative permeability curves were defined. These sets represented relative permeabilities of synthetic seawater and low salinity surfactant solutions, with interpolation between the curves being based on logarithm of capillary number. This setup was described in detail in section 4.4.

The simulation of the surfactant flood was run for 0.5 PV at an injection rate of 0.1 cm<sup>3</sup>/min. According to the laboratory data, 1 wt% of the surfactant “Recolas 18” was injected in combination with 5000 ppm low salinity brine. This corresponds to a Winsor type I system, as discussed in section 6.3.

The laboratory data did not provide any interfacial tension values, therefore the IFT values used by Jarlsby [58] were adopted. The interfacial tension was activated through the keyword IFTTABLE, and defined to only be a function of the surfactant concentration. The IFTTABLE used in the model can be seen in figure 7.13. The viscosity of the surfactant solution was not provided either, and therefore surfactant viscosity was treated as a history matching parameter.

Table 7 7: Simulated properties of “Recolas 18”.

Molecular weight [g/mol]	Injected mole fraction	IFT - no surfactant (mN/m)	IFT – max surfactant [mN/m]
426	0.000427	30	0.02

```

IFTTABLE
**  cift          SIGIFT
    0             30
    0.000001     0.1
    0.000005     0.05
    0.00001      0.02
    0.00005      0.02
    0.00026      0.02
    0.000427     0.02
  
```

Figure 7 13: IFTTABLE defining the interfacial tension in the model.

## 7.4 R14 – low salinity polymer (LSP) flooding

Directly after the surfactant flood, a slug of low salinity polymer (LSP) solution was injected. Due to the interpolation difficulties discussed in section 4.4, the polymer solution was not represented by its own set of relative permeability curves in the simulations. Instead, it was modelled as a viscosity effect only.

The simulation of the polymer flood was run for 0.5 PV at the same constant injection rate as in the surfactant flood. According to the laboratory data, the injected polymer solution consisted of 1500 ppm HPAM3230S and 5000 ppm NaCl. Additional properties can be seen in table 7.8.

Table 7 8: Simulated properties of HPAM3230S

Molecular weight [g/mol]	Injected mole fraction
$6.0 \cdot 10^6$	$4.51 \cdot 10^{-9}$

As mentioned in section 3.3, polymers solutions are known to have shear dependent viscosities. In the laboratory data from core R14 however, no such dependency was specified. In addition to this, due to the constant injection velocity, the shear rate interval was assumed to be constant during the polymer flooding. An assumption was therefore made that the viscosity of the polymer solution was independent of shear rate. As a result, the polymer viscosity was modelled as a function of the polymer concentration only. This was specified in the model through a shear rate table, which can be seen in figure 7.14.

```
SHEARTAB
** Darcy velocity Viscosity
** (cm/min) (cP)
0.00001      5.7
0.0001       5.7
0.001        5.7
0.01         5.7
0.1          5.7
```

Figure 7 14: shear rate table defining the polymer viscosity at different Darcy velocities.

## 7.5 R14 – combined low salinity surfactant polymer (LSSP) flooding

In this section, the history matching of all injection sequences performed on core R14 is presented. Due to the combined effects of low salinity surfactant and polymer injection, it is necessary to present the history match of the complete process, as opposed to presenting matches of surfactant and polymer floods separately.

History matching of all injection sequences required the implementation of a multiple interpolation scheme in the simulation model. A description of this setup was presented in section 4.4. In addition to this, alterations of multiple parameters related to the surfactant, polymer and low salinity water was necessary.

Due to the complexity of the experiment, the basic sensitivity studies presented in section 6.1 were not sufficient to predict the outcome of altering certain parameters. As a result, additional sensitivity studies specifically related to the history matching was conducted. These are presented in the following section.

### 7.5.1 Sensitivity of LSSP matching parameters

#### 7.5.1.1 Extended LS water relative permeability curve

Due to low salinity water being injected as chase water after the polymer slug, the low salinity relative permeability curves in rock type 2 had to be extended from those yielding the best match for the low salinity flood. To match the differential pressure of the chase water, the water relative permeability for the low salinity flood had to be increased significantly. Initially, a continuous transition from  $k_{rw}(S_{or})_{LS}$  to  $k_{rw}(S_{or})_{chase\ water}$  was attempted. This yielded a too high simulated differential pressure for the chase water. After extensive experimentation, it was found that an instantaneous transition was needed to achieve a low enough pressure. This is shown in figures 7.15-16.

End-point effective permeability of water was measured to be 315 mD after the chase water flood. This corresponds to an experimental  $k_{rw}(S_{or})$  of 0.60. Due to difficulties in achieving a low enough simulated pressure during 2. LS flood, this value was increased to 1.00 for the extended low salinity curve. This is shown in figures 7.17-18.

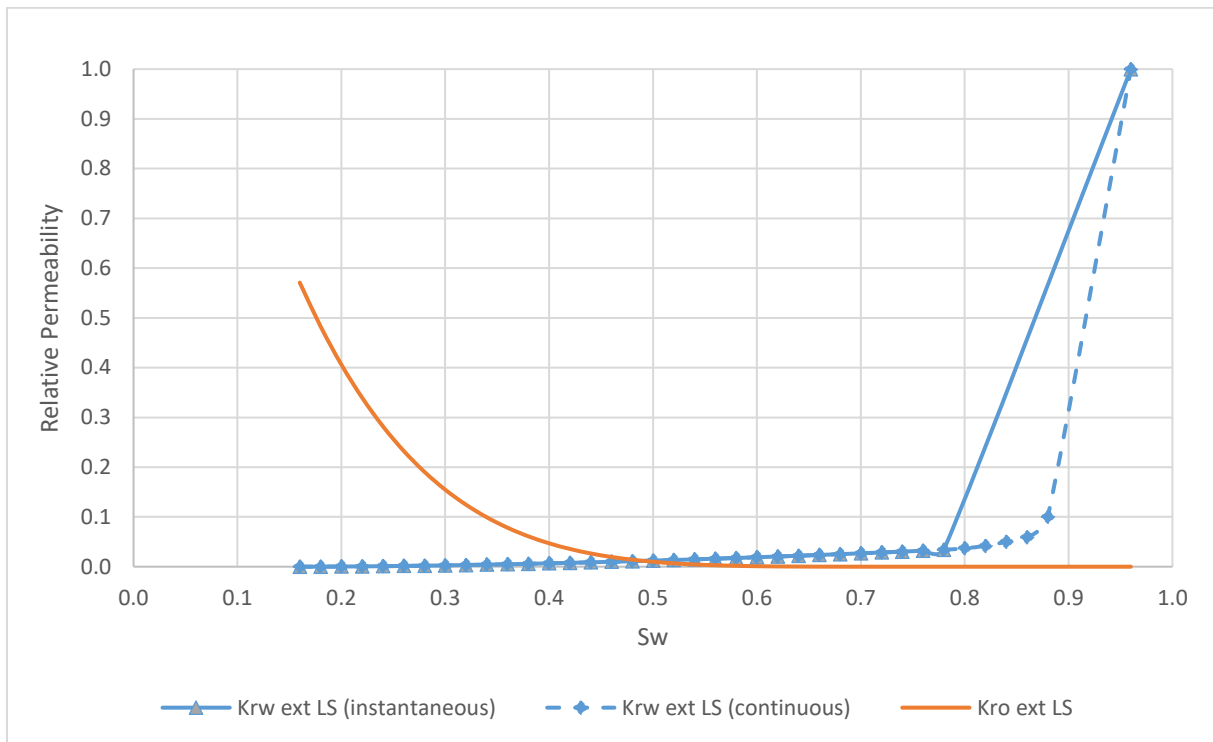


Figure 7 15: Extended LS relative permeability curves (instantaneous vs continuous)

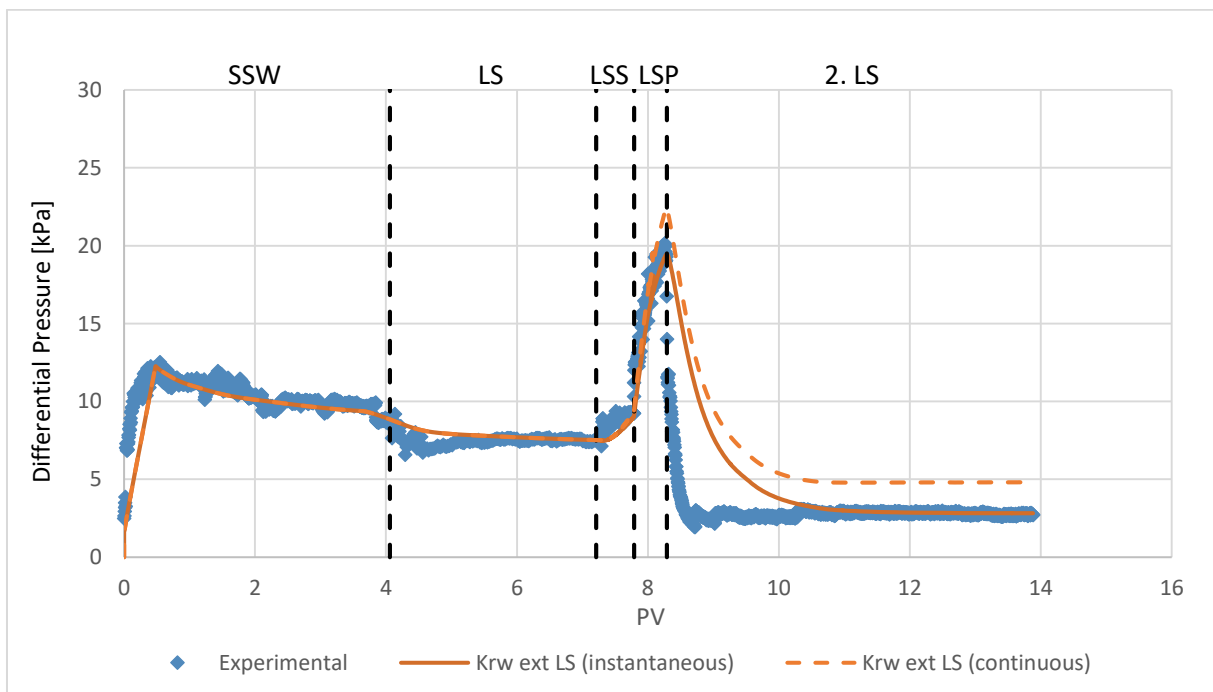


Figure 7 16: Differential pressure match for the different extended LS relative permeability curves (instantaneous vs continuous)

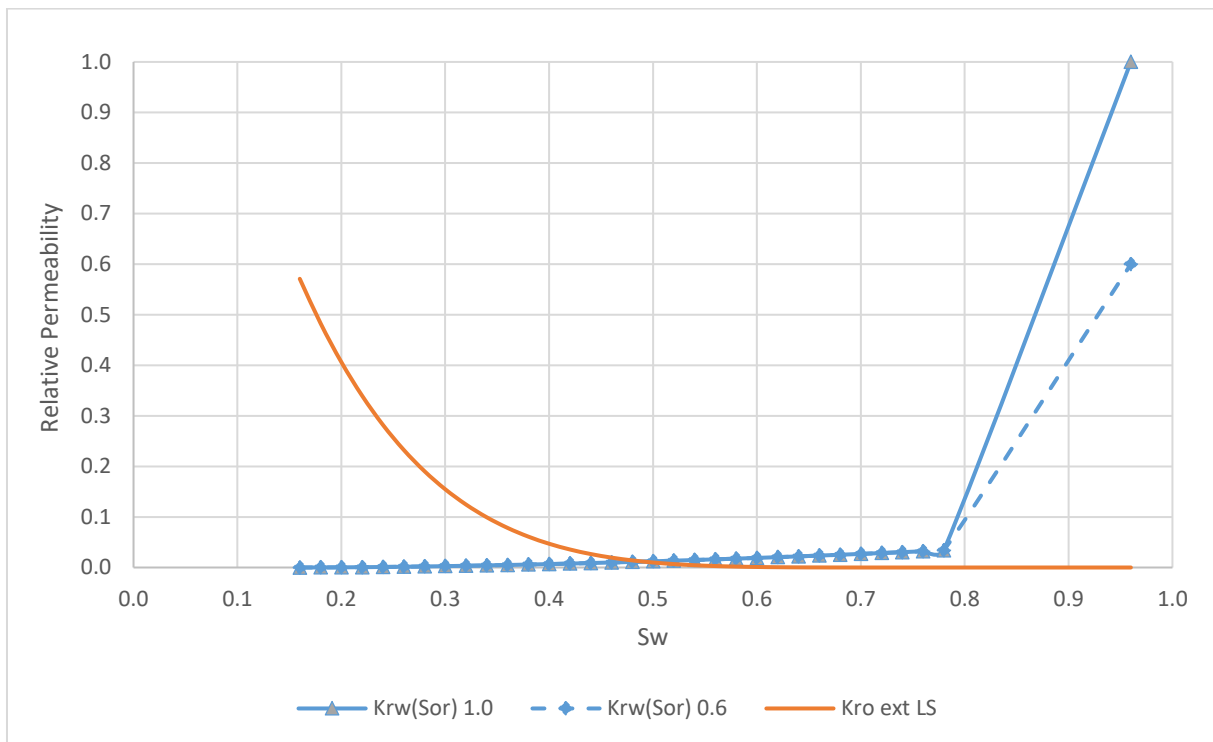


Figure 7 17: Extended LS relative permeability curves for different  $k_{rw}(S_{or})$  values

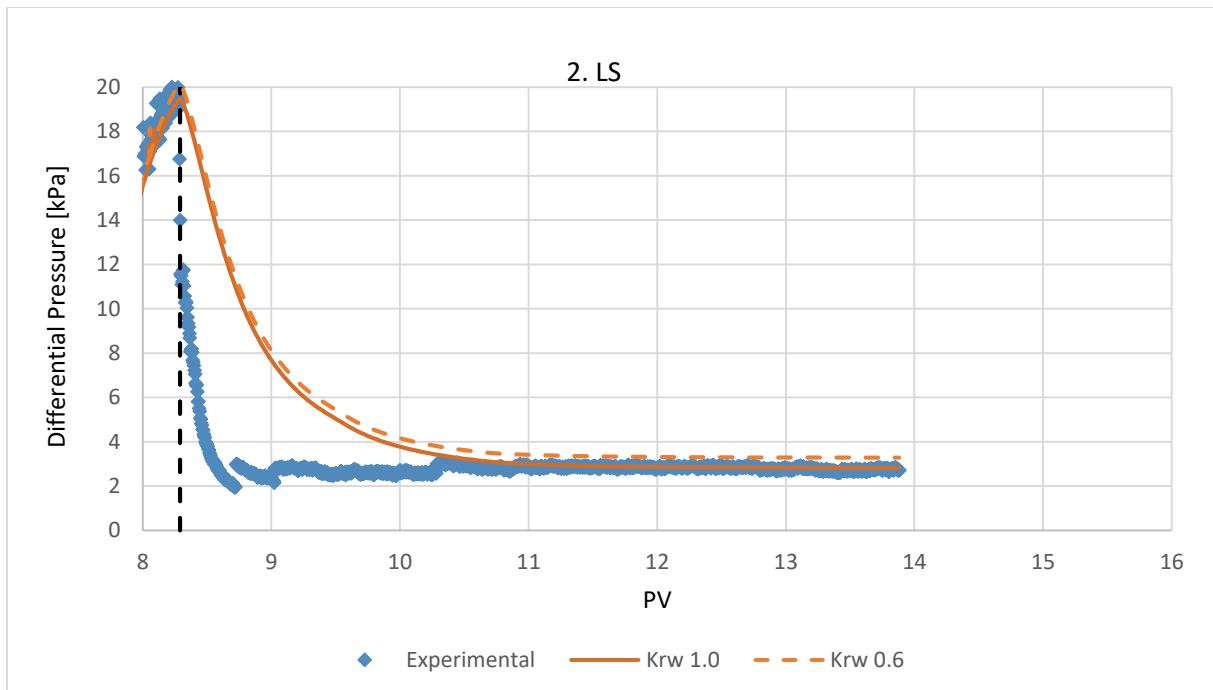


Figure 7 18: Differential pressure match for different  $k_{rw}(S_{or})$  values

### 7.5.1.2 LSS oil relative permeability curve

In order to capture the increased oil recovery from surfactant and polymer injection, the oil mobility had to be increased in the surfactant relative permeability curves. This was done by adjusting the Corey exponent  $n_o$ . The effect of adjusting  $n_o$  can be seen in figures 7.19-20.

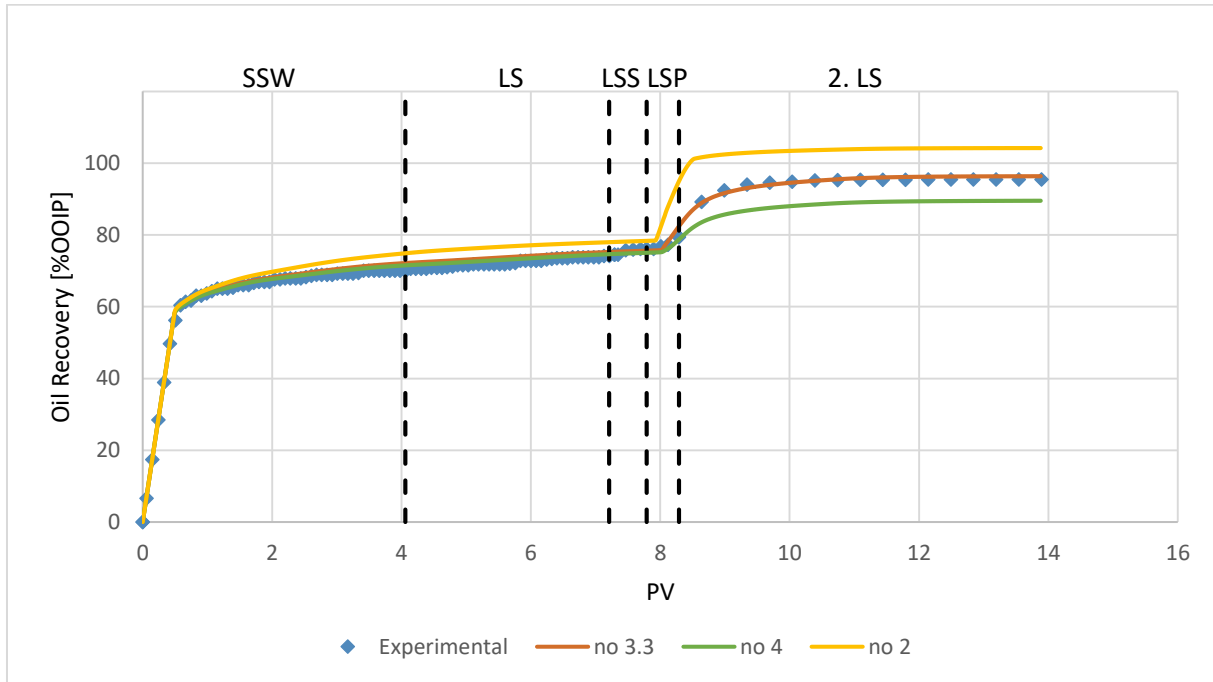


Figure 7 19: Oil recovery for varying  $n_o$

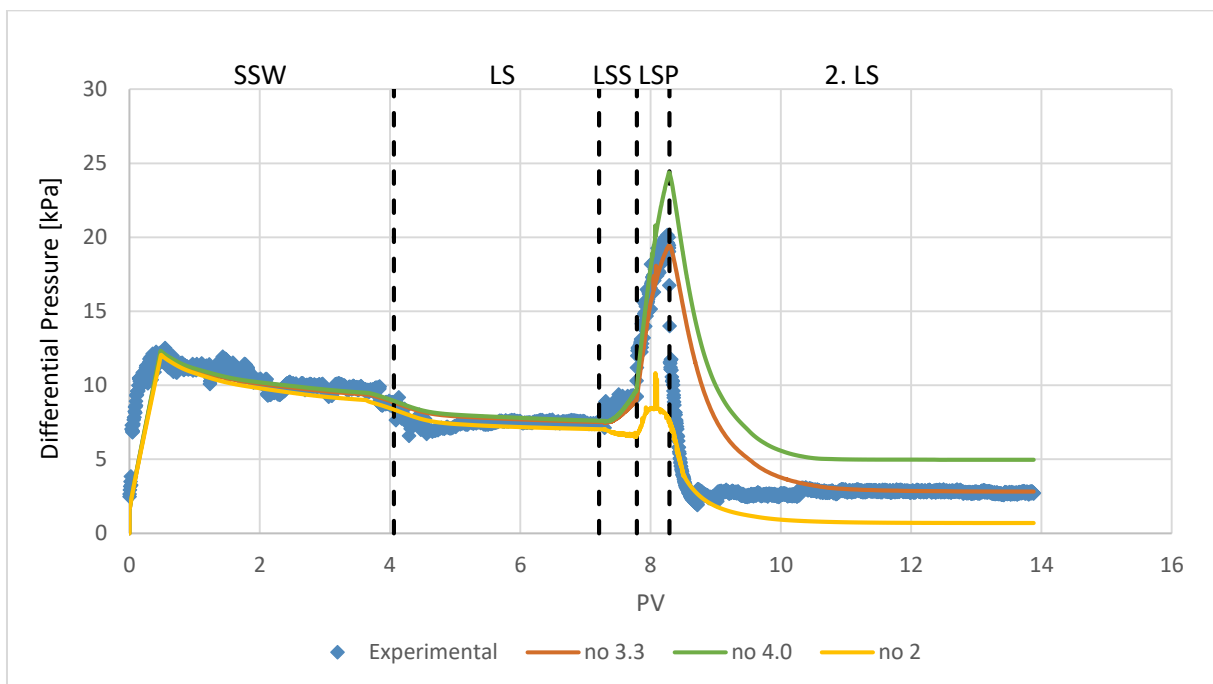


Figure 7 20: Differential pressure for varying  $n_o$

### 7.5.1.3 Polymer viscosity

The polymer viscosity had to be adjusted to 5.7 cP to obtain a best match. Altering the polymer viscosity had contrasting effects on the differential pressure during surfactant/polymer flooding and chase water flooding. In addition to this, altering the polymer viscosity affected the simulated oil recovery. This can be seen in figures 7.21-22.

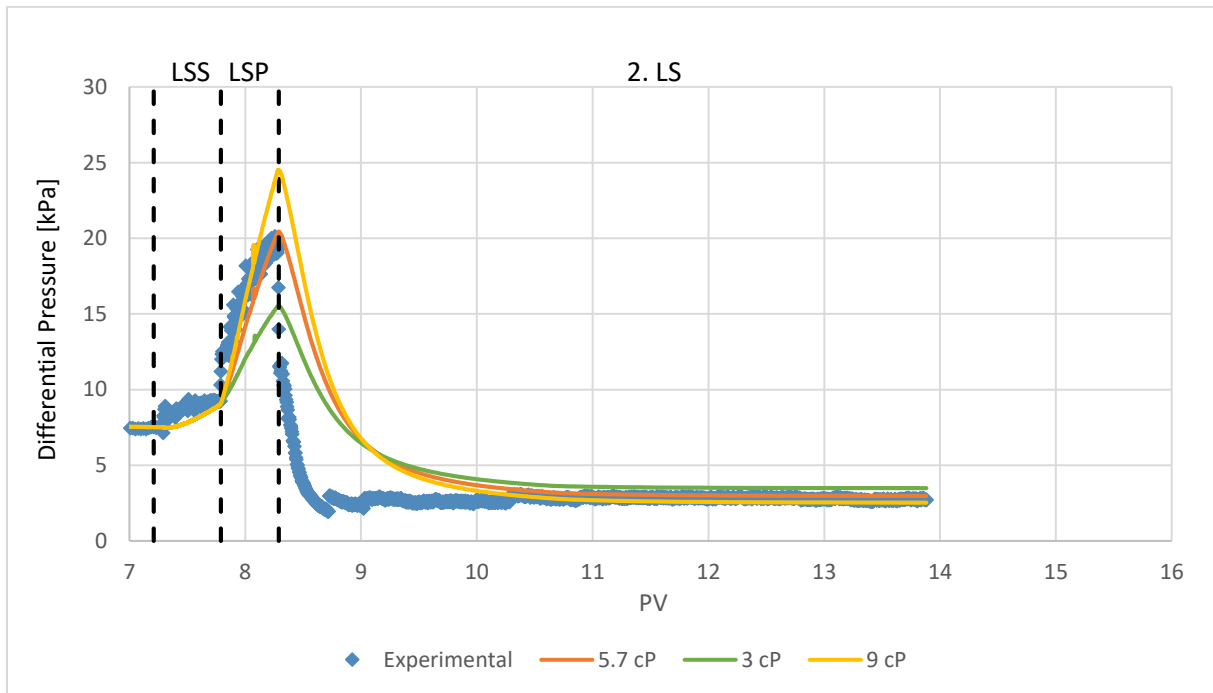


Figure 7 21: Differential pressure for varying polymer viscosity

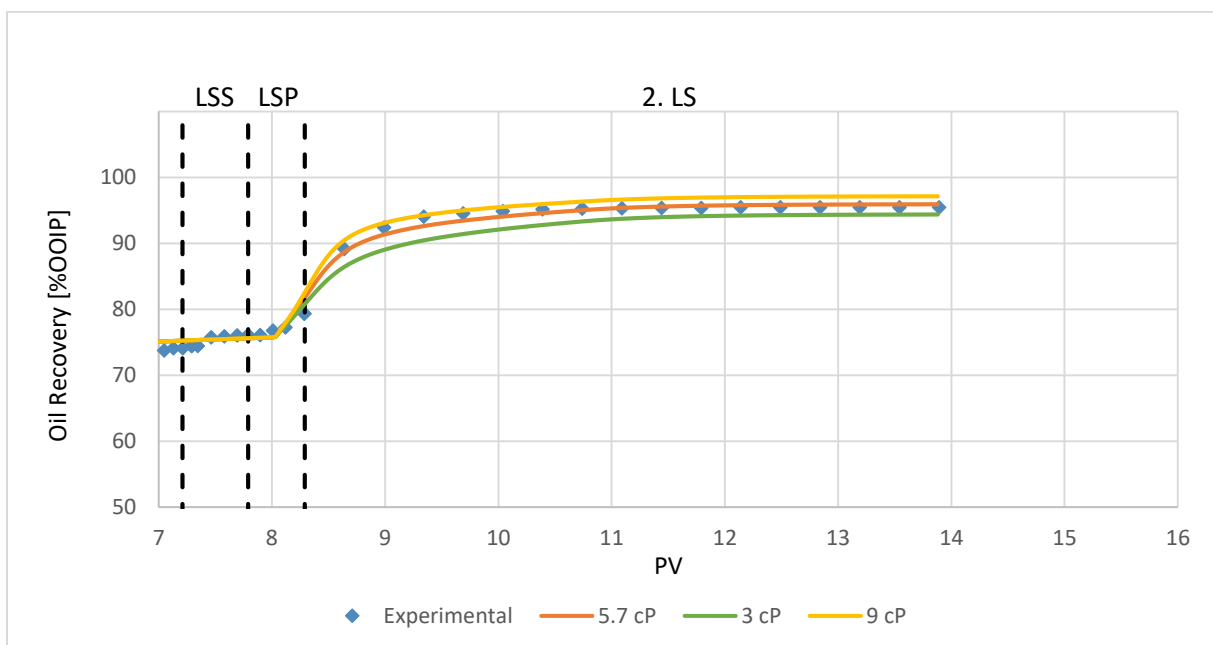


Figure 7 22: Oil recovery for varying polymer viscosity

### 7.5.1.4 Surfactant viscosity

The surfactant viscosity was mainly adjusted to match the differential pressure at the end of the surfactant flood. The oil recovery was also influenced, however not significantly.

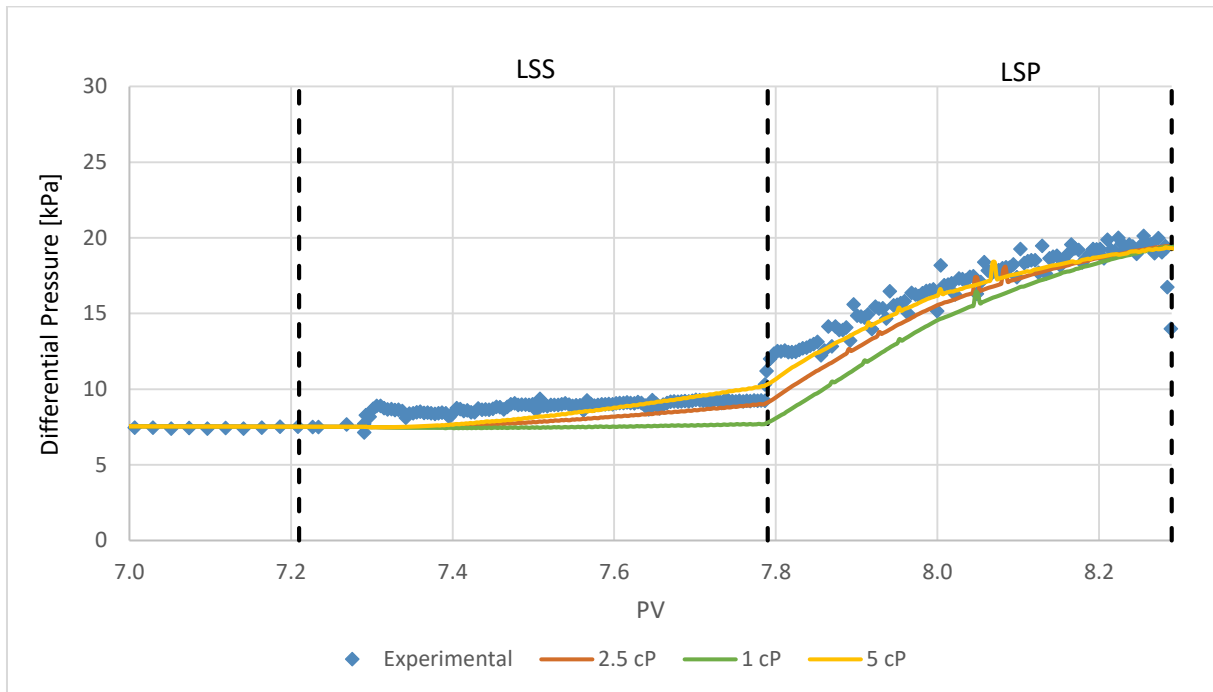


Figure 7 23: Differential pressure for varying surfactant viscosity

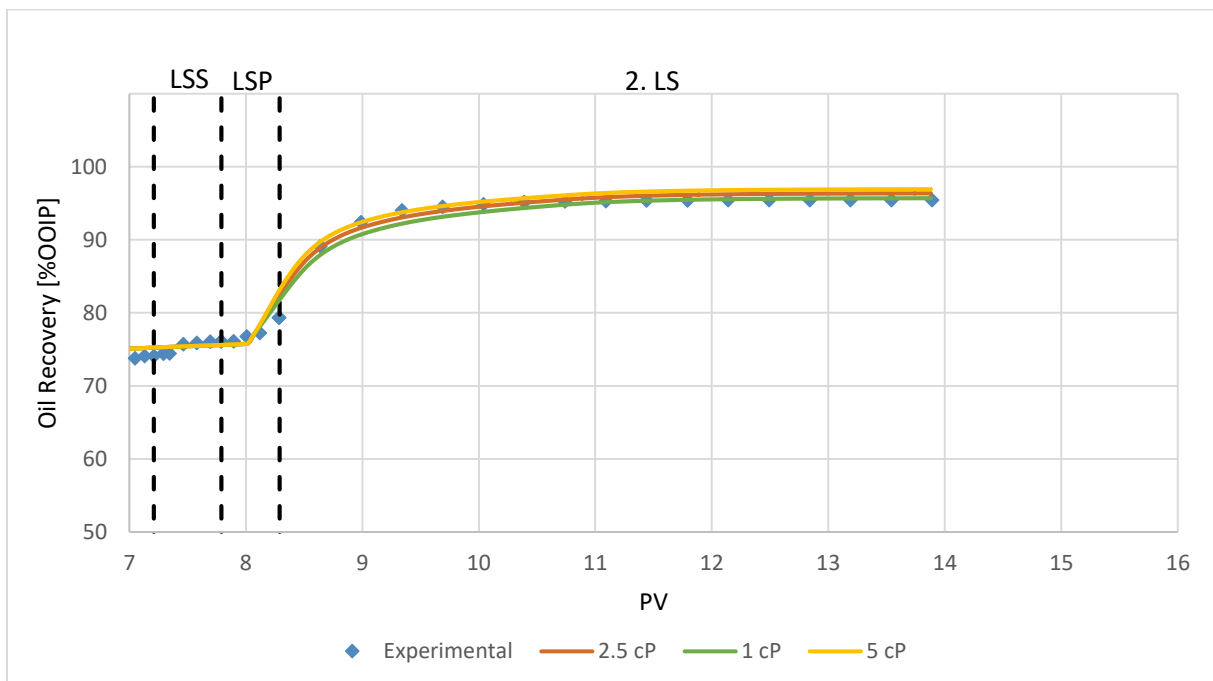


Figure 7 24: Oil recovery for different surfactant viscosity

### 7.5.1.6 Residual oil saturation

In the history matching of core R14, a best match was achieved using the experimental value for residual oil saturation. However, if a match had not been achieved, an adjustment of  $S_{or}$  could have been done. The effects of altering  $S_{or}$  is shown in figures 7.25-26.

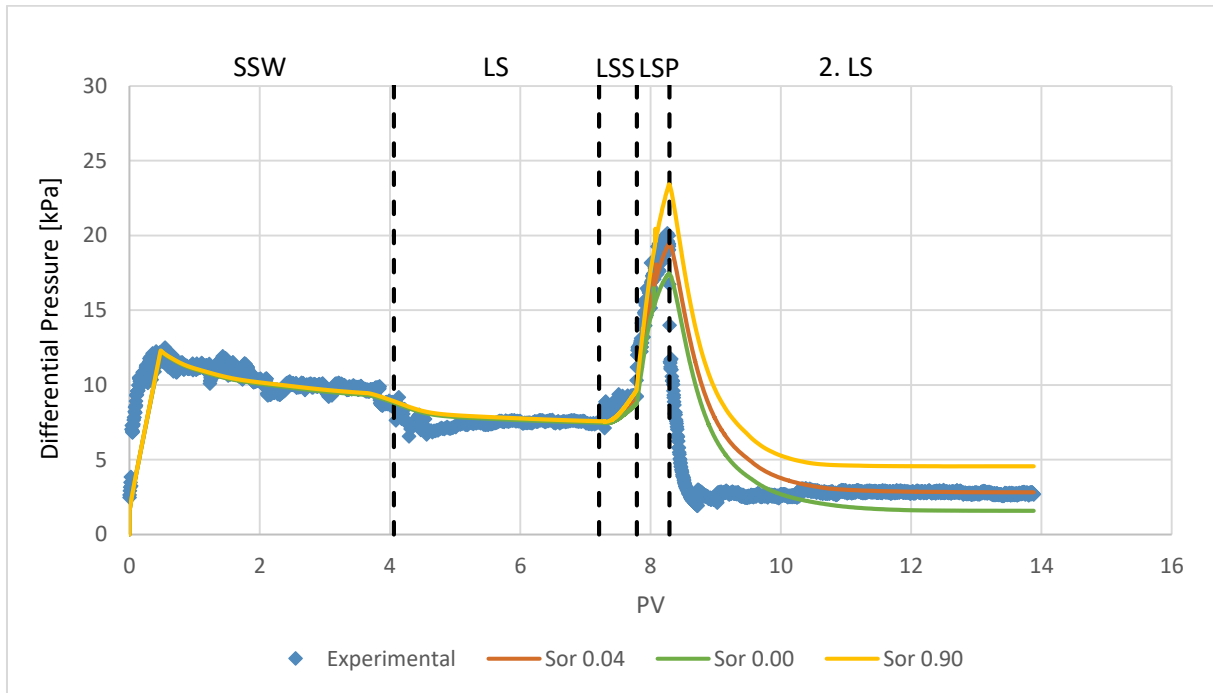


Figure 7.25: Differential pressure for varying  $S_{or}$

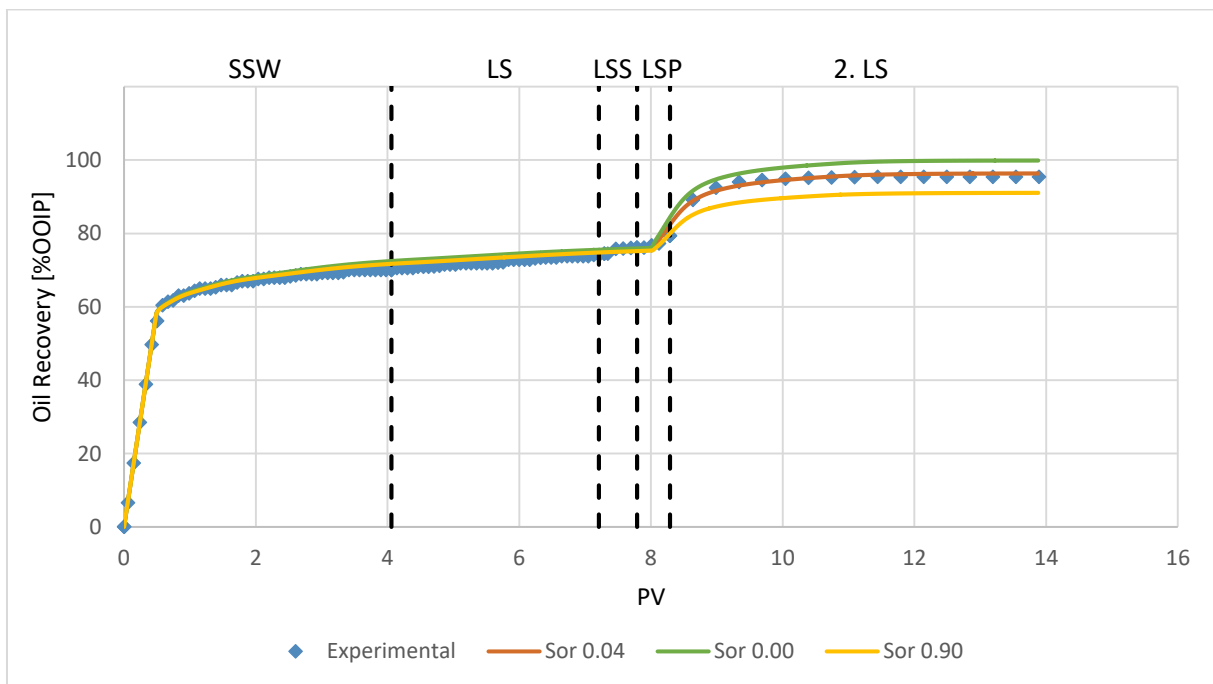


Figure 7.26: Oil recovery for varying  $S_{or}$

### 7.5.1.5 Inaccessible pore volume

Inaccessible pore volume was implemented in the model for the simulation of the polymer flooding. The value was set to 20% based on what was used in previous studies [57] [58]. Alterations within reasonable values proved to have little effect on the simulated results. This is illustrated in figures 7.27-28.

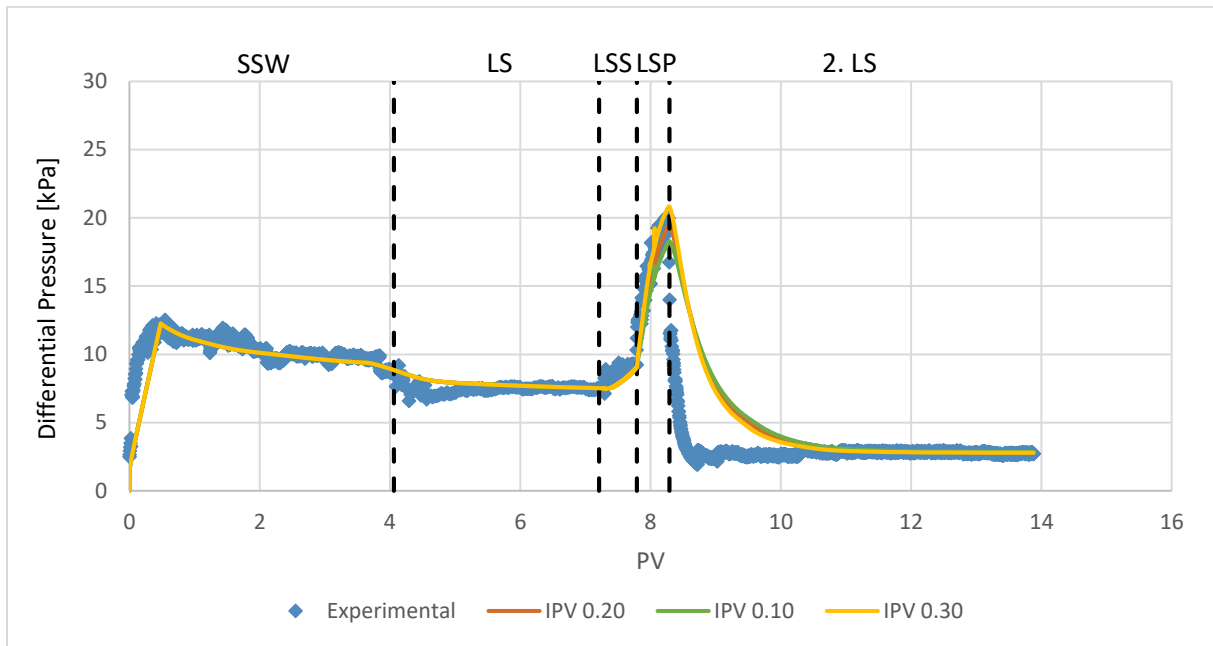


Figure 7 27: Differential pressure for varying inaccessible pore volume

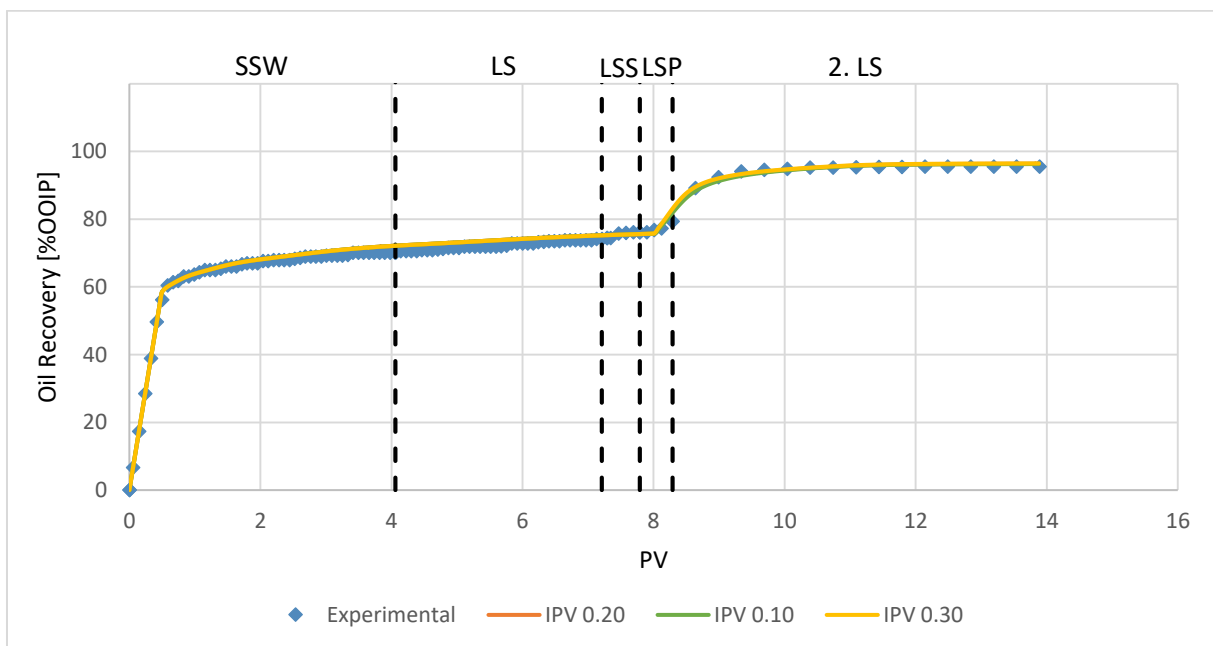


Figure 7 28: Oil recovery for varying inaccessible pore volume

### 7.5.1.7 Dispersion

During history matching, computational errors causing discontinuous differential pressure curves were encountered. Jarlsby [58] suggested that such errors could be a result of the simulator not being able to properly model very low polymer concentrations. Jarlsby solved this by reducing the molecular weight of polymer while simultaneously increasing the polymer concentration. In the simulations in this thesis, the problem was solved by increasing the dispersion of surfactant and polymer. Figures 7.29-7.30 show the computational errors that occurred at lower dispersion levels.

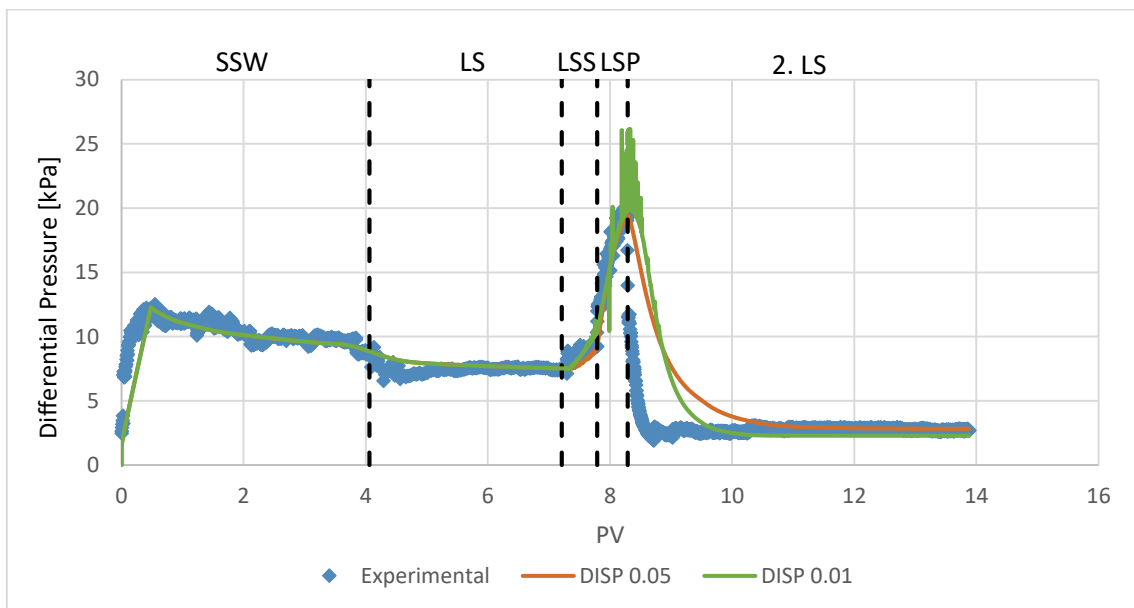


Figure 7 29: Differential pressure for varying surfactant and polymer dispersion

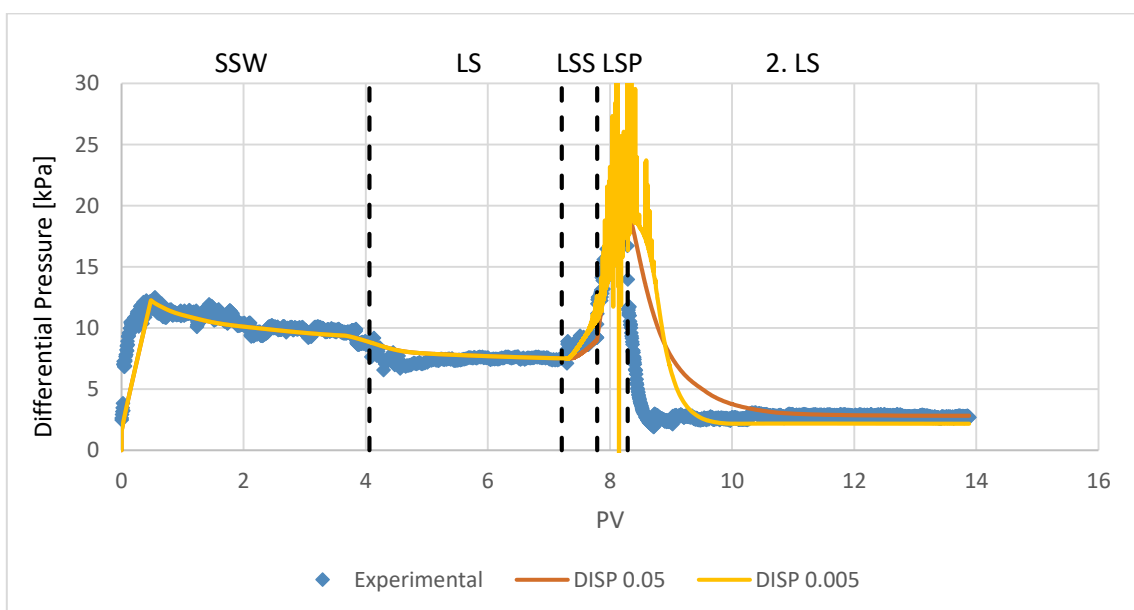


Figure 7 30: Differential pressure for varying surfactant and polymer dispersion

## 7.5.2 History matching

Oil recovery and differential pressure was successfully history matched for all flooding sequences performed on core R14. This was achieved by using the multiple interpolation scheme presented in section 4.4, and altering the parameters presented in section 7.5.1.

When history matching such a complex coreflooding experiment, a strategic approach is important. In this case, the differential pressure plateau for the chsae water was matched first. This was achieved by altering the extended low salinity water relative permeability curve as described in sections 7.5.1.1-2. Next, oil mobility was increased by altering the Corey exponent  $n_o$  in the surfactant relative permeability curves. This was to capture the oil mobilization from surfactant flooding. At the same time, polymer viscosity was reduced to obtain a lower differential pressure. The surfactant viscosity was increased to match the end-point differential pressure after surfactant flooding. As discussed in section 7.5.1.7, the dispersion of both surfactant and polymer was increased to avoid computational problems. Inaccessible pore volume and residual oil saturation was set to 0.20 and 0.04 from the start, and was not altered during matching.

Table 7.9 gives an overview of the Corey parameters used to obtain a best match for the LSSP flood. The corresponding relative permeability curves are shown in figure 7.31. In table 7.10, additional parameters values related to the surfactant and polymer are presented.

Table 7 9: Corey relative permeability values used in history matching of LSSP floods

	Synthetic seawater (SSW)*	Low Salinity Water (LS)	Low Salinity Surfactant (LSS)
$S_{wi}$	0.16	0.16	0.16
$S_{or}$	0.26	0.04	0.04
$k_{rw}(S_{or})$	0.025	1.00	0.069
$k_{ro}(S_{wi})$	0.057	0.057	0.057
$n_w$	1.6	1.7	1.7
$n_o$	4.9	5.1**	3.3

\* Same curves as those yielding best match of SSW flood.

\* After 1. LS flood. The extended part of the curve is adjusted manually.

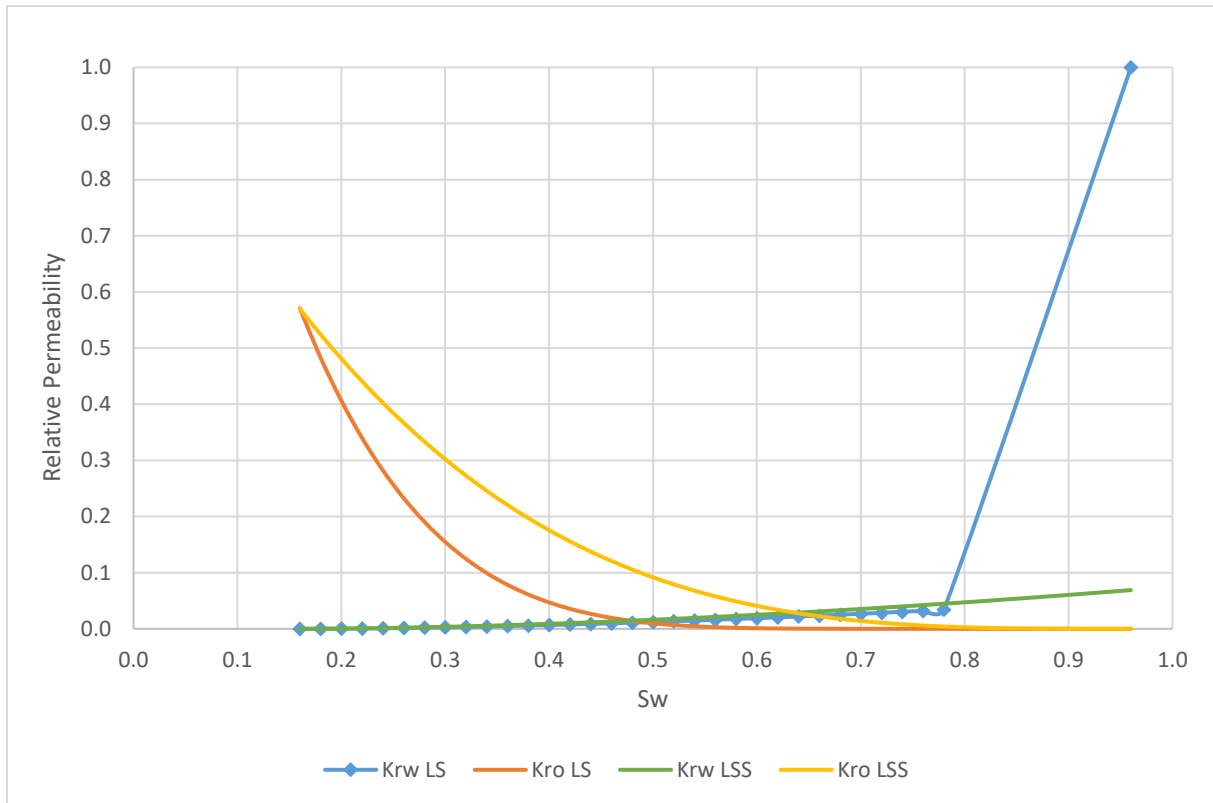


Figure 7.31: Relative permeability curves used in the history matching of LSSP flooding.

Table 7.10: Values of parameters related to the surfactant and polymer floods.

	Surfactant	Polymer
Viscosity [cP]	2.5	5.7
Dispersion [cm <sup>2</sup> /min]	0.05	0.05
Adsorption [gmol/cm <sup>3</sup> ]	$4.4 \cdot 10^{-7}$	$7.7 \cdot 10^{-11}$
DTRAPW (SSW)	-12.5	-
DTRAPW (LSS)	-9.5	-
Inaccessible Pore Volume	-	20%

The best match of oil recovery and differential pressure is shown in figures 7.32-33.

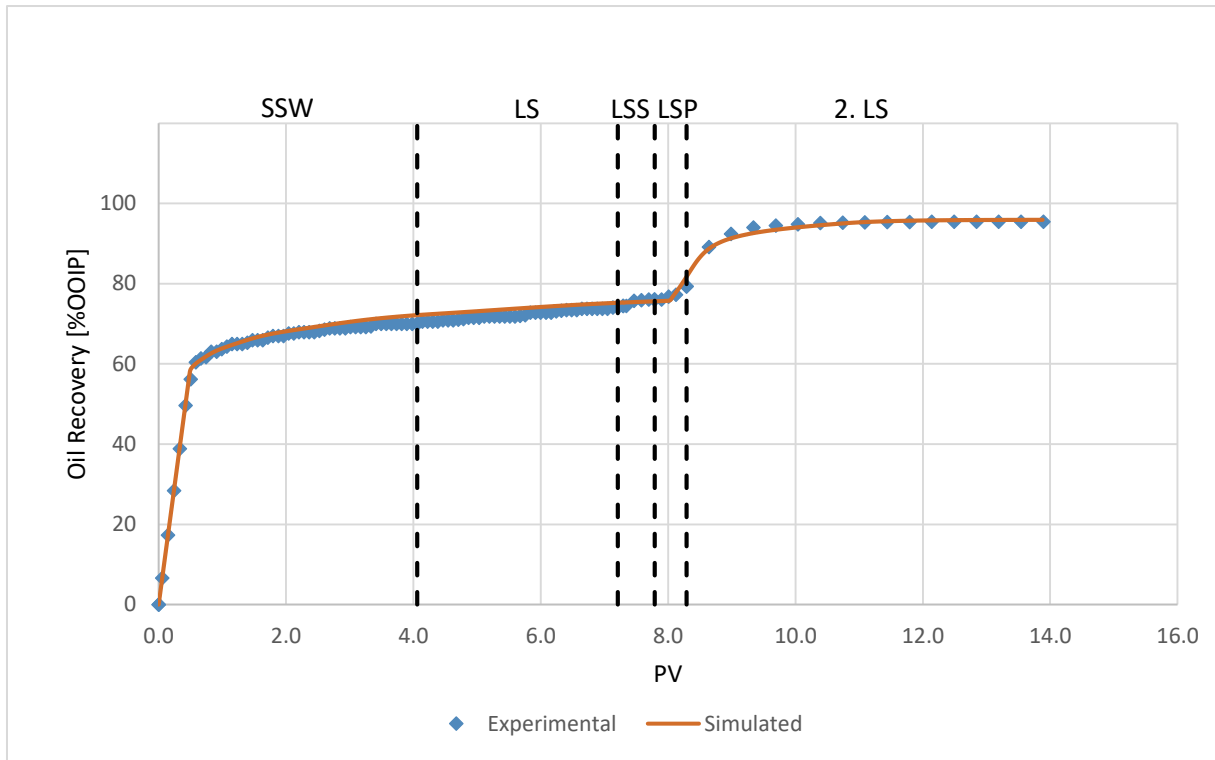


Figure 7 32: Best match of oil recovery for all flooding sequences.

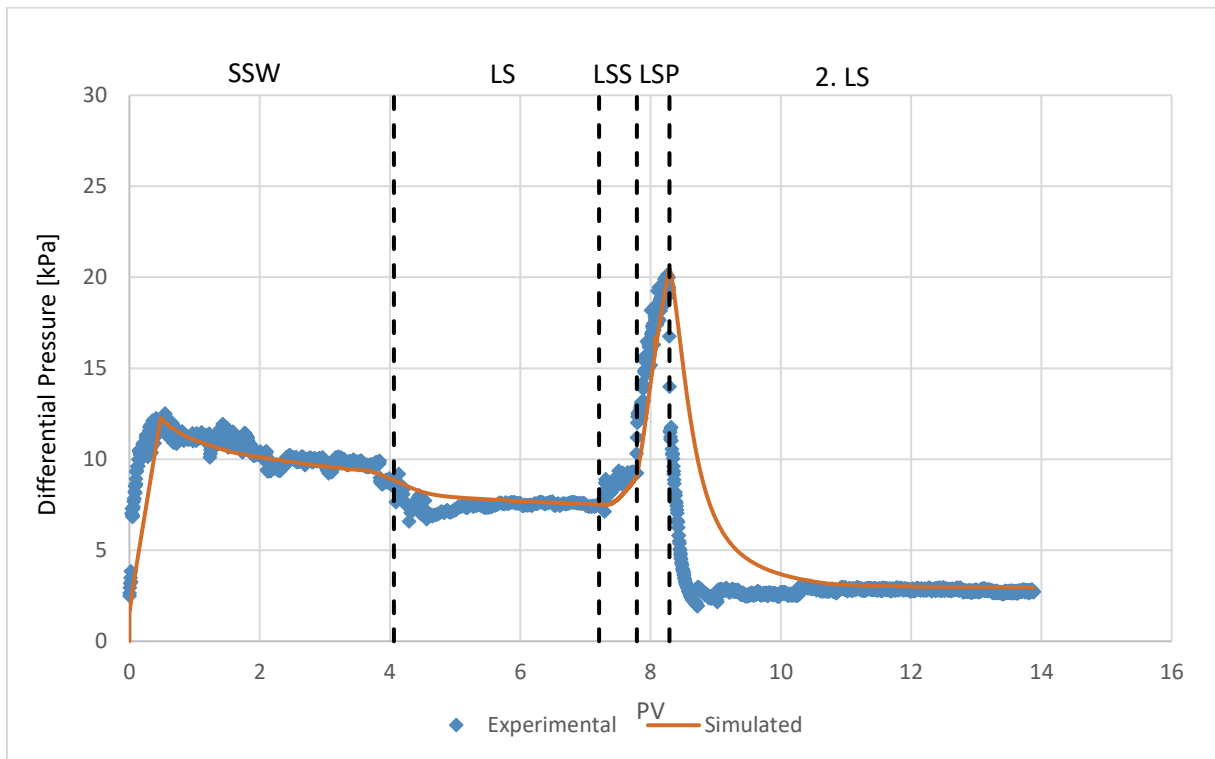


Figure 7 33: Best match of differential pressure for all flooding sequences

Figure 7.32 shows a significant increase in oil recovery as a result of surfactant and polymer injection. This is due to the combination of oil mobilization during low salinity and surfactant flooding, and increased volumetric sweep from polymer injection. The incremental production is initiated after approximately 8 PV, which is towards the end of the polymer injection. Figure 7.32 shows a good match between simulated and experimental oil recovery. The timing of the incremental oil production and the end-point residual oil saturation is accurately captured in the simulation.

Figure 7.33 shows that the injection of surfactant and polymer caused a considerable rise in differential pressure. This is due to the increased viscosity of the surfactant and polymer solutions compared to the low salinity water. For the chase water, an abrupt decline in experimental pressure is seen. This is due to the low viscosity of the chase water, and the formation of water channels yielding an early breakthrough of chase water.

The simulated differential pressure matches the experimental values at the start of the surfactant polymer injection. However, the simulation does not match the decline in pressure when chase water is injected. This is due to the one-dimensional simulation model not being able to account for the formation of water channels, i.e viscous fingering. Also, physical dispersion is added to the simulation model, which causes smearing of the curve, resulting in a higher phase viscosity in the simulation compared to in the experiment. Figure 7.34 illustrates how the simulated differential pressure follows the simulated water phase viscosity.

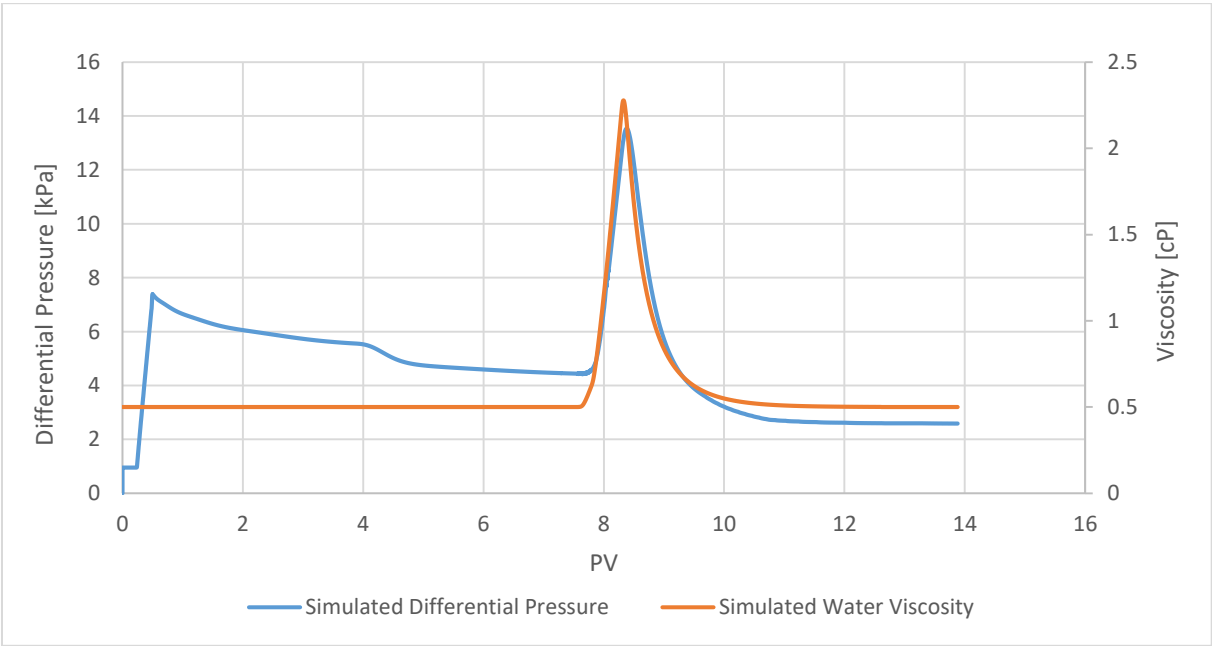


Figure 7 34: Comparison of water phase viscosity and differential pressure (block 50,1,1).

In order to investigate which phase contributed to the increased phase viscosity in the simulation, simulated surfactant and polymer concentrations were compared. This can be seen in figure 7.35. The results show that the polymer is the main contributor to the increased viscosity in the simulation for the chase water flood.

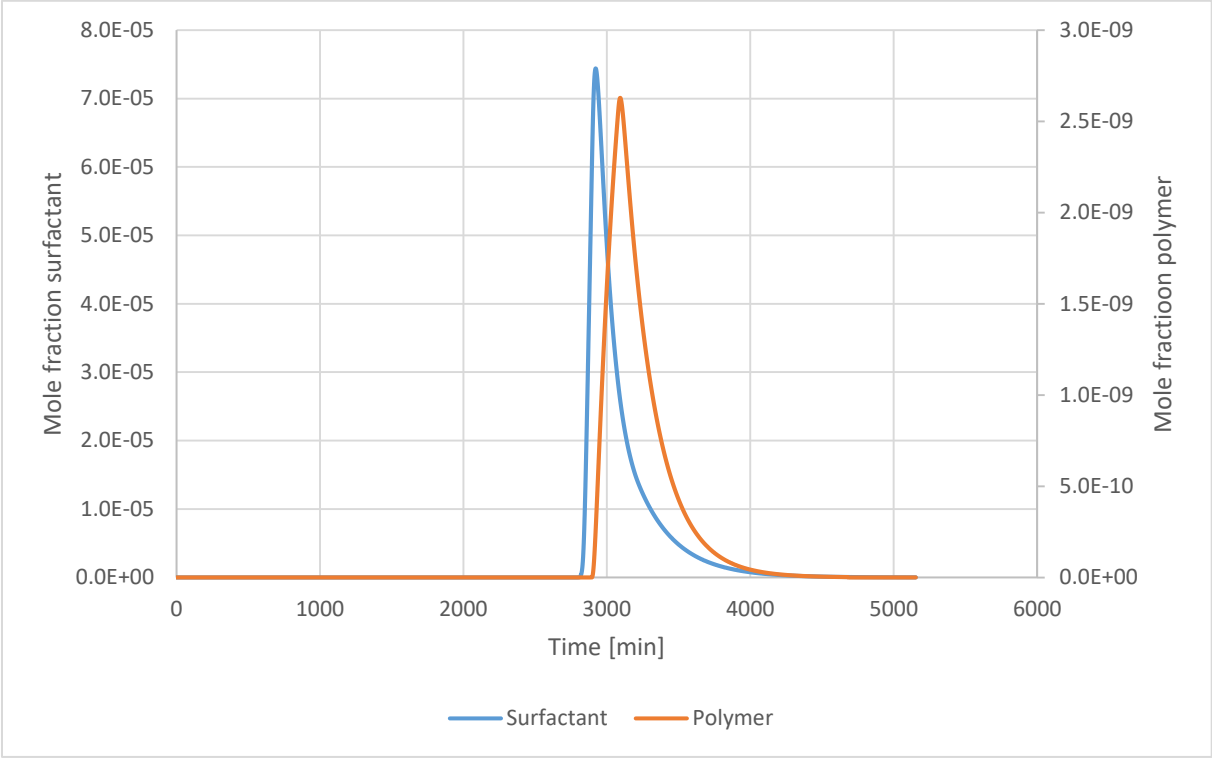


Figure 7 35: Mole fractions of surfactant and polymer in block 50,1,1

The history matching of oil recovery and differential pressure was achieved by enabling interpolation between multiple relative permeability sets, as described in section 4.4. Figures 7.36-37 show plots of simulated relative permeability curves from block 2,1,1 for the best match. As can be seen from the plots, interpolation of relative permeability occurs when flooding sequences are changed. Figure 7.37 shows that oil is mobilized during surfactant flooding due to an increase in oil relative permeability.

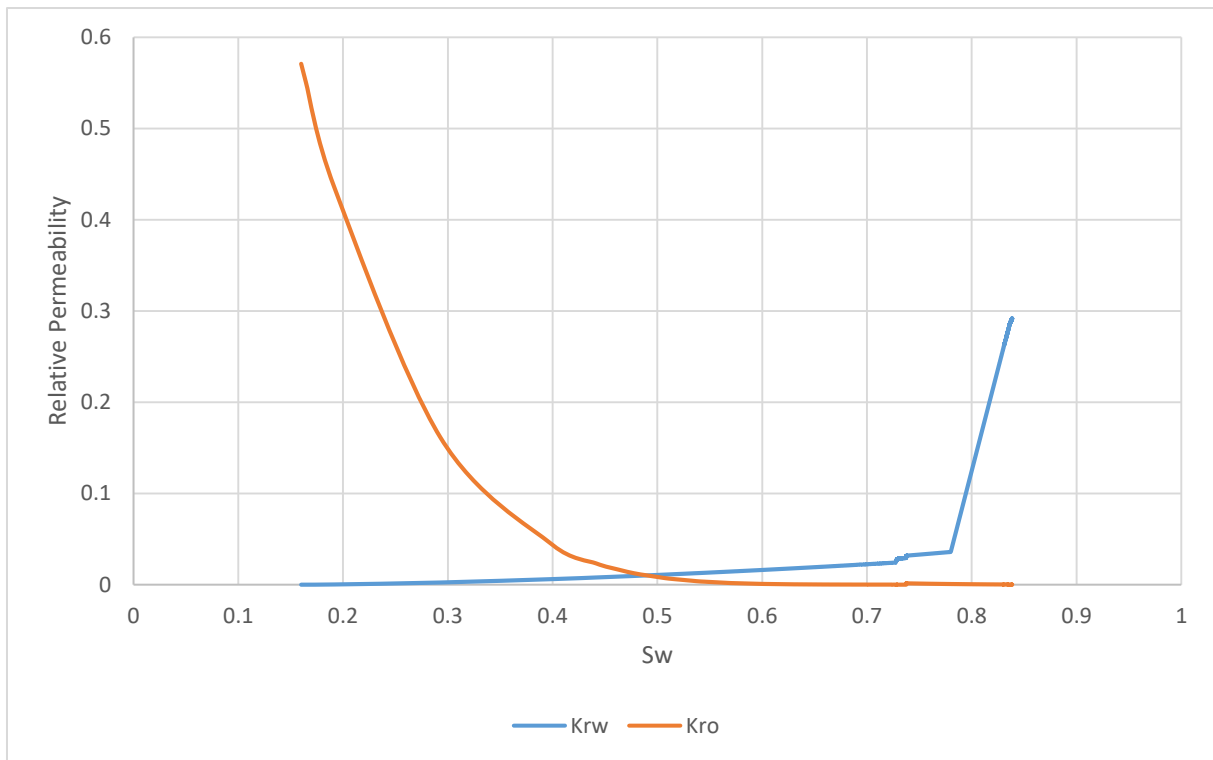


Figure 7 36: Relative permeability curves from block 2,1,1 of the LSSP best match simulation

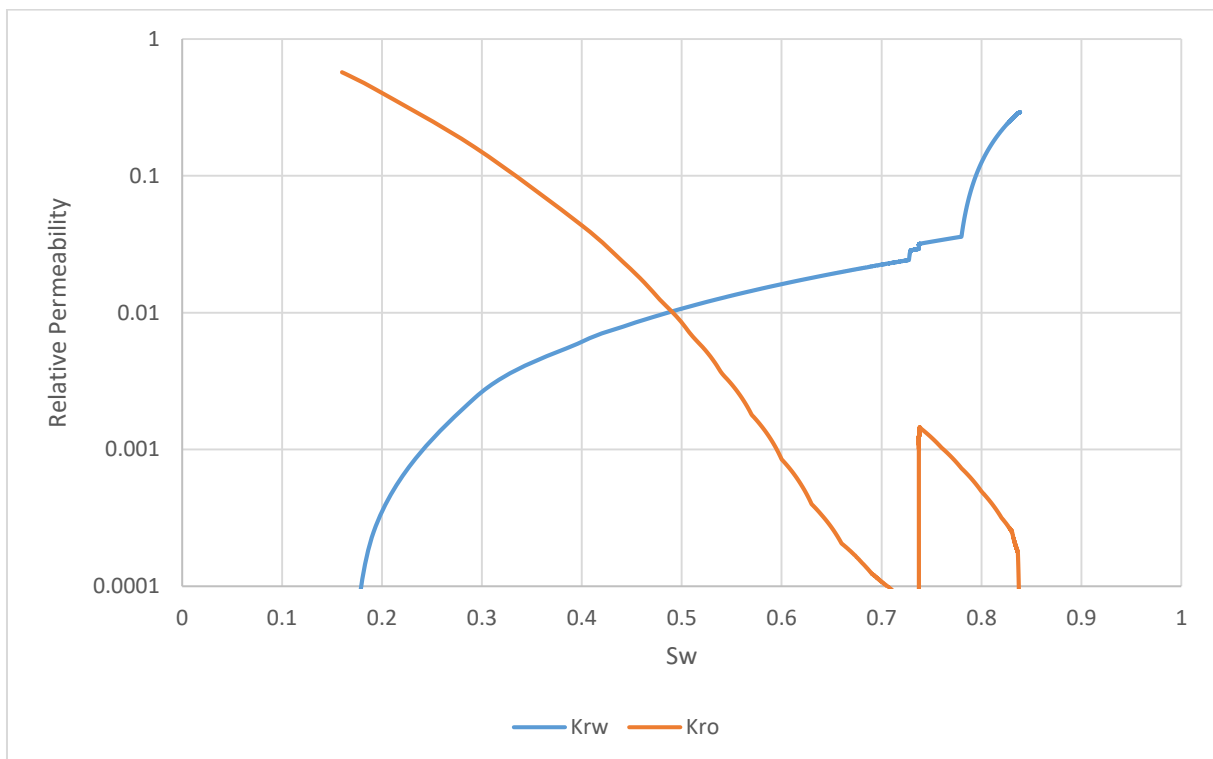


Figure 7 37: Relative permeability curves from block 2,1,1 of the LSSP best match simulation, with logarithmic scale on the y-axis.

## 8 Summary and Conclusions

In this thesis, modelling of low salinity surfactant polymer (LSSP) slug injections have been investigated. Laboratory data from the coreflood experiment performed on core R14 by UniResearch CIPR was provided, and the experiment was history matched using the chemical simulator STARS by CMG (Computer Modelling Group).

In preparation for the history matching, a series of sensitivity and verification studies were performed. These were presented in section 6. The effect of altering different Corey parameters was explored, and the observations were later used in the history matching of core R14. The impact of dispersion was also investigated, and a setup minimizing the numerical dispersion in the model was obtained. In addition to this, verification tests were conducted to ensure that STARS was able to calculate key parameters such as viscosity, interfacial tension, capillary number, and adsorption correctly.

Low salinity waterflooding was modeled by utilizing salinity dependent relative permeability. This was based on an assumption that injection of low salinity water induced a wettability alteration in the core. Salinity dependent relative permeability was enabled through salinity based interpolation between high salinity and low salinity relative permeabilities curves. A best match between simulated and experimental data was obtained, confirming STARS capabilities of accurately modelling waterflooding processes of varying salinity.

The combined effects of low salinity surfactant polymer (LSSP) flooding was modelled by implementing a multiple interpolation scheme. This setup was described in detail in section 4.4. It included the addition of a second rock type in which relative permeability curves for the surfactant solution was defined, and where interpolation was based on the capillary number. The polymer solution was modelled as a viscosity effect only, due to interpolation problems when adding a third interpolation routine in the model. Despite the polymer solution not being represented by its own set of relative permeability curves, successful history matching of oil recovery and differential pressure was achieved.

In summary, it was found that STARS was capable modelling low salinity surfactant polymer (LSSP) slug injections. However, the physical effects of the coreflood sequences were not adequately represented, since the polymer solution was modelled as a viscosity effect only. Therefore, the addition of a third interpolation routine would improve the modelling of such corefloods.

## 9 Further Work

The work done in this thesis confirms that CMG STARS is capable of modelling complex coreflood experiments such as low salinity surfactant polymer (LSSP) flooding. However, there are multiple approaches to modelling such processes, and further work on the topic is required. In addition, some of the problems encountered in this thesis needs to be investigated further.

It would be interesting to do a upscaling of the simulation model used in this thesis. By doing so, topics such as dispersion, wettability, hysteresis, reservoir heterogeneity, and in-situ rheology could be further evaluated.

History matching of other LSSP coreflood experiments would also be interesting. This could help verify the observations made in this study, and potentially discover new areas for further work.

It would also be interesting to model laboratory experiments where different coreflooding approaches have been used. For example, UniResearch CIPR have conducted several experiments of just low salinity surfactant (LSS) or low salinity polymer (LSP) flooding. Modeling of such experiments could give more knowledge on the mechanisms behind hybrid EOR processes. This knowledge could also be used to enhance the modelling of combined low salinity surfactant polymer (LSSP) floods.

Finally, modeling with different interpolation schemes should be investigated. In this thesis, the coreflooding experiment is modelled using two interpolation routines, with polymer only being modelled as a viscosity effect. In order to model LSSP floods more accurately, a third interpolation routine should be added where polymer is represented by its own set of relative permeability curves. This has not been properly achieved in STARS, and therefore further investigation is needed.

## 10 References

1. *Positive prospects for producing more.* in topics: Improved recovery, Norwegian Petroleum Directorate. 2017. <http://www.npd.no/en/Topics/Improved-Recovery/Temaartikler/Positive-prospects-for-producing-more/>.
2. Lake, L.W., *Enhanced oil recovery.* 1989: Upper Sadle River, N.J. Prentice Hall. ISBN 9780132816014.
3. Skarestad, M. and A. Skauge, *PTEK213 - Reservoarteknikk II.* 2012: Bergen. Universitetet i Bergen.
4. Zolotukhin, A.B. and J.R. Ursin, *Introduction to Petroleum Reservoir Engineering.* 2000: Høyskoleforlaget, Norwegian Academic Press. ISBN 82-7634-065-2.
5. Corey, A.T., *The interrelation between gas and oil relative permeabilities,* Producers monthly, 1954. **19**(1): p. 38-41.
6. Lien, J.R., *PTEK211 - Grunnleggende Reservoarfysikk.* 2004, Bergen: Universitetet i Bergen.
7. Kontogeorgis, G.M. and S. Kiil, *Introduction to Applied Colloid and Surface Chemistry.* 2016: Chichester, UK. Wiley. ISBN 9781118881187.
8. Skauge, A., *PTEK312 - Pore Scale Physics and Network Modelling.* 2017: Bergen.
9. Stegemeier, G.L., *Mechanisms of Entrapment and Mobilization of Oil in Porous Media.* Improved Oil Recovery by Surfactant and Polymer Flooding, R.S. Schechter, Editor. 1997: Academic Press. p. 55-91, <https://doi.org/10.1016/B978-0-12-641750-0.50007-4>.
10. Mohanty, K.K., *Multiphase Flow in Porous Media: III. Oil Mobilization, Transverse Dispersion, and Wettability.* SPE Annual Technical Conference and Exhibition. 1983. Society of Petroleum Engineers (SPE-12127-MS) San Francisco, California. p. 21. <https://doi.org/10.2118/12127-MS>.
11. Willhite, G.P. *Waterflooding.* SPE textbook series. Vol. 3. 1986: Richardson, TX. Society of Petroleum Engineers. ISBN 9781555630058.
12. Anderson, W.G., *Wettability Literature Survey-Part 6: The Effects of Wettability on Waterflooding.* Journal of Petroleum Technology. 1987: **39**(12). Society of Petroleum Engineers (SPE-16471-PA) p.1605-1622. <https://doi.org/10.2118/16471-PA>.
13. Anderson, W.G., *Wettability Literature Survey Part 5: The Effects of Wettability on Relative Permeability.* Journal of Petroleum Technology. 1987. **39**(11). Society of

- Petroleum Engineers (SPE-16323-PA). p. 1453-1468. <https://doi.org/10.2118/16323-PA>.
14. Craig, F.F., *The Reservoir Engineering Aspects of Waterflooding*. Henry L. Doherty series. Vol. 3. 1971: New York. Henry L. Doherty Memorial Fund of AIME.
  15. Buckley, J.S., Y. Liu, and S. Monsterleet, *Mechanisms of Wetting Alteration by Crude Oils*. SPE Journal, 1998. **3**(01): Society of Petroleum Engineers (SPE-37230-PA). p. 54-61. <https://doi.org/10.2118/37230-PA>.
  16. Smith, J.T., W.M. Cobb. *Waterflooding*. 1997: Midwest Office of the Petroleum Technology Transfer Council. p. 1-4.  
[http://www.prrc.nmt.edu/publications/media/pdf/workshop/95-99/Waterflooding%20\(1997\).pdf](http://www.prrc.nmt.edu/publications/media/pdf/workshop/95-99/Waterflooding%20(1997).pdf)
  17. Bernard, G.G., *Effect of Floodwater Salinity on Recovery Of Oil from Cores Containing Clays*, SPE California Regional Meeting. 1967: Society of Petroleum Engineers (SPE-1725-MS). Los Angeles, California. p. 8.  
<https://doi.org/10.2118/1725-MS>.
  18. Jadhunandan, P.P. and N.R. Morrow, *Effect of Wettability on Waterflood Recovery for Crude-Oil/Brine/Rock Systems*. SPE Reservoir Engineering, 1995: **10**(01). Society of Petroleum Engineers (SPE-22597-PA) p. 40-46. <https://doi.org/10.2118/22597-PA>.
  19. Yildiz, H.O. and N.R. Morrow, *Effect of brine composition on recovery of Moutray crude oil by waterflooding*. Journal of Petroleum Science and Engineering, 1996. **14**(3): p. 159-168. [https://doi.org/10.1016/0920-4105\(95\)00041-0](https://doi.org/10.1016/0920-4105(95)00041-0)
  20. Yildiz, H.O., M. Valat, and N.R. Morrow, *Effect of Brine Composition On Wettability And Oil Recovery of a Prudhoe Bay Crude Oil*. Journal of Canadian Petroleum Technology, 1999. **38**(01): Petroleum Society of Canada. p. 6.  
<https://doi.org/10.2118/99-01-02>
  21. Tang, G.Q. and N.R. Morrow, *Salinity, Temperature, Oil Composition, and Oil Recovery by Waterflooding*. SPE Reservoir Engineering, 1997. **12**(04): Society of Petroleum Engineers (SPE-36680-PA) p. 269-276. <https://doi.org/10.2118/36680-PA>
  22. Tang, G.-Q. and N.R. Morrow, *Influence of brine composition and fines migration on crude oil/brine/rock interactions and oil recovery*. Journal of Petroleum Science and Engineering, 1999. **24**(2): p. 99-111. [https://doi.org/10.1016/S0920-4105\(99\)00034-0](https://doi.org/10.1016/S0920-4105(99)00034-0)
  23. Sharma, M.M. and P.R. Filoco, *Effect of Brine Salinity and Crude-Oil Properties on Oil Recovery and Residual Saturations*. SPE Journal, 2000. **5**(03): Society of Petroleum Engineers (SPE-65402-PA) p.293-300. <https://doi.org/10.2118/65402-PA>

24. Zhang, Y. and N.R. Morrow, *Comparison of Secondary and Tertiary Recovery With Change in Injection Brine Composition for Crude-Oil/Sandstone Combinations*, in *SPE/DOE Symposium on Improved Oil Recovery*. 2006: Society of Petroleum Engineers (SPE-99757-MS). Tulsa, Oklahoma. p. 14. <https://doi.org/10.2118/99757-MS>
25. Shaker Shiran, B. and A. Skauge, *Wettability and Oil Recovery by Low Salinity Injection*, in *SPE EOR Conference at Oil and Gas West Asia*. 2012, Society of Petroleum Engineers (SPE-155651-MS). Muscat, Oman. p. 15. <https://doi.org/10.2118/155651-MS>
26. Webb, K.J., C.J.J. Black, and H. Al-Ajeel, *Low Salinity Oil Recovery - Log-Inject-Log*, in *Middle East Oil Show*. 2003, Society of Petroleum Engineers (SPE-81460-MS). Bahrain. p. 8. <https://doi.org/10.2118/81460-MS>.
27. Skrettingland, K., et al., *Snorre Low-Salinity-Water Injection--Coreflooding Experiments and Single-Well Field Pilot*. SPE Reservoir Evaluation & Engineering, 2011. **14**(02). Society of Petroleum and Engineering (SPE-129877-PA). p. 182-192. <https://doi.org/10.2118/129877-PA>.
28. Lager, A., et al., *LoSal Enhanced Oil Recovery: Evidence of Enhanced Oil Recovery at the Reservoir Scale*, in *SPE Symposium on Improved Oil Recovery*. 2008, Society of Petroleum Engineers (SPE-113976-MS). Tulsa, Oklahoma, USA. p. 12. <https://doi.org/10.2118/113976-MS>.
29. Vledder, P., et al., *Low Salinity Water Flooding: Proof Of Wettability Alteration On A Field Wide Scale*, in *SPE Improved Oil Recovery Symposium*. 2010, Society of Petroleum Engineers (SPE-129564-MS). Tulsa, Oklahoma, USA. p. 10. <https://doi.org/10.2118/129564-MS>.
30. Seccombe, J., et al., *Demonstration of Low-Salinity EOR at Interwell Scale, Endicott Field, Alaska*, in *SPE Improved Oil Recovery Symposium*. 2010, Society of Petroleum Engineers (SPE-129692-MS): Tulsa, Oklahoma, USA. p. 12. <https://doi.org/10.2118/129692-MS>.
31. Skauge, A., et al., *Theoretical and experimental evidence of different wettability classes*. Journal of Petroleum Science and Engineering. 2007. **57**(3-4). p. 321-333. <https://doi.org/10.1016/j.petrol.2006.11.003>.
32. Filoco, P.R. and M.M. Sharma, *Effect of Brine Salinity and Crude Oil Properties on Relative Permeabilities and Residual Saturations*, in *SPE Annual Technical*

- Conference and Exhibition*. 1998, Society of Petroleum (Engineers SPE-49320-MS). New Orleans, Louisiana. p. 10. <https://doi.org/10.2118/49320-MS>.
33. Lager, A., et al., *Low Salinity Oil Recovery - An Experimental Investigation I*. Petrophysics. 2008. **49**(1). Society of Petrophysics and Well-log Analysts. p. 28-35. <https://www.onepetro.org/journal-paper/SPWLA-2008-v49n1a2>.
  34. Yousef, A.A., S.H. Al-Salehsalah, and M.S. Al-Jawfi, *New Recovery Method for Carbonate Reservoirs through Tuning the Injection Water Salinity: Smart Water Flooding*, in *SPE EUROPEC/EAGE Annual Conference and Exhibition*. 2011, Society of Petroleum Engineers (SPE-143550-MS). Vienna, Austria. p. 16. <https://doi.org/10.2118/143550-MS>.
  35. Valocchi, A.J., R. Street, and P.V. Roberts, *Transport of ion-exchanging solutes in groundwater: chromatographic theory and field simulation*. Water Resources Research. 1981. **17**(5). p. 1517-1527. <https://doi.org/10.1029/WR017i005p01517>.
  36. Secombe, J.C., et al., *Improving Waterflood Recovery: LoSal™ EOR Field Evaluation*, in *SPE Symposium on Improved Oil Recovery*. 2008, Society of Petroleum Engineers (SPE-113480-MS). Tulsa, Oklahoma, USA. p. 19. <https://doi.org/10.2118/113480-MS>.
  37. Jerauld, G.R., et al., *Modeling Low-Salinity Waterflooding*. SPE Reservoir Evaluation & Engineering, 2008. **11**(06). Society of Petroleum Engineers (SPE-102239-PA). p. 1000-1012. <https://doi.org/10.2118/102239-PA>.
  38. Wu, Y.-S. and B. Bai, *Efficient Simulation for Low Salinity Waterflooding in Porous and Fractured Reservoirs*, in *SPE Reservoir Simulation Symposium*. 2009, Society of Petroleum Engineers (SPE-118830-MS). The Woodlands, Texas. p. 13. <https://doi.org/10.2118/118830-MS>.
  39. Omekeh, A.V., et al., *Modeling of Ion-Exchange and Solubility in Low Salinity Water Flooding*, in *SPE Improved Oil Recovery Symposium*. 2012, Society of Petroleum Engineers (SPE-154144-MS). Tulsa, Oklahoma, USA. p. 13. <https://doi.org/10.2118/154144-MS>.
  40. Dang, C.T.Q., et al., *Modeling Low Salinity Waterflooding: Ion Exchange, Geochemistry and Wettability Alteration*, in *SPE Annual Technical Conference and Exhibition*. 2013, Society of Petroleum Engineers (SPE-166447-MS). New Orleans, Louisiana, USA. p. 22. <https://doi.org/10.2118/166447-MS>.

41. Healy, R.N. and R.L. Reed, *Physicochemical Aspects of Microemulsion Flooding*. Society of Petroleum Engineers Journal, 1974. **14**(05). Society of Petroleum Engineers (SPE-4583-PA) p. 491-501. <https://doi.org/10.2118/4583-PA>.
42. Huh, C., *Interfacial tensions and solubilizing ability of a microemulsion phase that coexists with oil and brine*. Journal of Colloid and Interface Science. 1979. **71**(2). p. 408-426. [https://doi.org/10.1016/0021-9797\(79\)90249-2](https://doi.org/10.1016/0021-9797(79)90249-2).
43. Spildo, K., et al., *A Strategy for Low Cost, Effective Surfactant Injection*. Journal of Petroleum Science and Engineering. 2011. Vol. 117. p. 8-14. <https://doi.org/10.1016/j.petrol.2014.03.006>.
44. Alagic, E. and A. Skauge, *Combined Low Salinity Brine Injection and Surfactant Flooding in Mixed–Wet Sandstone Cores*. Energy & Fuels, 2010. **24**(6): p. 3551-3559. <https://doi.org/10.1021/ef1000908>.
45. Alagic, E., et al., *Effect of crude oil ageing on low salinity and low salinity surfactant flooding*. Journal of Petroleum Science and Engineering, 2011. **78**(2). p. 220-227. <https://doi.org/10.1016/j.petrol.2011.06.021>.
46. Spildo, K., A.M. Johannessen, and A. Skauge, *Low Salinity Waterflood at Reduced Capillarity*, in *SPE Improved Oil Recovery Symposium*. 2012, Society of Petroleum Engineers (SPE-154236-MS). Tulsa, Oklahoma, USA. p. 13. <https://doi.org/10.2118/154236-MS>.
47. Skauge, A., G. Z, and M. Delshad, *Simulation of Combined Low Salinity Brine and Surfactant Flooding*. 16<sup>th</sup> European Symposium on Improved Oil Recovery. 2011. Cambridge, UK. p.14. <https://doi.org/10.3997/2214-4609.201404792>.
48. Sorbie, K.S., *Polymer-improved oil recovery*. 1991: Boca Raton, Florida. Blackie. ISBN 9780849371370.
49. Ayirala, S.C., et al., *A Designer Water Process for Offshore Low Salinity and Polymer Flooding Applications*, in *SPE Improved Oil Recovery Symposium*. 2010, Society of Petroleum Engineers (SPE-129926-MS). Tulsa, Oklahoma, USA. p. 12. <https://doi.org/10.2118/129926-MS>.
50. Shaker Shiran, B. and A. Skauge, *Enhanced Oil Recovery (EOR) by Combined Low Salinity Water/Polymer Flooding*. Energy & Fuels, 2013. **27**(3): p. 1223-1235. <https://doi.org/10.1021/ef301538e>.
51. Vermolen, E.C.M., et al., *Low-Salinity Polymer Flooding: Improving Polymer Flooding Technical Feasibility and Economics by Using Low-Salinity Make-up Brine*,

- in *International Petroleum Technology Conference*. 2014, International Petroleum Technology Conference: Doha, Qatar. p. 15. <https://doi.org/10.2523/IPTC-17342-MS>.
52. Rotondi, M., et al., *Low Salinity Water Injection: eni's Experience*. Abu Dhabi International Petroleum Exhibition and Conference. 2014. Society of Petroleum Engineers (SPE-171794-MS). Abu Dhabi, UAE. p. 16. <https://doi.org/10.2118/171794-MS>.
  53. Mohammadi, H. and G. Jerauld, *Mechanistic Modeling of the Benefit of Combining Polymer with Low Salinity Water for Enhanced Oil Recovery*, in *SPE Improved Oil Recovery Symposium*. 2012, Society of Petroleum Engineers (SPE-153161-MS). Tulsa, Oklahoma, USA. p. 11. <https://doi.org/10.2118/153161-MS>.
  54. Skauge, A. and B. Ottesen, *A summary of Experimentally derived Relative Permeability and Residual Oil Saturation on North Sea Reservoir Cores*. 2002. International Symposium of the Society of Core Analysts (SCA). Monterey, California, USA. p.12. [https://www.researchgate.net/publication/265850274\\_A\\_Summary\\_of\\_Experimentally\\_derived\\_Relative\\_Permeability\\_and\\_Residual\\_Saturation\\_on\\_North\\_Sea\\_Reservoir\\_Cores](https://www.researchgate.net/publication/265850274_A_Summary_of_Experimentally_derived_Relative_Permeability_and_Residual_Saturation_on_North_Sea_Reservoir_Cores)
  55. *CMG STARS User Guide 2016*.
  56. *CMG Results User Guide 2016*.
  57. Drønen, I., *Modelling of Waterflood Hybrid EOR*. 2015. Master thesis. Centre for Integrated Petroleum Research. University of Bergen: Bergen. p. 239.
  58. Jarlsby, D.O., *Mechanistic Modelling of Combined Low Salinity Waterflood and Surfactant- Polymer Flooding*. 2018. Master thesis. Centre for Integrated Petroleum Research. University of Bergen: Bergen. p. 165. <http://hdl.handle.net/1956/18460>.
  59. Fanchi, J.R., *Multidimensional Numerical Dispersion*, in *Society of Petroleum Engineers Journal*. 1983. Society of Petroleum Engineers (SPE-9018-PA). p. 9. <https://doi.org/10.2118/9018-PA>.
  60. Nordaker, V., *Grid Sensitivity Simulation of Low Salinity and Polymer Flooding*. 2015. Master thesis. Centre for Integrated Petroleum Research. University of Bergen. Bergen. p. 171. <http://hdl.handle.net/1956/10356>.
  61. Mahadevan, J., L.W. Lake, and R.T. Johns, *Estimation of True Dispersivity in Field Scale Permeable Media*, in *SPE/DOE Improved Oil Recovery Symposium*. 2002. Society of Petroleum Engineers (SPE-75247-MS). Tulsa, Oklahoma. p. 9. <https://doi.org/10.2118/75247-MS>.

62. Sheng, J.J., *Modern Chemical Enhanced Oil Recovery: Theory and Practice*. ed. J.J Sheng. 2010. Gulf Professional Publishing. p. 648. ISBN 978-1-85617-745-0.

## A Appendix

This section contains the experimental data from the coreflooding of core R14. In addition, the STARS input files used for sensitivity studies and history matching is presented.

### A.1 Experimental data

*Table A 1: Petrophysical data of core R14.*

Length [cm]	Diameter [cm]	Porosity [%]	PV [ml]	$S_{wi}$	$S_{oi}$	Abs $K_w$	$K_o(S_{wi})$
14.83	3.79	22.19	37.13	0.16	0.84	525	300

*Table A 2: Experimental properties of injected fluids*

	Viscosity at 70 °C * [cP]	NaCl concentration [ppm]	Surfactant concentration [ppm]	Polymer concentration [ppm]
Synthetic seawater (SSW)	0.5	11 159	-	-
Low Salinity water (LS)	0.5	5000	-	-
Low Salinity Surfactant (LSS)	-	5000	10 000	-
Low Salinity Polymer (LSP)	-	5000	-	1500

\* Viscosity of LSS and LSP was not listed in laboratory data.

Table A 3: Experimental properties of injection sequences

	Residual Oil Saturation ( $S_{or}$ )	End-point water effective permeability ( $k_w$ )	PV injected	PV injected cumulative	Injection start time [min]
Synthetic Seawater Flood (SSW)	0.25	15	4.06	4.06	0
Low Salinity Water Flood (LS)	0.22	18	3.23	7.29	1506
Low Salinity Surfactant (LSS)	0.20		0.50	7.79	2707
Low Salinity Polymer (LSP)	0.17		0.50	8.29	2891
2. Low Salinity Water Flood (2. LS)	0.04	315	5.60	13.89	3075*

\* Injection sequence ends after 5154 min.

### A.3 STARS input file – History Matching of R14

```
RESULTS SIMULATOR STARS 201210
INUNIT LAB
WSRF WELL 1
WSRF GRID 1
WSRF SECTOR 1
OUTSRF GRID ADSORP ADSPCMP CAPN IFT KRO KRW LOGCAPN MASDENO
MASDENW MOLDENO MOLDENW
      PRES RFO RFW SG SO SW TEMP VELOCRC VISO VISW W KRSETN
KRINTER
      X
OUTSRF GRID ALL
OUTSRF WELL MASS COMPONENT ALL
OUTSRF WELL MASS COMPONENT 'Na'
**OUTSRF SPECIAL MASSFRAC WATER
OUTSRF SPECIAL MASSFRAC 'INJTR' 'Na'
OUTSRF SPECIAL MOLEFRAC 'INJTR' 'Na'
OUTSRF SPECIAL MASSFRAC 'PRODN' 'Na'
OUTSRF SPECIAL MOLEFRAC 'PRODN' 'Na'
OUTSRF SPECIAL MASSFRAC 'PRODN' 'Cl'
OUTSRF SPECIAL MOLEFRAC 'PRODN' 'SURF'
OUTSRF SPECIAL MASSFRAC 'PRODN' 'SURF'
OUTSRF SPECIAL MOLEFRAC 'PRODN' 'POLYMER'
OUTSRF SPECIAL MASSFRAC 'PRODN' 'POLYMER'
OUTSRF SPECIAL VOLFRAC 'PRODN' 'Na'
OUTSRF SPECIAL DELPBLK 2 1 1 99 1 1
```

\*\*\*\*\*

```
** Definition of fundamental cartesian grid
```

\*\*\*\*\*

\*\* ===== GRID AND RESERVOIR DEFINITION ===== \*\*

GRID CART 100 1 1

KDIR DOWN

DI IVAR 0.056 98\*0.1502 0.056

DJ 100\*3.79

DK 100\*3.79

DTOP 100\*1

POR ALL

0.999 98\*0.22194 0.999

PERMI

100000 98\*525.4 100000

PERMJ EQUALSI

PERMK EQUALSI

END-GRID

\*\* ===== ROCK THERMAL PROPERTIES ===== \*\*

PRPOR 1000

CPOR 2.96e-8

\*\* ===== COMPONENT PROPERTIES ===== \*\*

MODEL 6 6 6 5

COMPNAME 'H2O' 'Na' 'Cl' 'SURF' 'POLYMER' 'DEAD\_OIL'

CMM

0.018 0.02299 0.035453 0.426 6000 0.4

PCRIT

0 0 0 0 0 0

TCRIT

0 0 0 0 0 0

PRSR 1000

TEMR 70

PSURF 101.1

TSURF 25

MASSDEN

0.001 0.001 0.001 0.001 0.001 0.0008784

AVISC

\*\*'H2O' 'Na' 'Cl' 'SURF' 'POLYMER' 'DEAD\_OIL'

0.5 0.5 0.5 2.5 5.7 3.0

VSMIXCOMP 'Na'

VSMIXENDP 0 0.00885

VSMIXFUNC 0 0 0.075 0.166 0.255 0.345 0.43 0.515 0.6 0.683 0.764

VSMIXCOMP 'SURF'

VSMIXENDP0 0.000427

VSMIXCOMP 'POLYMER'

VSMIXENDP 0.0 4.51E-09

SHEARTAB

\*\* Darcy velocity Viscosity

\*\* (cm/min) (cP)

0.00001 5.7

0.0001 5.7

0.001 5.7

0.01 5.7

0.1 5.7

SOLID\_DEN 'Na' 0.001 0 0

SOLID\_DEN 'Cl' 0.001 0 0

SOLID\_DEN 'SURF' 0.001 0 0

SOLID\_DEN 'POLYMER' 0.001 0 0

\*\* ===== ROCK-FLUID DATA ===== \*\*

ROCKFLUID

DISPI\_WAT 'Na' CON 0.005

DISPJ\_WAT 'Na' CON 0.005

DISPK\_WAT 'Na' CON 0.005

DISPI\_WAT 'Cl' CON 0.005

DISPJ\_WAT 'Cl' CON 0.005

DISPK\_WAT 'Cl' CON 0.005

DISPI\_WAT 'SURF' CON 0.05

DISPJ\_WAT 'SURF' CON 0.05

DISPK\_WAT 'SURF' CON 0.05

DISPI\_WAT 'POLYMER' CON 0.05

DISPJ\_WAT 'POLYMER' CON 0.05

DISPK\_WAT 'POLYMER' CON 0.05

RPT 1 WATWET

INTCOMP 'SURF' WATER

IFTTABLE

**	cift	SIGIFT
	0	30
	0.000001	0.1
	0.000005	0.05
	0.00001	0.02
	0.00005	0.02
	0.00026	0.02
	0.000427	0.02
	0.05	0.02

\*\* ----- Synthetic seawater, no surfactant ----- \*\*

INTCOMP 'SURF' WATER

KRINTRP 1

DTRAPW -12.5

SWT

SMOOTHEND QUAD

0.16	0.000000	0.571000
0.18	0.000114	0.480795
0.20	0.000347	0.402317

0.22	0.000663	0.334392
0.24	0.001051	0.275926
0.26	0.001501	0.225902
0.28	0.002010	0.183380
0.30	0.002572	0.147488
0.33	0.003509	0.104347
0.36	0.004551	0.071908
0.39	0.005691	0.048059
0.42	0.006925	0.030979
0.45	0.008247	0.019124
0.48	0.009654	0.011200
0.51	0.011142	0.006142
0.54	0.012709	0.003097
0.57	0.014352	0.001396
0.60	0.016069	0.000539
0.63	0.017857	0.000165
0.66	0.019715	0.000035
0.69	0.021642	0.000003
0.72	0.023635	0.000000
0.74	0.025000	0.000000

\*\* ----- Low salinity water, max surfactant ----- \*\*

INTCOMP 'SURF' WATER

KRINTRP 2

DTRAPW -9.5

SWT

SMOOTHEND QUAD

0.16	0.000000	0.570000
------	----------	----------

0.18	0.000130	0.524312
0.20	0.000424	0.481241
0.22	0.000844	0.440700
0.24	0.001377	0.402601
0.26	0.002012	0.366861
0.28	0.002743	0.333394
0.30	0.003565	0.302115
0.32	0.004473	0.272943
0.34	0.005465	0.245794
0.36	0.006537	0.220586
0.38	0.007686	0.197238
0.40	0.008912	0.175670
0.42	0.010211	0.155804
0.44	0.011581	0.137559
0.46	0.013023	0.120859
0.48	0.014533	0.105627
0.50	0.016111	0.091786
0.52	0.017755	0.079263
0.54	0.019464	0.067983
0.56	0.021237	0.057873
0.58	0.023074	0.048861
0.60	0.024973	0.040877
0.62	0.026933	0.033850
0.64	0.028954	0.027712
0.66	0.031035	0.022396
0.68	0.033174	0.017836
0.70	0.035372	0.013967
0.72	0.037628	0.010724
0.74	0.039941	0.008048
0.76	0.042311	0.005876

0.78	0.044736	0.004150
0.80	0.047217	0.002814
0.82	0.049753	0.001811
0.84	0.052343	0.001089
0.86	0.054987	0.000597
0.88	0.057685	0.000286
0.90	0.060435	0.000111
0.92	0.063238	0.000029
0.94	0.066093	0.000003
0.96	0.069000	0.000000

\*\* -----

RPT 2 WATWET

RPT\_INTRP

COMP 'Na' WATER

LOWER\_BOUND 0.00155

UPPER\_BOUND 0.00885

UPPERB\_RPT 1

INTCOMP 'Na' WATER

\*\* ----- Synthetic seawater, no surfactant ----- \*\*

KRINTRP 1

DTRAPW 0.00885

SWT

SMOOTHEND QUAD

**Sw	krw	kro
0.16	0.000000	0.571000
0.18	0.000114	0.480795
0.20	0.000347	0.402317
0.22	0.000663	0.334392
0.24	0.001051	0.275926
0.26	0.001501	0.225902
0.28	0.002010	0.183380
0.30	0.002572	0.147488
0.33	0.003509	0.104347
0.36	0.004551	0.071908
0.39	0.005691	0.048059
0.42	0.006925	0.030979
0.45	0.008247	0.019124
0.48	0.009654	0.011200
0.51	0.011142	0.006142
0.54	0.012709	0.003097
0.57	0.014352	0.001396
0.60	0.016069	0.000539
0.63	0.017857	0.000165
0.66	0.019715	0.000035
0.69	0.021642	0.000003
0.72	0.023635	0.000000
0.74	0.025000	0.000000

\*\* ----- Low salinity water, no surfactant ----- \*\*

KRINTRP 2

DTRAPW 0.00155

## SWT

0.160	0.000000	0.571000
0.180	0.000099	0.483070
0.200	0.000322	0.406370
0.220	0.000642	0.339780
0.240	0.001046	0.282258
0.260	0.001529	0.232839
0.280	0.002085	0.190627
0.300	0.002709	0.154799
0.320	0.003400	0.124596
0.340	0.004153	0.099322
0.360	0.004968	0.078345
0.380	0.005842	0.061086
0.400	0.006773	0.047026
0.420	0.007760	0.035693
0.440	0.008802	0.026667
0.460	0.009897	0.019575
0.480	0.011045	0.014085
0.500	0.012244	0.009907
0.520	0.013494	0.006789
0.540	0.014793	0.004514
0.560	0.016140	0.002896
0.580	0.017536	0.001781
0.600	0.018979	0.001041
0.620	0.020469	0.000571
0.640	0.022005	0.000289
0.660	0.023586	0.000132
0.680	0.025213	0.000052
0.700	0.026883	0.000017
0.720	0.028598	0.000004

0.740 0.030356 0.000000  
0.760 0.032157 0.000000  
0.780 0.034000 0.000000  
0.960 1.000000 0.000000

KRTYPE CON 2

\*\* ----- Adsorption Data ----- \*\*

ADSCOMP 'SURF' WATER

ADSLANG 0.045 0 100200

ADMAXT 4.4E-07

ADRT 4.4E-07

ADSCOMP 'POLYMER' WATER

ADSLANG 102960 0 1.00E+07

ADMAXT 7.7E-11

ADRT 7.7E-11

PORFT 0.80

\*\* ===== INITIAL CONDITIONS ===== \*\*

INITIAL

VERTICAL OFF

\*\*INITREGION 1

PRES CON 1200

TEMP CON 70

SW CON

0.16

SO CON

0.84

MFRAC\_OIL 'DEAD\_OIL' CON 1

MFRAC\_WAT 'H2O' CON 0.98079

MFRAC\_WAT 'Na' CON 0.00885

MFRAC\_WAT 'Cl' CON 0.01036

MFRAC\_WAT 'SURF' CON 0

MFRAC\_WAT 'POLYMER' CON 0

\*\* ===== NUMERICAL CONTROL ===== \*\*

NUMERICAL

TFORM SXY

ISOTHERMAL

\*\* ===== RECURRENT DATA ===== \*\*

RUN

TIME 0

DTWELL 0.01

DTMAX 1

\*\* ----- Injecting synthetic seawater (SSW) ----- \*\*

WELL 'INJTR'

INJECTOR UNWEIGHT 'INJTR'

\*\* 'H2O' 'Na' 'Cl' 'SURF' 'POLYMER' 'DEAD\_OIL'

INCOMP WATER 0.98079 0.00885 0.01036 0 0 0

OPERATE MAX STW 0.1 CONT

\*\*0.1 cm<sup>3</sup>/min i rate tilsvare 6 cm<sup>3</sup>/time (Eclipse enhet)

\*\* rad geofac wfrac skin

GEOMETRY K 0.01 0.249 1. 0.

PERF TUBE-END 'INJTR'

\*\* UBA ff Status Connection

1 1 1 1. OPEN FLOW-FROM 'SURFACE'

WELL 'PRODN'

PRODUCER 'PRODN'

OPERATE MIN BHP 1200 CONT REPEAT

\*\* rad geofac wfrac skin

GEOMETRY K 0.01 0.249 1. 0.

PERF TUBE-END 'PRODN'

\*\* UBA ff Status Connection

100 1 1 1. OPEN FLOW-TO 'SURFACE'

TIME 1

TIME 1350

\*\* ----- Injecting low salinity water (LS) ----- \*\*

WELL 'INJTR'

INJECTOR UNWEIGHT 'INJTR'

\*\* 'H2O' 'Na' 'Cl' 'SURF' 'POLYMER' 'DEAD\_OIL'

INCOMP WATER 0.99690 0.00155 0.00155 0 0 0

OPERATE MAX STW 0.1 CONT

\*\* Q=0.1 cc/min

TIME 2707

\*\* ----- Injecting low salinity surfactant (LSS) ----- \*\*

WELL 'INJTR'

INJECTOR UNWEIGHT 'INJTR'

\*\* 'H2O' 'Na' 'Cl' 'SURF' 'POLYMER' 'DEAD\_OIL'

INCOMP WATER 0.996473 0.00155 0.00155 0.000427 0 0

OPERATE MAX STW 0.1 CONT

\*\*0.1 cm<sup>3</sup>/min

TIME 2891

\*\* ----- Injecting low salinity polymer (LSP) -----\*\*

WELL 'INJTR'

INJECTOR UNWEIGHT 'INJTR'

\*\* 'H2O' 'Na' 'Cl' 'SURF' 'POLYMER' 'DEAD\_OIL'

INCOMP WATER 0.9968999955 0.00155 0.00155 0 4.51E-09 0

OPERATE MAX STW 0.1 CONT

TIME 3075

\*\* ----- Injecting low salinity water (2. LS) ----- \*\*

WELL 'INJTR'

INJECTOR UNWEIGHT 'INJTR'

\*\* 'H2O' 'Na' 'Cl' 'SURF' 'POLYMER' 'DEAD\_OIL'

INCOMP WATER 0.99690 0.00155 0.00155 0 0 0

OPERATE MAX STW 0.1 CONT

\*\* Q=0.1 cc/min

TIME 5154

STOP

### A.3 STARS input file – Sensitivity and verification studies

```
INUNIT LAB
INTERRUPT *STOP
WSRF WELL 1
WSRF GRID TIME
WSRF SECTOR TIME
OUTSRF GRID VOL ADSORP MASS ADSORP MOLE ADSORP CMPVISW PPM KRO
KRW PRES SG SHEARW SO SW
    TEMP VISCVELW VISW VISWCOM W X Y
OUTSRF SPECIAL DELPBLK 2 1 1 99 1 1
OUTSRF SPECIAL DELP 'INJ' 'PRODN'
OUTSRF SPECIAL MOLEFRAC 'PRODN' 'SALT'
OUTSRF SPECIAL MASSFRAC 'PRODN' 'SALT'
OUTSRF GRID ALL
OUTSRF WELL LAYER NONE
WPRN GRID 0
OUTPRN GRID POREVOL
OUTPRN RES NONE
WPRN ITER 1
OUTPRN ITER NEWTON
PARTCLSIZE 1e-017
```

```
** ===== GRID AND RESERVOIR DEFINITION ===== **
```

```
GRID CART 100 1 1
KDIR DOWN
DI CON 1
DJ CON 1
DK CON 1
```

NULL CON 1

POR 0.999 98\*0.25 0.999

PERMI ALL

20000 98\*2000 20000

PERMJ CON 2000

PERMK CON 200

PINCHOUTARRAY CON 1

END-GRID

\*\* ===== COMPONENT PROPERTIES ===== \*\*

MODEL 3 3 3 2

COMPNAME 'WATER' 'SALT' 'DEAD\_OIL'

CMM 0.018 0.058 0.4

PCRIT 0 0 0

TCRIT 0 0 0

CP 0 0 0

MASSDEN 0.0010 0.0019 0.00010

AVISC 1 5 13.8

BVISC 0 0 0

SOLID\_DEN 'SALT' 0.0182482 0 0

PRSR 2528.25

TEMR 31

PSURF 101

TSURF 31

\*\* ===== ROCK-FLUID DATA ===== \*\*

ROCKFLUID

RPT 1 WATWET

\*\* ----- Relative Permeability Curves ----- \*\*

DTRAPW 0.0400

SWT

SMOOTHEND QUAD

**Sw	krw	kro
0.20	0.0000000	1.0000000
0.22	0.0004800	0.9216000
0.24	0.0019200	0.8464000
0.26	0.0043200	0.7744000
0.28	0.0076800	0.7056000
0.30	0.0120000	0.6400000
0.32	0.0172800	0.5776000
0.34	0.0235200	0.5184000
0.36	0.0307200	0.4624000
0.38	0.0388800	0.4096000
0.40	0.0480000	0.3600000
0.42	0.0580800	0.3136000
0.44	0.0691200	0.2704000
0.46	0.0811200	0.2304000
0.48	0.0940800	0.1936000
0.50	0.1080000	0.1600000
0.52	0.1228800	0.1296000
0.54	0.1387200	0.1024000
0.56	0.1555200	0.0784000

0.58	0.1732800	0.0576000
0.60	0.1920000	0.0400000
0.62	0.2116800	0.0256000
0.64	0.2323200	0.0144000
0.66	0.2539200	0.0064000
0.68	0.2764800	0.0016000
0.70	0.3000000	0.0000000

DISPI\_WAT 'SALT' \*CON 0.05  
DISPJ\_WAT 'SALT' \*CON 0.01  
DISPK\_WAT 'SALT' \*CON 0.01

\*\* ===== INITIAL CONDITIONS ===== \*\*

INITIAL  
VERTICAL OFF  
INITREGION 1  
PRES CON 101  
TEMP CON 31

SW ALL  
1 98\*0 1

MFRAC\_OIL 'DEAD\_OIL' CON 1.0  
MFRAC\_WAT 'SALT' CON 0.0400  
MFRAC\_WAT 'WATER' CON 0.9600

\*\* ===== NUMERICAL CONTROL ===== \*\*

NUMERICAL

TFORM SXY  
ISOTHERMAL

\*\* ===== RECURRENT DATA ===== \*\*

RUN

TIME 0

DTWELL 0.001

WELL 'INJ'

INJECTOR MOBWEIGHT 'INJ'

INCOMP WATER 0.9600 0.0400 0

OPERATE MAX STW 0.1 CONT

GEOMETRY K 0.01 0.2 1.0 0.0

PERF TUBE-END 'INJ'

1 1 1 1. OPEN FLOW-FROM 'SURFACE'

WELL 'PRODN'

PRODUCER 'PRODN'

OPERATE MIN BHP 101.1 CONT REPEAT

GEOMETRY K 0.01 0.2 1.0 0.0

PERF GEO 'PRODN'

100 1 1 1. OPEN FLOW-TO 'SURFACE'

TIME 20000

STOP